

Delft University of Technology
FACULTY OF CIVIL ENGINEERING AND GEOSCIENCES

Graduation project on topic
Reliability-based updating of anchor capacity

By
Moritz Effenberger

to obtain degree

Master of Science

ASSESSMENT COMMITTEE:

Chair: Dr. ir. Bram van den Eijnden (TU Delft)

Dr. ir. Alfred Roubos (TU Delft / Port of Rotterdam)

M.Sc. ir. Antonis Mavritsakis (Deltares)

M.Sc. ir. Camille Habets (Royal HaskoningDHV)



Delft, 14 November 2022

Symbols, indeces and abbreviations

Anchor Modelling

| | |
|--------------|-------------------------|
| α_t | Shaft friction factor |
| Δ | -change |
| μ | Viscosity |
| ν | Poisson's ratio |
| τ | Shear stress |
| τ_{avg} | Average tension stress |
| τ_{ult} | Ultimate tension stress |
| A | Grout body |
| k | Characteristic |
| M | -Maxwell |
| t | Tension |
| KV | -Kelvin-Voigt |
| A | Cross-sectional area |
| D | Diameter |
| f_{eff} | Efficiency factor |
| G | Shear modulus |
| k_s | Creep value |

| | |
|-----------|------------------------|
| L | Length |
| P | Force |
| R | Resistance |
| t | Time |
| T_{ult} | Ultimate tension force |
| u | Displacement |

Bayesian Updating

| | |
|------------|---|
| δ_u | Dirac mass at the random variable |
| ℓ | Scaling constant |
| λ | Scaling parameter |
| Ω | Failure domain |
| ϕ_n | Posterior distribution |
| π | Structural reliability random variable |
| ρ | Cross-Correlation coefficient |
| θ | Random variable |
| i,j | Counter for the nested failure domains |
| $iter$ | Counter for the correlation coefficient calculation |
| a | Acceptance probability in Markov Chain |
| c | Normalizing constant |
| c_E | Evidence |
| D | Data |
| F | Nested failure domain in standard normal space |

| | |
|-----------|---|
| G | Limit-state function in standard normal space |
| g | Limit-state function |
| h | Threshold level |
| I_{F_j} | Indicator function for specific failure domain |
| K | Total amount of posterior samples |
| k | Counter for accepted samples |
| L | Likelihood |
| M | Model assumptions |
| m | Amount of nested failure domains |
| n | Counter of proposed samples |
| P | Probability |
| P_0 | Prior probability distribution |
| P_D | Posterior probability distribution |
| P_f | Probability of Failure |
| q | Proposal probability density function |
| u | Random variable in standard normal space |
| U_n | Indicator for the state of the Markov Chain |
| v | Accepted random variable in standard normal space |
| Z | Nested failure domain |

General

| | |
|----------|--------------------------------|
| μ | Statistical mean |
| σ | Statistical standard deviation |

aBUS – SuS adaptive Bayesian updating using structural reliability methods with Subset Sampling

Cal Calibration

Disp Displacement

MCMC Markov Chain Monte Carlo

Abstract

This research focuses on reliability-based, Bayesian updating of grout anchors' bearing capacity. Firstly, grouted anchors are commonly used in practice, even though large uncertainties surround their bearing capacity. Secondly, every anchor must be tested on their working load for quality assurance. Because of the combination of those two factors, Bayesian updating on grout anchors yields large potential. The measurement data can be used in the design process, to reduce uncertainties. The main goal of this research was to establish how reliability-based updating can be applied in the context of grout anchor bearing capacity. The motivation to use such techniques is to increase the efficiency of existing structures, like in this case study for quay walls, or to adapt the design during construction, effectively cutting costs in both cases.

This research was conducted using measurement data from the HHTT quay wall at the port of Rotterdam, applying a recently developed analytical anchor displacement model, and the Bayesian updating technique 'aBUS-SuS'. The combination of both of these methods in this context is a novelty approach to the subject. The first step was to derive the soil parameters necessary to reproduce the measurements to prove firstly, that the model is capable to capture anchor behavior, secondly to get a better understanding of how the model functions in this context, and thirdly to establish a baseline of the parameters necessary for the estimation of prior distributions.

The second step was the application of the Bayesian updating algorithm. There, the prior distributions, which are needed as an input, are generated using the results from the first step. The resulting posterior distributions are then related to failure limits of the critical soil parameters that were derived according to a common anchor failure criterion. This gives an indication of the anchor's utilization and disposition to failure.

The results exhibited failure conditions for those anchors that were at failure, verifying that the novelty approach can be applied to the problem. Another finding was that depending on the soil parameter, conclusions can be drawn about the likeliness of the failure type. This means how brittle or elastic the failure might be.

The analyses showed that the studied procedure has potential and the anchor's proneness to failure can be assessed. The underlying analytical model is suitable for the applied type of Bayesian updating because the results are in the same range as for the calibration, but on average slightly lower in their mean magnitude. Thus, additional information is obtained, and the overall uncertainty is reduced. Furthermore, the analyses of the suitability tests gave a quantifiable indication of the anchors' reliability under *failure load* that was in line with measured failure indication under *working load*.

Even though the uncertainty that surrounds the anchor-design was reduced, limitations to the framework arose. The analytical model requires uncommon soil parameters as an input. Those parameters need to be specifically determined in laboratory investigations and cannot be tested for on site. The model in- and output needs to match the measurements to the failure criterion of the anchors, and in anchor design, advanced analytical models, like the one used in this research are scarce. The measurement always have certain errors inherent. These errors can lead to diffuse and noisy posterior distributions. Furthermore, a minimum amount of measurements must be available in the first place, otherwise the algorithm does not converge properly towards a solution.

This is why it is recommended to get detailed insight of the soil parameters at question also under higher stresses and strains than the anticipated working loads. This helps to give better estimations of the prior distributions and their bounds, and also gives larger confidence in the posterior distributions as a result. Furthermore, this also helps to establish precise parametric limits corresponding to failure, for which the reliability can be evaluated.

Acknowledgements

First, I want to thank my supervisors Bram van den Eijnden and Alfred Roubos for always providing me with constructive feedback and giving me proper guidance throughout the entire graduation project.

I also would like to thank Antonis Mavritsakis for helping me understand the Bayesian framework and always asking critical questions that improved my understanding of the topic and the quality of the thesis.

I would like to specially thank Camille Habets and Jelle van der Zon for the insightful discussions and extensive support revolving all aspects of the graduation project.

Lastly, I thank my family and friends for supporting me throughout my time in Delft and for making this graduation possible.

Moritz Effenberger
Delft, November 2022

Contents

| | | |
|----------|--|-----------|
| 1 | Introduction | 1 |
| 1.1 | Research question | 3 |
| 1.2 | Outline | 3 |
| 2 | Methodology | 5 |
| 2.1 | Limitations to this research | 5 |
| 2.2 | Data and Tools | 6 |
| 3 | Theoretical Background | 7 |
| 3.1 | Grout anchors | 7 |
| 3.2 | Grout anchor Design | 8 |
| 3.2.1 | Ostermayer Method | 9 |
| 3.2.2 | CUR166 Method | 12 |
| 3.2.3 | Analytical creep model | 13 |
| 3.2.4 | Numerical Methods | 19 |
| 3.3 | Anchor Testing | 20 |
| 3.3.1 | Test procedures | 20 |
| 3.3.2 | Creep Value | 22 |
| 3.3.3 | Apparent free length | 23 |
| 3.3.4 | Test Limits | 23 |
| 3.4 | Bayesian Updating Methods | 24 |
| 3.4.1 | Bayes Theorem | 24 |
| 3.4.2 | aBUS - Theory: | 25 |
| 3.4.3 | Subset Simulation - Theory: | 26 |
| 3.4.4 | Markov Chain Monte Carlo (MCMC) simulation | 27 |
| 4 | Practical elaboration | 33 |
| 4.1 | Site description | 33 |
| 4.2 | Ostermayer method | 34 |
| 4.3 | CUR method | 35 |
| 4.4 | Analytical model | 35 |

| | | |
|----------|--|-----------|
| 4.5 | Comparison | 36 |
| 5 | Anchor Modelling Results | 37 |
| 5.1 | Limits | 38 |
| 5.2 | Calibration | 38 |
| 5.2.1 | Sensitivities | 40 |
| 5.2.2 | Investigation Tests | 45 |
| 5.2.3 | Suitability tests | 48 |
| 5.2.4 | Acceptance Tests | 51 |
| 5.2.5 | Summary | 53 |
| 5.3 | Parameter distribution | 54 |
| 5.3.1 | Shear modulus | 54 |
| 5.3.2 | Kelvin-Voigt shear modulus | 55 |
| 5.4 | Parametric limits at failure | 56 |
| 6 | Bayesian Updating Results | 59 |
| 6.1 | Artificial Case | 60 |
| 6.2 | Investigation Test Results | 61 |
| 6.2.1 | Set 1 - 5 Parameters | 61 |
| 6.2.2 | Set 3 - 2 Parameters | 64 |
| 6.2.3 | Set 4 - 3 Parameters | 65 |
| 6.2.4 | Large Sample Size Investigation | 66 |
| 6.3 | Suitability Test Results | 68 |
| 6.3.1 | Set 1 - 5 Parameters | 68 |
| 6.3.2 | Set 3 - 2 Parameters | 69 |
| 6.3.3 | Set 4 - 3 Parameters | 69 |
| 6.3.4 | Credible Intervals | 70 |
| 6.4 | Reliability analysis | 71 |
| 6.4.1 | Investigation Tests | 71 |
| 6.4.2 | Suitability Tests | 74 |
| 7 | Discussion | 77 |
| 7.1 | Calibration Comparison | 77 |
| 7.2 | Parameter Evolution | 77 |
| 7.3 | Non-time dependent Failure Criterion | 79 |
| 7.4 | Multimodality, Post-processing | 80 |
| 7.4.1 | Example 1 | 80 |

| | | |
|----------|---|------------|
| 7.4.2 | Example 2 | 81 |
| 7.5 | Reliability - Parametric Limits | 83 |
| 7.6 | Practical Suitability | 83 |
| 8 | Conclusions | 85 |
| 9 | Limitations and Recommendations | 87 |
| 9.1 | Limitations | 87 |
| 9.1.1 | General Limitations | 87 |
| 9.1.2 | Detailed Limitations | 87 |
| 9.2 | Recommendations | 88 |
| 9.3 | Further research | 89 |
| A | Appendix - Theoretical Background | 93 |
| A.1 | Anchor design | 93 |
| A.2 | Bayesian updating | 94 |
| A.2.1 | Algorithms | 94 |
| B | Appendix - Practical Elaboration | 97 |
| C | Appendix - Anchor Modelling | 99 |
| C.1 | HHTT Test Data: | 99 |
| C.2 | HHTT Structural Parameters: | 99 |
| C.3 | Results Investigation tests, Set 1 - tabular: | 102 |
| C.4 | Results Investigation tests | 102 |
| C.4.1 | Set 1 | 102 |
| C.4.2 | Set 3 | 103 |
| C.5 | Results Suitability tests | 103 |
| C.5.1 | Set 1 | 103 |
| C.5.2 | Set 2 | 104 |
| C.5.3 | Set 3 | 105 |
| D | Appendix - Bayesian Updating | 107 |
| D.1 | Investigation Tests | 107 |
| D.1.1 | Set 1 - Results second anchor | 107 |
| D.1.2 | Set 3 - Results second anchor | 107 |
| D.1.3 | Set 4 - Results second anchor | 108 |
| D.1.4 | Comparison with truncated normal priors | 109 |
| D.2 | Suitability Tests | 109 |

| | | |
|----------|---|------------|
| D.2.1 | Reliability investigation | 109 |
| E | Appendix - Codes | 111 |
| E.1 | Analytical model | 111 |
| E.1.1 | General Displacements | 111 |
| E.1.2 | Calibration - Least squares | 114 |
| E.1.3 | Limit Parameters | 114 |
| E.2 | Bayesian Updating | 116 |
| E.2.1 | aBUS-SuS Call, general | 116 |
| E.2.2 | Multiprocessing function call | 116 |

1. Introduction

Over the last centuries, grouted anchors became a standard element of geotechnical construction projects. They are commonly used to tie back structural forces in sheet pile walls, quay walls or similar structures. Especially in deep excavations, they show advantages because a 'strut-free', open excavation pit can be constructed. Also in quay wall construction their application became standard practice. The first anchors were installed by Karl Bauer in 1958 [15]. After the initial research programs, grout anchors became a more common anchorage system and the first design methods were developed. Since then, the demands have changed, anchors became larger and the capacities increased, however, the design methods only changed marginally. Proven methods for the design and installation of anchors have been used for decades, yet due to the large uncertainties, each anchor must be tested for verification. Once a project is completed, and all anchors passed the test, all of this data remains typically unused for back-analysis purposes. All uncertainties increase the costs of projects because more generous reserves in the design need to be appointed. Therefore, there is a large potential to utilize this data to make a statement about the anchor's capacity, its reliability or other characteristics. This way, the efficiency of the anchored structure can be increased, which leads again to a higher utilization of the structure that has also environmental benefits.

The design of grout anchors is specified within the framework of European and national standardization codes. In the Netherlands, anchor design and specifications to the installation are regulated in CUR166, [8]. During the years, different methods for the design evolved, all mainly of empirical or semi-empirical nature. One of the main contributions towards anchor design were the efforts and publications by Ostermayer [17], [16], [15]. The author provides detailed explanations on the design and installation techniques. While the recommendations and the content have not changed over time, the earlier publications like [15] provide more background data and the later ones elaborate more on previous case studies to reflect the limits of grout anchors. Based on large scale testing efforts, Ostermayer developed diagrams which can be used to estimate anchor capacity. In [16] recommendations are provided about the soil-structure interaction aspects of the design of anchored structures.

An alternative method is provided by the authors of [14]. The presented method is not a design method in the conventional sense, comparable to the CUR-method or the Ostermayer charts, since no maximum bearing capacity is calculated. The procedure was developed to calculate creep displacements over larger time periods with an ultimate limit loading as an input. In this research, it is adapted for analytical anchor modelling of shorter time periods. The details and the theory are explained in the following chapters.

The work of Baecher et al. [1] functions well as a basis for familiarizing oneself with the basic concepts of statistical analyses in a geotechnical engineering environment. In addition, it provides the theory behind Bayesian theory, sampling methods and reliability analyses. Fellin et al. [10] provides a good alternative to the previous publication, but the authors discuss a broader range of topics in a more practical approach while providing several examples along the way. Reliability or Bayesian updating procedures are mainly focused outside of anchor modelling. There has not been a single publication identified that investigated Bayesian updating on grout anchors.

The motivation of applying Bayesian updating techniques is the incorporation of monitoring data or other measurements/observations to update the reliability in a mechanical model. The basis for all of Bayesian computation is Bayes theorem, which states how observations or measurement data can be used in a mathematical calculation procedure to update previous parameter estimates. Different computational approaches revolve around an efficient approximation for the solution of Bayes equation. One of the most beneficial Bayesian inference tools are Markov-Chain-Monte-Carlo algorithms [12], [3]. Another efficient Bayesian updating algorithm was developed by Straub, firstly presented in [23]. The method was continuously improved and updated, [24], [25], until the latest version where "adaptive Bayesian updating using Structural reliability methods with Subset sampling", short, aBUS-SuS is introduced [4]. The main idea behind this approach is that the Bayesian updating problem is translated into a reliability problem, with the goal of drawing samples directly from a posterior distribution that lies in an artificial failure domain of the reliability problem [12]. The author of [6] gives a comprehensive overview of other common reliability updating techniques and compares them regarding their suitability for a sheet pile wall reliability updating analysis. The author comes to the conclusion that aBUS-SuS algorithm is the most optimal since it can deal with non-linear problem definitions and its ability to calculate small failure probabilities.

In [2] the principles of inverse analysis are elaborated by using the maximum likelihood approach on a case study of a sheetpile wall deep excavation. This gives insight on how measurements and monitoring data can be utilized to back-calculate forces, stresses and other parameters, referring to the theoretical background as well. However, for the discussed case study within the publication, there was no attention being paid to the anchor capacity and its inherent uncertainty, it revolved mainly around the sheetpile wall. Another simple procedure for the back-analysis of measurements to loads is described in [9] by calculating the secant shear modulus from the measured strain increments on piles. In [21], the authors give a comprehensive overview of the theory and application on reliability assessments of geotechnical structures with several variables involved, also providing recommendations for a step wise approach towards a solution. As an example, a retaining wall structure is provided without any anchors involved. Recently, there has been more research conducted regarding the reliability assessment of quay walls using finite element analysis [26], [29], [13]. One of the main findings in [26] is that the anchor capacity and the parameters influencing it are governing in the reliability assessment. The author in [29] recommends that the target reliability for anchor failure should be increased in fault trees when investigating the reliability. However, the failure condition of the investigated anchor were less of geotechnical but more of structural nature, namely steel failure of the rod. Therefore, the relevance for this research is limited, where the geotechnical anchor failure plays the major role. Regarding quay walls, [19] functions as a state-of-the-art report. Within this research, anchor failure is regarded structurally and geotechnically. The geotechnical limit state function adapts the CUR-method for the estimation of the anchor's bearing capacity. One of the most relevant conclusions that was drawn is that the sensitivity of non-time dependent parameters is the largest along with the geometrical measurements of the structure, which could be observed within the resulting sensitivity factors. To summarize, most analyses have been carried out numerically, since the complexity of the researched structures does not allow for analytical solutions. Grout anchors are often a part of the structural system, but no research has been identified that investigates the influence of Bayesian updating techniques on anchor capacity itself.

In practice, reliability-based or Bayesian updating approaches are not widespread. One of the limitations of the past was the lack of affordable computational power in combination with efficient algorithms. As illustrated, the scientific community is advancing with the development of these tools, however, within the civil engineering sector their application is scattered. There is little experience in the application of these methods, and case studies are mostly not published. Scientific publications mainly show simple examples of less practical relevance.

1.1. Research question

The identified gap in literature and within research compared to the industry's interest in efficiency and safely increasing utilization of structures to extend their lifespan justifies the need for further research of grout anchors in the context with Bayesian updating techniques. In the following, the research questions and sub-questions are presented.

How can anchor measurement data be used for reliability-based updating of anchor bearing capacity?

- How can analytical models be used to predict anchor failure?
- What is the effect of Bayesian updating on the anchor capacity?
- What are the limitations of Bayesian updating using analytical models?

1.2. Outline

In the first part, the theoretical background of the relevant literature and applied procedures is presented. It shall serve as a comprehensive overview, without repeating the source literature too closely. The different components of the research are split accordingly throughout the report, beginning with anchor modelling and followed by Bayesian updating. The second part discusses the application of the chosen anchor modelling technique to reproduce the anchor measurement data to establish a parametric benchmark through back analysis. Within this part, the models sensitivities and parametric dependencies are illustrated. In the third part the effects of Bayesian updating are investigated incorporating the modelling approach from the previous chapter and the same measurement data. This chapter focuses mainly on the parametric influences and the deviations compared to the previously presented results from the calibration. In the fourth part, the results of the previous parts are summarized, interpreted and put into context concerning the effects on the reliability of the anchor itself. Lastly, conclusions, recommendations and limitations are formulated.

2. Methodology

A quantitative research was set up to investigate Bayesian updating on anchor capacity. First, a desk study was conducted to familiarize oneself with the theoretical aspects intertwined with the investigated topic and to check which research has already been conducted within the field. Within this step, the analytical models for the anchor modelling and the Bayesian updating algorithms were identified. As a next step, those models and procedures that seemed the most innovative and promising were chosen for further investigation by application in the preceding chapters. The analytical model presented in [14] was chosen because the model's possibilities are vast, and the limitations according to the authors are negligible. An initial investigation showed that precise fits to the measurement data were possible for a physically realistic range of parameters - comparable to the range derived in [14], which gave a promising outline for the follow-up research. The calibration process was done by utilizing the 'least-squares' algorithm, implemented in the Python-library 'SciPy'. This procedure is commonly applied in the context of curve fitting, which is the essence of the initial analysis, since the complex soil parameters were treated as unknowns. There are many approaches for Bayesian updating. For this research, the suitable procedure was chosen based on the previous research for similar problems and based on advice of the members of the committee for this graduation project.

2.1. Limitations to this research

In the following, the limitations of this research are discussed. Several knowledge gaps were identified involving anchor modelling. This research shall combine the two new approaches, reliability-based updating on anchor capacity. The underlying analytical model was recently developed for the purpose of modelling long term anchor creep displacement. The Bayesian updating algorithm is a more efficient adaptation of Markov Chain Monte Carlo analyses. Both methods together have not been investigated before. Throughout the investigation, knowledge gaps arose about both methods independently. Those gaps were not the major focus of the research, since both methods themselves are regarded as sound concepts, and the focus was in their combination.

- One of the major gaps is the definition of an anchor's geotechnical failure criterion. Based on the investigated literature, its origin and magnitude cannot be fully related. The current consensus is that the anchor's creep is governing in the assessment of its failure condition, but the current limit values seem rather arbitrary and interchangeable.
- This work is limited to the effects of Bayesian updating using an analytical anchor model. Numerical anchor modelling techniques are outside the scope, since their calculation times are too long for Bayesian updating unless surrogate modelling or virtual machines are employed.
- Literature suggests that anchor bearing behavior can be influenced by the installation method, boring techniques, structural detailing or type of loading. This analysis does not aim to investigate these dependencies, but focuses on the standard anchor installation with standard boundary conditions.
- Regarding the reliability-based updating procedure, this research does not focus on the development, comparison or improvement of approximate Bayesian computing and the involved algorithms. The

procedures are selected according to reviews in state-of-the-art literature and applied to the anchor problem.

- Another limitation is that given the scope and the data, the validation and verification steps of the results could not be conducted in a way that the presented and developed procedures allow to be applied in a practical environment.

Limitations of the more technical kind are discussed within the corresponding chapters.

2.2. Data and Tools

The measurement data was provided by Port of Rotterdam through the supervisors of this graduation project. With this data, a case study is conducted to illustrate the possibilities of the analytical anchor model and the effects of Bayesian updating. This list illustrates what the used data consists of for the **HHTT-Rotterdam** data set.

- Design and test report for investigation tests incl. test results (2 anchors)
- Test results suitability tests (9 anchors)
- Test results acceptance tests (81 anchors)

The measurement data consisted of .pdf files of digital tables or analogue scans, which means it was necessary to digitalize them by transferring them into Microsoft Excel sheets to be flexible for further data analysis purposes. The analytical model was implemented in a calculation sheet in the programming language "Python" with common inherent libraries. By reproducing the results with the data presented in [14] it was ensured that the model implementation functions correctly. The Bayesian updating algorithm, called 'aBUS-SuS', was made available, open-source, by the developers at the Technological University Munich and can be downloaded on their website. It consists of one script that has the 'adaptive conditional sampling' Markov chain Monte Carlo method according to [18] implemented and another script that has the 'adaptive Bayesian updating using Structural Reliability methods' algorithm according to [25] and [4] implemented. The most important equations and snippets necessary for reproduction of the results of this research can be found in Appendix E.

3. Theoretical Background

3.1. Grout anchors

Grout anchors are used in various structures. The most common applications are in retaining wall construction, quay walls and in tunneling. Grout anchors only work in a single direction, there is no bearing capacity in compression. The tension bearing capacity of grout anchors is obtained by mobilizing friction at the interface of the grout body to the surrounding soil. The following figure shows the main components of a grout anchor in a simplified way.

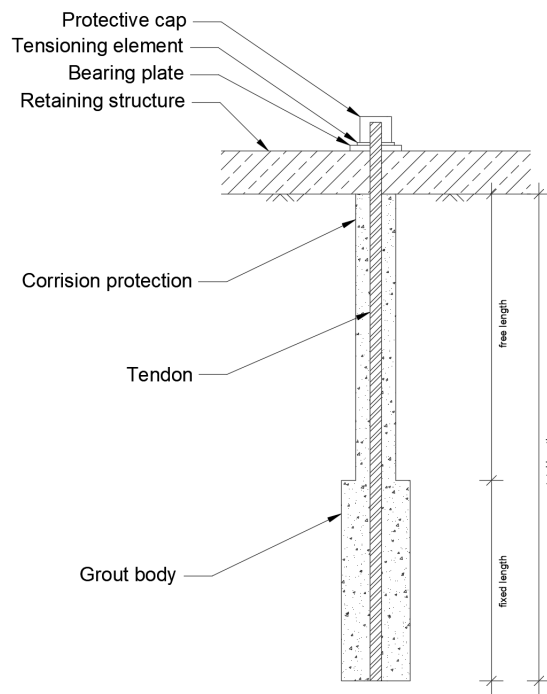


Figure 3.1: Grout anchor components simplified

The figure shows the grout anchor in a vertical installation, however, the inclination of grout anchors installation purely depends on the force that needs to be tied back and the equilibrium of the soil-structure system. In retaining walls and quay walls, the anchors are normally installed with an inclination to the horizontal, from 10° to 45° . The installation process is easier for larger inclinations, but the efficiency of the anchor decreases since the vertical component of the force becomes larger while the horizontal one becomes smaller. Anchors are often used for temporary works, like for retaining walls for deep excavations, since it enables an open construction pit compared to the alternative of using struts. Anchors in quay walls are always permanent.

There are several different types of grout anchors, of which only the standard, common strand anchor is focussed on. The typical construction process first involves the drilling of the hole, second the insertion of the anchor tendon, often covered in a tube as a protection against corrosion, and then third higher pressure

grouting. The anchor generates its tension resistance on the soil-grout interface mainly due to this procedure. Normally, the grouting is done in several steps, while the first step ensures the complete coverage of the steel tendon at around 5 bar pressure while usually the second step then fabricates the load bearing grout body under pressures of 30 - 50 bar. Due to the grouting, the diameter increases. For sands, this increase is usually estimated to be 2 cm in diameter. However, the grouting procedures and pressures vary, depending on the soil types, soil conditions and the contractor [20].

Screw in-injection anchors provide an alternative to classic grout anchors. The working principle is similar, but the grout body reaches over the entire length of the steel tendon. Furthermore, the anchor body is grouted with lower pressures, which means that the borehole diameter is assumed not to increase. A lost drilling tip is fixed on a tubular steel element, where the drilling and the grouting is a continuous process. Since the tendon is commonly a steel tube and the soil-grout interface is so large, those anchors are also capable of bearing compression [27].

Grouted anchors are differentiated into two groups, long term anchors with a duration of use longer than two years and short term anchors with a duration shorter than two years. Usually, depending on the steel tendon, grouted anchors are considered short term anchors, since their structural safety is strongly influenced by possible corrosion. The grout body is considered to develop cracks and fissures when being under tension, through which water can contact the steel. For long term anchors, compression type anchors are used to limit the influence of corrosion. The main idea is to keep the whole grout body under compression by introducing the force into the end of the grout body instead of the beginning. This way, no tension cracks develop, and the steel does not get in contact with water. This mainly becomes a problem with pre-tensioned steel rods that are extremely sensitive to corrosion. For tubular steel rods, corrosion effects can often be estimated and accounted for in the design [20].

3.2. Grout anchor Design

The available anchor design methods are mainly of empirical or semi-empirical nature. The presented methods follow similar procedures as for pile design equations, where the shaft friction is quantified and governing in the calculation. The empirical coefficients vary from the ones for piles.

In Europe, the design is regulated in the Eurocode 7, giving the boundary conditions for the safety philosophy. In the Netherlands, the actual calculation procedure is described in the CUR 166. The anchor installation and regulations about the testing are described in EN 1537.

The main proofs concerning their design involve sufficient tension resistance of the anchor steel and sufficient resistance on the soil-grout interface, which is the pull-out resistance. Naturally, the smaller value is governing. The steel strength is assessed by comparing the tension stress in the cross-sectional area with its resistance according to Eurocode 3, which depends on the steel type, taking corrosion into account. Since the steel quality is more precisely predictable and controllable, the material factors concerning steel resistance are lower than for geotechnical resistance, usually around 1.0 to 1.1 for steel. However, the safety factors on the loading are larger for the steel strength assessment compared to the geotechnical one. Within this research, design calculations are not made, which is why generally no safety factors are applied, and characteristic values are kept.

$$R_{t,k} = A_t \cdot f_{t,k} \quad (3.1)$$

The focus of this research is the assessment of the geotechnical bearing capacity of grout anchors. The steel strength assessment is not further discussed. The geotechnical bearing capacity is more complex to derive,

the practical methods are mainly of semi-empirical nature. One of the earliest and most proven methods is Ostermayer's approach, which is discussed in the following.

3.2.1 Ostermayer Method

The Ostermayer method originates from research conducted by H. Ostermayer in 1960 to 1980 for application in various soils. For different ground conditions, the bearing mechanism at the interfaces changes accordingly. For rocks the strength is mobilized by interlocking of the grout at a rough interface, for non-cohesive soils the resistance is related to dilatancy effects along the grout body while for cohesive soils, grout fissures contribute most to the bearing capacity. For a large test database the capacity has been quantified and is expressed in graphs in which, for example, the non-linear bond stress distribution over the length of the grout body is incorporated. Alternatively, the ultimate bearing capacity can also be estimated by adapting a similar procedure as for calculating pile bearing capacity [17]:

$$T_{ult} = \pi \cdot D \cdot L \cdot \tau_{ult} \quad (3.2)$$

However, since the stress distribution along the anchor is non-linearly dependent on the fixed length the following relation holds [17].

$$T_{ult} = \pi \cdot D \cdot L \cdot \tau_{avg} \quad (3.3)$$

$$T_{ult} = \pi \cdot D \cdot L \cdot \tau_{ult} \cdot f_{eff} \quad (3.4)$$

With,

$$f_{eff} = 1.6 \cdot L^{-0.57} \quad (3.5)$$

The factor f_{eff} can be understood as an efficiency factor dependent on the length of the grout body. It decreases the bearing capacity stress with increasing length. This can be visualized by putting the factor into context with the bond stress distribution over the fixed length.

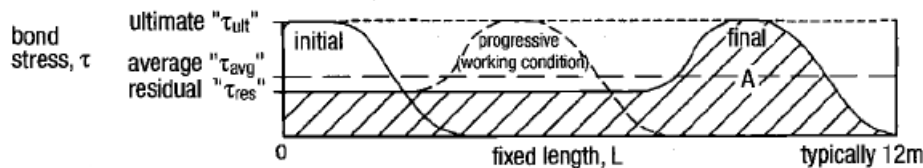


Figure 3.2: Bond stress distribution along grout body [17]

Using figure 3.2, the factor f_{eff} can be expressed as the fraction of the area of τ over the area below the τ_{ult} line.

$$f_{eff} = \frac{Area \ \tau}{Area \ \tau_{ult}} \quad (3.6)$$

The purpose of the efficiency factor is to quantify a decrease of capacity with an increasing length, since for anchors the stress distribution is not comparable to the one of piles [17].

Furthermore, for some soil conditions the bearing capacity can show that it does not increase proportionally with a larger diameter which is why [17] suggests the incorporation of a T_M [kN/m] value, that is a fixed value, inserted in equation 3.4, replacing π , d , and τ_{ult} . Its estimation is not further explained in [17], only a range for different soils is provided. For fine sands T_M should be around 200 kN/m up to 400 kN/m for

dense gravels. The authors note that the mentioned values were only valid for short grout body lengths and a certain grout pressure, here 7-10 bar per casing. This means that the authors observed an influence of the installation technique and pressurization, but could not quantify it.

Within the publication, there is limited information about how to estimate the strength parameters τ_{ult} and τ_{avg} . It is suggested that τ_{ult} can be estimated, for cohesive soils with a factor multiplied with the undrained shear strength c_u and for non-cohesive soils a factor multiplied with the standard penetration test value N_{30} as shown in Fig. 3.3, which suggests that also a correlation to CPT data should be possible. Specific values for these factors are not given.

The following figure presents the approach of how to estimate the ultimate bearing capacity with the input parameters 'fixed length' and SPT data.

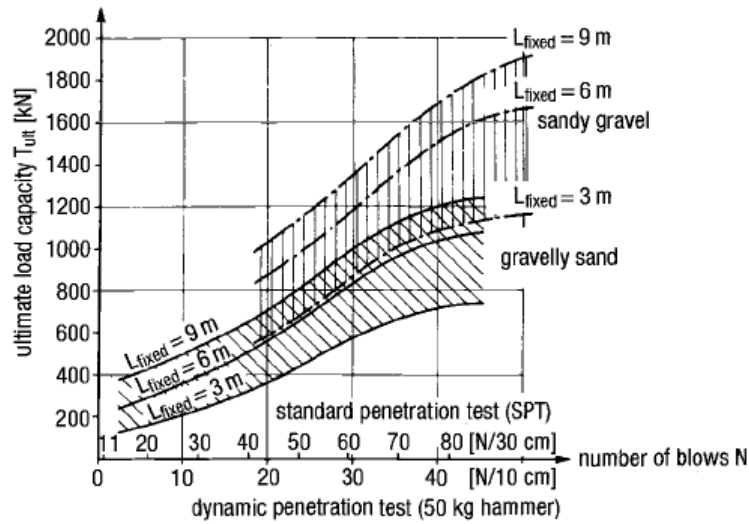


Figure 3.3: Ultimate bearing capacity with SPT data

Figure 3.3 has quantifiable SPT data as a basis, but this basis is not provided to the reader, which makes the implementation for computational Bayesian updating analysis cumbersome.

The general design approach is to make use of the provided diagrams, in which non-linearity and soil conditions are accounted for. For cohesive soils, they can be found in Appendix A. For non-cohesive soils, the following figure is used to estimate the bearing capacity, with input parameters of the fixed length and a known soil type and condition.

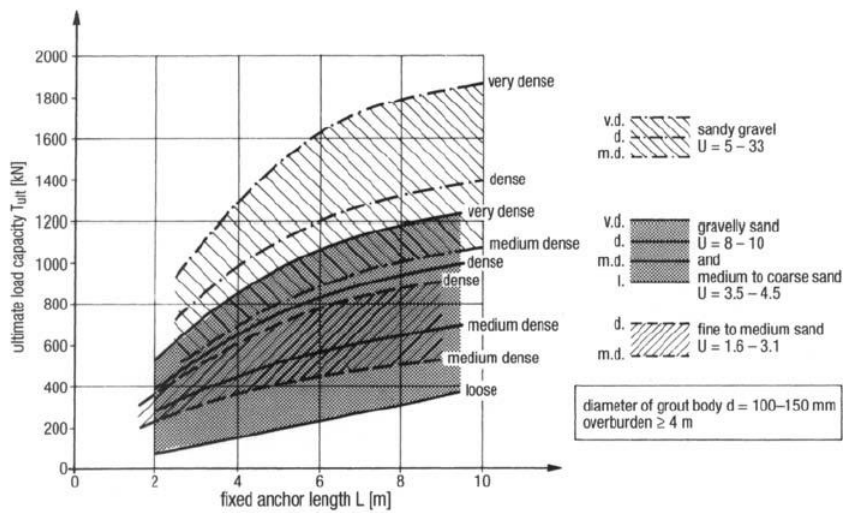


Figure 3.4: Ultimate bearing capacity for non-cohesive soils

It can be concluded that the Ostermayer method is an empirical method based on anchor test data. The diagrams provide a quick indication on how much bearing capacity could be mobilized. Although the general application is straight forward and a proven concept, it is difficult to utilize this method for the purpose of Bayesian updating, without trying to reverse-engineer the necessary factors for each different soil type to generate the input necessary to derive an independent mechanical model.

3.2.2 CUR166 Method

The CUR Method has its origins closer to the pile capacity calculation procedure. For this semi-empirical approach, the anchor dimension and the average cone resistance in the soil around the grout body are needed as an input parameter. The equation below gives the geotechnical bearing capacity.

$$\begin{aligned} R_{a,min} &= O \cdot L_A \cdot \alpha_t \cdot q_{c,avg} \\ R_{a,min} &= \pi \cdot d \cdot L_A \cdot \tau_{mob} \end{aligned} \quad (3.7)$$

With, $\alpha_t = 0.015$ as a suggested value, O being the circumference of the grout body, L_A being the fixed grout body length, and $q_{c,avg}$ being the average cone resistance around the grout body [8].

The 'shaft friction factor' α_t is an empirical value, which indicates how much of the theoretical resistance available from the soil can be mobilized along the structure's interface. Multiplied with the cone resistance, it quantifies the mobilized friction along the shaft of the grout body τ_{mob} . This illustrates that α_t can be also derived from tests, since it is the mobilized friction divided by the cone resistance:

$$\alpha_t = \frac{\tau_{mob}}{q_{c,avg}} \quad (3.8)$$

This method is only applied in non-cohesive soils, with the cone resistance being the only parameter related to the soil strength. For sands specifically, Table 7.2 in [8] provides the value $f_{k,rep}$ [kN/m], dependent on the cone resistance, which eliminates the need for an estimation of the circumference of the grout body.

For cohesive soils, [8] provides an estimation for the resistance, but it is only applicable for 'screw-in'-type anchors and therefore not further discussed.

In [17] the decreasing efficiency of the anchors with increasing length is one of the main components of the design equations. The tendency, that the forcing cannot be increased linearly with larger dimensions, as equation 3.7 suggests, can be observed in the graphs presented previously, Fig. 3.4 and Fig. 3.3. However, the CUR method does not suggest that a similar phenomenon applies. The resistance calculated with equation 3.7 could continuously increase with the anchor dimensions. The contribution made by the soil strength to the bearing capacity formulation is limited to an average cone resistance of 17.5 MPa [8].

3.2.3 Analytical creep model

This model was recently presented in [14] and is able to capture the force change in the anchor over time as well as the creep strains and displacements. The calculation of a limit force as with the previous methods is not directly possible. The basis is the Burger mechanical model, supported by the Borowicka hypothesis of settlement and movement generated by a force in an elastic semi-space and the Mindlin equations. The authors recommend deriving the belonging soil parameters from laboratory tests and transferring them into time dependent quantities.

Model description

In the following figure, all displacement components are shown.

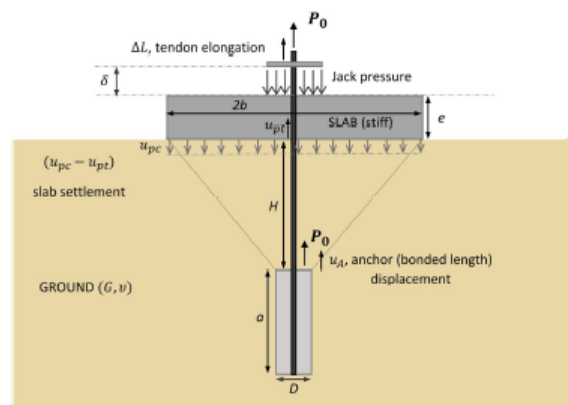


Figure 3.5: Model components

The governing components of the model are thus the following:

- Tendon elongation, L_{Δ}
- Ground compression displacement from the anchored structure, u_{pc}
- Lift of the anchored structure due to the displacement of the grout body, u_{pt}
- Anchor fixed length displacement, u_A

Therefore, there are two mechanical systems that are working against each other, by producing displacements in opposite directions: The displacements that are resulting directly from the force acting on the anchor, in the same direction, u_A and L_{Δ} and the displacements resulting from the pressure of the jack action on the anchored structure, in Fig. 3.5 a slab [14].

The total displacement δ is thus computed in the following way.

$$\delta = \Delta L + u_A + (u_{pc} - u_{pt}) \quad (3.9)$$

The following describes how each of these components are derived:

For linear elastic behavior of the tendon, the relationship in eq. 3.10 holds.

$$\Delta L = \frac{L}{EA} \cdot P_0 \quad (3.10)$$

For the ground compression, the Borowicka solution of settlement is applied. The theoretical model is shown in Fig. 3.6 below.

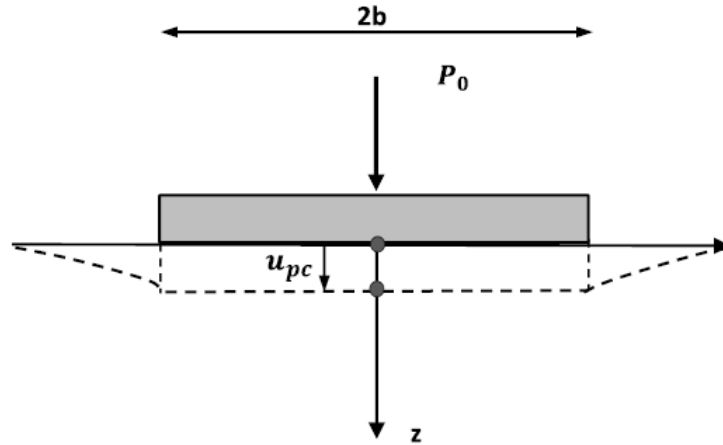


Figure 3.6: Scheme of Borowicka model for u_{pc}

The displacement component is calculated with the following equation.

$$u_{pc} = \frac{1 - \nu}{(1 + \nu)G} \frac{P_0}{4b} \quad (3.11)$$

For the u_{pt} component, the lift of the anchored structure due to the anchor force from the fixed length, the Mindlin surface equations for an elastic ground are applied. The theoretical scheme and the general form of the equation is presented in the following.

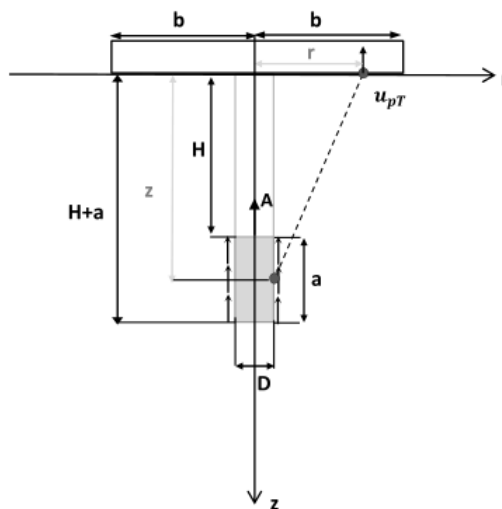


Figure 3.7: Scheme of Mindlin model for u_{pt}

$$u_{pt} = P_0 \left(\frac{1 - \nu}{\pi a b^2 G} \int_H^{H+a} \frac{\tau(z) \phi_{31}(z)}{\beta} dz + \frac{1}{2\pi a b^2 G} \int_H^{H+a} \frac{\tau(z) \phi_{32}(z)}{\beta} dz \right) \quad (3.12)$$

$$R_2 = \sqrt{(z + H)^2 + r^2}$$

$$M = 2Hz(z + H)^2$$

$$K = (3 - 4\nu)(z + H)^2 - 2Hz$$

$$B = 3 - 4\nu$$

$$C = 5 - 12\nu + 8\nu^2$$

These displacements are then related to the stiffness of each component.

$$P_0 = u \cdot k$$

$$k = \frac{P_0}{u}$$

This principle is applied to all components to derive the general system stiffness k_s .

$$k_s = \frac{1}{\frac{1}{k_L} + \frac{1}{k_{pc}} - \frac{1}{k_{pt}} + \frac{1}{k_A}} \quad (3.19)$$

From this, the instantaneous system's displacement can then be derived.

$$\delta = \frac{P_0}{k_s} \quad (3.20)$$

However, one of the key aspects of this model is the capability of dealing with time dependent parameters, to model the system's creep characteristics. The loading is considered constant, thus the stiffness of the model varies with time as well. This incorporation is straight forward for the stiffness components, which were derived above, as they are only dependent on the shear modulus G , and the Poisson's ratio ν . Considering the Burgers mechanical model, they can be expressed as described in the following way.

The Burger Model is a rheological model that is used to model the time dependent components of the calculated displacements. It consists of two viscosity parameters represented by dash-pods and two shear modulus parameters represented by springs. The Maxwell components are set 'in row' while the Kelvin-Voigt parameters are set 'parallel'.

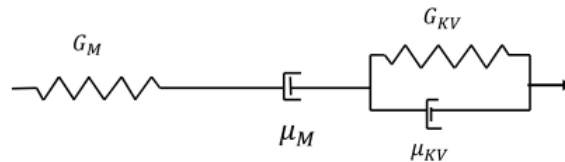


Figure 3.9: Scheme of Burger model for calculation of time dependent displacements

The main parameters of the soil, regarded as a linear elastic medium, are the shear modulus and the Poisson's ratio. The Burger model adds time dependency to calculate the time dependent shear modulus and Poisson's ratio, defined in Eq. 3.21 and Eq. 3.22.

$$G(t) = \frac{1}{\frac{1}{G_M} + \frac{t}{\mu_M} + \frac{1 - \exp\left(-\frac{tG_{KV}}{\mu_{KV}}\right)}{G_{KV}}} \quad (3.21)$$

$$\nu(t) = \frac{3K - 2G(t)}{2(3K + G(t))} \quad (3.22)$$

This strain-time expression, under constant load, is the result of Laplace inverse transformation. These two time dependent quantities can now be substituted for the instantaneous components in the expressions regarding the component's stiffness.

Since ground creep occurs delayed from the initial pre-stressing, the resulting elongation of the tendon gets slowly recovered over time, which results in a decreasing load in the anchor itself. Therefore, the following algorithm must be considered when it comes to the implementation to account for the compatibility between wall head deformation and deformation from the anchor at each time step [14].

Time Algorithm:

- instantaneous displacement δ_0 is calculated, Eq. 3.20
- elastic time dependent soil parameters for the next time step are calculated, Eq. 3.21 and Eq. 3.22
- change in displacement δ from previous to current time step is computed:

$$\Delta\delta_1 = \delta_1 - \delta_0$$

- The change in load ΔP between time steps is computed:

$$\Delta P_1 = \frac{\Delta\delta_1}{\frac{1}{k_{str}} + \frac{1}{k_L}} \text{ with the wall stiffness according to Blum: } k_{str} = \frac{3E_{str}I_{str}}{L_T^3}; s = \frac{H_L}{\sqrt{K_p/K_a - 1}}; L_T = H_L + s$$

- then the actual change in displacements Δu_1 between time steps is calculated:

$$\Delta u_1 = \Delta\delta_1 - \Delta L_1; \text{ with } L_1 = \frac{\Delta P_1}{k_L}$$

This formulation now depicts the first time step. The following shows the general form.

$$\begin{aligned} \Delta\delta_i &= \delta_i - \delta_{i-1} \\ \Delta P_i &= \frac{\Delta\delta_i}{\frac{1}{k_{str}} + \frac{1}{k_L}} \\ \Delta u_i &= \Delta\delta_i - \Delta L_i \end{aligned} \quad (3.23)$$

Summary:

The model utilizes three different analytical solutions and sums up their contribution to calculate a displacement of the anchor head. This can be achieved with just the Poisson's ratio and the shear modulus as input soil parameters for the instantaneous displacement. Then, the procedure above is applied and combines the time dependent Burger model with single displacement components to calculate the anchor's behavior over time. To capture time dependency, more soil parameters are necessary.

The model above is according to the authors capable of modelling creep of anchors and was verified numerically and applied in a practical case for a piled wall in Scotland within Strahov Claystone. However, the authors do not mention the validity for different soil types or specific strain ranges.

3.2.4 Numerical Methods

The use of numerical methods for anchor modelling are increasing. They are a common technique in practical applications. In [28] anchor failure in cohesive soils is investigated, using advanced constitutive models to capture the behavior of the grout anchors. These were for example the Hardening soil model (HS) due to its versatile fields of application, with decent computation times, or the Shotcrete model (SC), which was developed initially for tunnel-lining applications. It is capable of capturing cracking within cemented materials, which makes it suitable to model the anchor grout body. The main focus was set on the application of the Multilaminate soil model (MLSM). This advanced model is capable of capturing small strain stiffness and complex hardening and softening phenomena in heavily overconsolidated soils. [28]. Due to the computational intensity of numerical models, their suitability for Bayesian updating techniques, where thousands of model evaluations are performed, is limited. Therefore, numerical anchor modelling is not further investigated. An opportunity to overcome this limitation is by surrogate modelling. There, a surrogate model is employed that is able to capture the behavior of the numerical model but with a fraction of the calculation time at the expense of accuracy. However, within this research, no surrogate modelling approach was undertaken.

3.3. Anchor Testing

The following deals with the different kind of anchor tests and what kind of information can be obtained from conducting them. This is relevant since the upcoming case studies are based on anchor test data, thus, an in-depth understanding of the fundamentals is crucial.

3.3.1 Test procedures

There are three main procedures common within Europe, corresponding to the main practice in Germany, the UK and France. The procedures differ in how long the load is held at each step, if the load is reset to the pre-stressing after each step, and what parameters are measured once each load step is reached. It should be noted that these procedures are mainly relevant for the comparison of suitability testing methods [11]. Specifications to the measurements, the devices and the presentation of the results are regulated in EN-ISO-22477-5 [7].

The first method is the common method for anchor testing for German and Dutch practice. Here, the load is applied in cyclic increments of its working load, while for each cycle the displacement of the anchor head is measured at the peak load of each cycle.

For the second method, the load is applied in cyclic increments of its working load as well. At the peak of each cycle, the loss of load at the anchor head is measured over time.

For the third method, the anchor is loaded step-wise in increments of the anchor's working load. At the peak of each step, the load is held for a specific time interval, where the displacement at the anchorage point is measured.

The following descriptions of investigation and suitability tests refer to this first test method. For acceptance tests, the first and the third method are applicable.

Investigation Tests

Investigation tests or failure tests are normally carried out on sites where the ground conditions and the corresponding bearing behavior is uncertain and thus, more information is necessary. This is mostly due to limited experience with the soil type or due to uniquely high loading conditions.

The maximum bearing capacity for which the test is set up is calculated according to the CUR-method (Equation 3.7), and multiplied with the factor of 1.5¹. This limit load should not exceed 90 % of the design resistance of the steel rod [8]. The test usually stops as soon as the creep value (displacement over time) reaches 2 mm and/or when the load reaches the 150 % limit [20]. The creep value is explained in more detail in 3.3.2.

The cycles and the common holding times are depicted in the following figure. P denotes the anchor load, while P_{max} is the maximum expected bearing capacity.

¹This is valid for the Dutch practice with the CUR 166 method. Depending on the inherent safety factors of the working load, the maximum bearing capacity can be estimated in the same way with other procedures for calculating the working load. This is supposed to be a rough approach for reverse engineering.

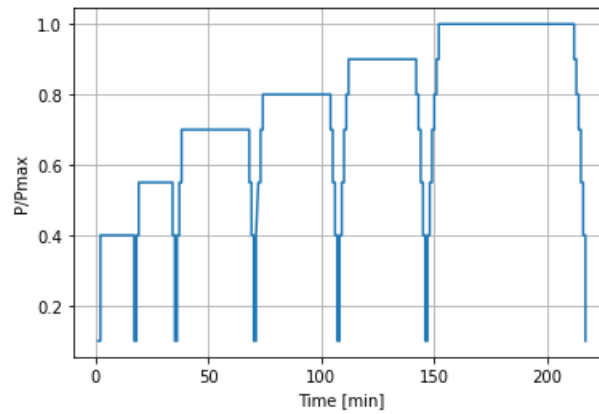


Figure 3.10: Procedure Investigation Tests

The time period during which the load is hold at each loading increment continuously increases as the increment gets closer to 100 % loading. Investigation tests should give insight about the maximum bearing capacity, sufficient free anchor length, verify sufficient capacity under the anticipated working load, and give insight about the creep characteristics [11].

Suitability Tests

Suitability tests are similar to investigation tests, but their loading does not reach failure level, but just the working load. Furthermore, they typically need to be carried out at $\approx 5\%$ of all the anchors on the site, with a minimum of 3 per site. There are only five cycles compared to the six cycles in investigation tests, with a 15 % load increase with each step.

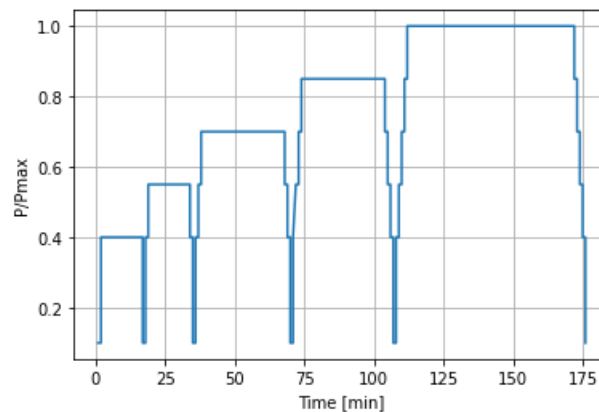


Figure 3.11: Procedure Suitability Tests

Suitability test give insight about similar characteristics of the system as investigation tests, however their loading level equals their anticipated working load, instead of exceeding it by the factor of 1.5 as for the previously discussed investigation tests. This means that the informative value is of the data is closer related to the conditions used on site. Thus, suitability tests should verify the capacity for the working load, sufficient free anchor length and give insight about the creep characteristics. [20], [8].

Acceptance Tests

Acceptance Tests need to be carried out on every anchor that is installed, apart from those that are tested within the suitability test framework. The test is shorter and also yields less informative value, especially

concerning the creep characteristics.

The following figure shows the procedure of this kind of test. The full working load is held only for 5 minutes, with the whole test being finished within 11 minutes. During an acceptance test, the loads are generally applied in a non-cyclic, progressive fashion.

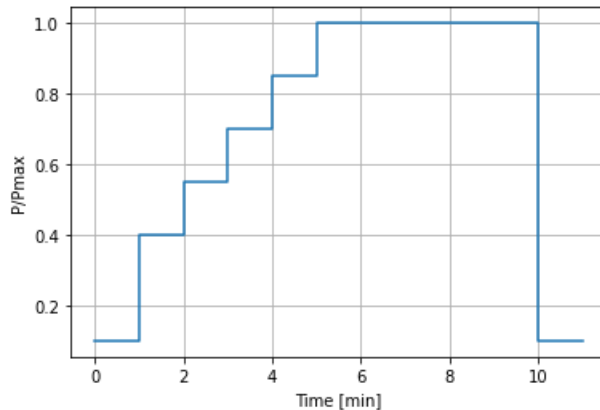


Figure 3.12: Procedure Acceptance Tests

Thus, an acceptance test should verify that each anchor is able to sustain the working load and that the apparent free length is within its limits [11].

3.3.2 Creep Value

The creep value is a measurement of the displacement of the rod over time under constant loading. It can be derived from the anchor test data.

$$k_s = \frac{\Delta s}{\Delta \log(t)} \tag{3.24}$$

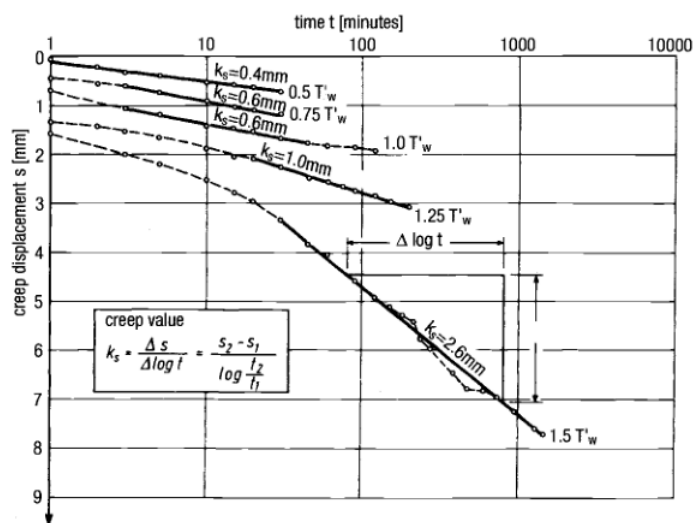


Figure 3.13: Creep value definition [17]

The creep value is displacement over time. The European guidelines are uniform and define the anchor’s failure limit once a creep value of 2.0 mm is reached [8], not considering the steel strength for this investigation. The exact time frame of evaluation is dependent on the type of test. For acceptance tests the time frame is

$t_1 = 2 \text{ min}$ and $t_2 = 5 \text{ min}$, for suitability and investigation test, for 15 min long loading, $t_1 = 7 \text{ min}$ and $t_2 = 15 \text{ min}$, for 30 min long loading $t_1 = 20 \text{ min}$ and $t_2 = 30 \text{ min}$, and for 60 min long loading $t_1 = 30 \text{ min}$ and $t_2 = 60 \text{ min}$ [8], [7]. These time frames are common for non-cohesive soils. For cohesive soils, the loading cycles tend to be longer, because creep is expected to be larger.

At this point it is mentioned that there is a knowledge gap around this particular limit since it is set at 2.0 mm independent of the site, soil, stress level or other influences. In this research however, the creep value limit is not the main focus of investigation.

3.3.3 Apparent free length

The apparent free length is a value that is calculated using the following equation.

$$L_{app} = \frac{\Delta s \cdot EA}{\Delta P} \quad (3.25)$$

The variable ΔP [kN] denotes the difference between full load and pre-stressing or lock-off load. The lock-off load is usually 10 % of the full load, since it is the point where the measurements start and where they end. The difference in displacement Δs [m] is being computed at said loading points, where the 10 % increment is basically the last measurement of the test, after reaching 100 % in the previous loading step, that represents the full plastic deformation of the system. The stiffness EA [kN] denotes the stiffness of the steel rod.

Equation 3.25 tries to capture the theoretical free length of the anchor by subtracting the total displacement from the elastic displacement. The idea is to prove that the actual free length is not too different from the apparent free length, to show that the rod along the free part of the anchor does not develop an inadmissible amount of friction. Especially in the back calculation of the α_t value, an odd, non-linear distribution of the stresses is distorting the results, since the assumption of uniform stress distribution and the one of no friction along the shaft does not hold anymore. However, this friction is a part that usually adds further capacity and robustness to the system, which is why it is often not regarded within the design process. This is mainly due to the fact that an accurate quantification method is lacking.

3.3.4 Test Limits

There are two limit criteria to the results of the measurements of the anchors. The first one is that the creep value within one loading step does not exceed a certain limit, and the second one is that the apparent free length L_{app} does not exceed the set limits.

For the investigation tests, the creep value is limited to 2.0 mm for a specific time frame which is mentioned in 3.3.2. Since the time frames are set and do not change, the creep value limit can also be translated into a maximum allowable net displacement within said time frame. For an investigation test, this would for example be $\approx 0.60 \text{ mm}$ within 30 min and 60 min.

For suitability tests and acceptance tests, the limit creep value is 1 mm [8]. For investigation tests, where the loading is 150 % of the working load, the limit of the creep value is set to be 2 mm [8]. There is limited knowledge regarding the origin of the creep limit. In [15] it is recommended to set the limit for 150 % at 1 mm as well, because then, for the time interval between 30 min and 50 years, the additional displacement would be 6 mm. Why exactly 6 mm would make a good limit is not specified. However, usually the guidelines have the 1 mm and 2 mm creep limit specified.

The limits of the apparent free length are precisely defined within [11]. For bond anchors the upper limit

$L_{app} = L_{tf} + L_e + 0.5 \cdot L_{tb}$, where L_{tf} denotes the tendon free length, L_{tb} is the tendon bond length and L_e is the length between the anchor head and the measurement point in the stressing jack. The lower limit is given as $L_{app} = 0.8 \cdot L_{tf} + L_e$.

3.4. Bayesian Updating Methods

3.4.1 Bayes Theorem

The main idea of Bayesian updating originates from Bayes Theorem. The standard formulation can be expressed as shown in Eq. 3.26.

$$P[A|B] = \frac{P[A \text{ and } B]}{P[B]} = \frac{P[A]P[B|A]}{P[A]P[B|A] + P[\bar{A}]P[B|\bar{A}]} \quad (3.26)$$

In this notation, A and B denote two separate events [1].

Another way of expressing Bayes theorem in a more specific way is shown in the following equation [3].

$$\theta = \text{random variables}; \quad D = \text{Data}; \quad M = \text{Model assumption} \quad (3.27)$$

$$P[\theta|D, M] = P_D(\theta) = \frac{P[D|\theta, M] \cdot P_0[\theta|M]}{P[D|M]}$$

Equation 3.27 consists of several components. $P[\theta|D, M] = P_D[\theta]$ is the updated, or posterior distribution. It denotes the probability of a single or a set of parameters given a data set. The term $P_0[\theta|M]$ is the prior distribution, which is an estimate of what the updated distribution could look like. This does not necessarily need to be a close approximation, a uniform distribution with parametric limits can be sufficient, depending on the problem. The term $P_D[D|\theta, M]$ gives the probability of obtaining the data or measurements D , based on a specific model M for a certain set of parameters θ . These two terms in the numerator in equation 3.27 are the main input that is necessary for the solution of the equation. The denominator $P[D|M]$ is a normalizing constant that can be expressed as follows.

$$P[D|M] = \int P[D|\theta, M] \cdot P_0[\theta|M] \quad d\theta \quad (3.28)$$

The normalizing constant is often called c .

$$c^{-1} = \int P[D|\theta, M] \cdot P_0[\theta|M] \quad d\theta \quad (3.29)$$

Thus, equation 3.27 is becoming the following expression, now with an implicit M for model assumption.

$$P_D[\theta] = \frac{P[D|\theta] \cdot P_0[\theta]}{P[D]} \quad (3.30)$$

$$P_D[\theta] = \frac{P[D|\theta] \cdot P_0[\theta]}{\int P[D|\theta] \cdot P_0[\theta]}$$

$$P_D[\theta] = c^{-1} \cdot P[D|\theta] \cdot P_0[\theta]$$

Now, the probability $P[D|\theta]$ can be regarded as the likelihood function of θ for a given set of data: $P[D|\theta] = L[\theta|D]$. Therefore, the baseline of a Bayesian updating algorithm evolves around the solution of the following

term or a similar version of it [4] [3].

$$P[\theta|D] = c^{-1} \cdot L[\theta|D] \cdot P_0[\theta] \quad (3.31)$$

In the following, two different but related procedures are presented in their theory.

3.4.2 aBUS - Theory:

This Bayesian inference method translates the Bayesian equation into a structural reliability problem. The authors describe this 'Bayesian Updating with structural reliability methods' - BUS, as an extension of rejection sampling. The procedure is described in [4] and explained below.

From Bayes theorem, one ends up with the equation 3.31, which is repeated here again for completion.

$$P[\theta|D] = c_E^{-1} \cdot L[\theta|D] \cdot P_0[\theta] \quad (3.32)$$

Again, $P[\theta|D]$ denotes the posterior or updated distribution, $L[\theta|D]$ is the likelihood function, $P_0[\theta]$ is the prior distribution.

The c_E -constant is often referred to as either, 'evidence', 'marginal likelihood' or 'integrated likelihood' and can be expressed like in 3.29. The evaluation of this multidimensional integral is difficult.

In the original BUS-method, [23], [24] the evaluation of a different c-constant was necessary as an input parameter for the algorithm. This c-constant has to normalize the calculation, and it should be chosen to be larger than or equal to the maximum of the likelihood function.

For the original BUS, different methods were proposed and depending on the problem a suitable method could be chosen for evaluating c . The c-constant must always be larger than the maximum of the likelihood function. However, the larger the c-constant is, and the further it overshoots, the smaller the efficiency of the algorithm since more proposed samples get rejected. Within the adapted method, 'aBUS', the algorithm functions in a way that the c-constant is not required as an input parameter anymore.

The idea of interpreting the Bayesian equation as a structural reliability problem yields that the Bayesian problem becomes a 'rare event estimation' [4]. This means that structural reliability methods are used to evaluate the equation. To do so, an additional random variable, that is uniformly distributed, is employed to formulate a limit state function for the artificial failure domain Ω .

$$\Omega = [\pi \leq c \cdot L[\theta|D]] \quad (3.33)$$

With the limit state function g :

$$g[\pi, \theta] = \pi - c \cdot L[\theta|D] \quad (3.34)$$

For numerical optimization, the limit state function is described in logarithmic form.

$$g_1[\theta, \pi] = \ln(\pi) - \ln(c \cdot L[\theta, D]) \quad (3.35)$$

Thus, the artificial failure domain is defined in a way that once the limit state function of a sample is smaller equal to zero within Ω and outside for values larger than zero. This is illustrated in figure 3.14.

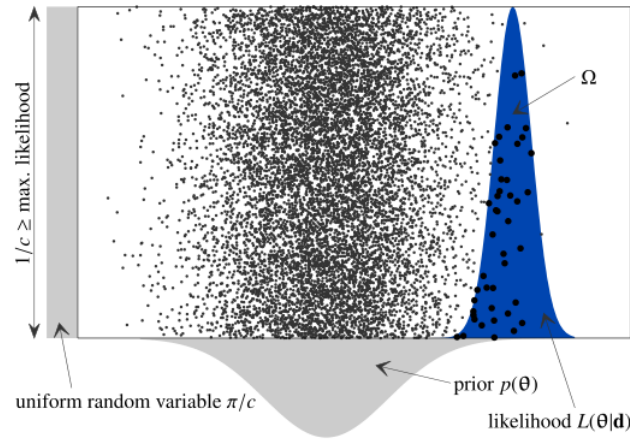


Figure 3.14: Illustration of the artificial failure domain [4]

Ideally, the inverse normalizing constant is chosen to the maximum of the likelihood function. Then, the condition $c \cdot L[\theta|D] \leq 1$ always holds.

3.4.3 Subset Simulation - Theory:

The concept of Subset simulation is an advanced version of the Monte Carlo method [18]. This can be illustrated by discussing the evolution of the algorithms and their way of functioning. The original BUS method, utilizes a standard rejection sampling algorithm. There, a sample of the prior distribution of the random variables θ and a sample of the limit-state function in Eq. 3.34 is initially generated. The parameter π in Eq. 3.34 is uniformly distributed and has 0 and 1 as its limits. If both samples get accepted, which means that the limit state function 3.34 evaluated for these samples is smaller or equal to 0, the samples are appended to the posterior distribution. This is done, until the counters that specify the amount of posterior samples anticipated to be generated reach the limit (K). There are two counters within this algorithm. One counts the total amount of samples proposed (n) and one counts the amount of samples accepted (k). The loop is executed and generates samples until the counter k reaches the specified limit K . The counter n gives insight about the probability of failure p_Ω of the inherent structural reliability problem: $p_\Omega \approx \frac{K-1}{n-1}$. This probability of failure is the probability that the generated samples fall into the artificial failure domain Ω . It is used to calculate the evidence c_E : $c_E = p_\Omega \cdot c^{-1}$. [4]

The principle of the subset simulation is similar, but with several subsets introduced. For common rejection sampling, the limit state function draws the boundaries, to decide if a sample is accepted or not. For subset simulation, the main idea is to introduce intermediate failure events, describing intermediate failure domains, which all depend on the initial limit state function. The main motivation for Subset sampling is to increase efficiency for higher dimensional problems with low probabilities of failure.

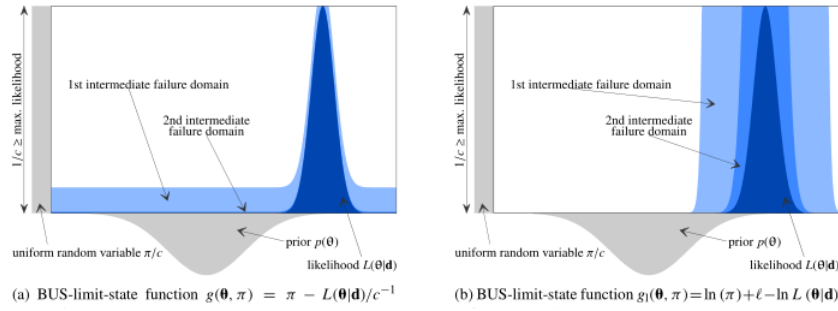


Figure 3.15: Failure domain with nested, intermediate domains [4]

The total domain Ω is composed of m intermediately, nested domains Z_i . The intermediate failure events are defined as $g[\theta, \pi] \leq h_i$. The constant h_i is a threshold level, that decreases to zero for each level of convergence. To calculate the threshold level, first, the limit state function is evaluated for all posterior samples of the initial step and then sorted in ascending order $S_{po,s}^K$ ². Then, h_i is calculated as the specific percentile of the sorted, generated posterior set, $S_{po,s}^K$. This percentile is one of the input parameters of the algorithm, p_t , which gives the probability of the intermediate subsets (usually set around 10 %). Once h_i is established, n is introduced, which gives the number of the sorted, generated samples that once evaluated for the limit state function are smaller than h_i , $S_{po,s,g < h}^n$. This is only necessary once the threshold h_i becomes smaller than zero. Then, p_t becomes $p_i = n/K$.

After the calculation of the threshold, the samples in the intermediate failure domain Z_i are generated. For this, the Markov Chain Monte Carlo simulation method is adapted. First, the samples generated above, $S_{po,s,g < h}^n$, are randomized in their order to generate $S_{po,r,g < h}^n$. Then Markov chains are used to generate the intermediate samples, where the samples $S_{po,r,g < h}^n$ are used as seeds, since they are already laying within the intermediate domain. The length of the chains is given as, K/n and the number of Markov Chain Monte Carlo samples is $K - n$. The total probability of failure is then given by the product of p_i , $p_\Omega = \prod p_{i=1}^m$. The evidence is calculated in the same way as previously presented. [4]

3.4.4 Markov Chain Monte Carlo (MCMC) simulation

Within the aBUS-SuS algorithm, Markov Chain Monte Carlo (MCMC) simulation is applied. MCMC is a class of algorithms that are used for sampling from distributions, with the most common method being the Metropolis-Hastings algorithm. In [18], different existing approaches and methods are discussed, and a new approach is introduced.

MCMC is a combination of two statistical concepts, Markov chains and Monte Carlo simulation. Markov chains, or Markov processes, are sequences in which the probability of the next state only depends on the current state and not on any previous states. There exist different methods, but they mainly differ from one another in the way how the Markov chain is constructed. MCMC simulation is mainly used to evaluate structural reliability problems with small probabilities of failure but before entering the algorithms, the random variables are transformed into standard normal random variables by performing the Rosenblatt transformation. Thereby, the parameters are mapped one-to-one, as $U = T(\theta)$. This means that the initial reliability problem is changing in the following way.

$$P_f = \int_{g(\theta) \leq 0} f_\theta(\theta) d\theta \quad (3.36)$$

$$P_f = \int_{G(u) \leq 0} \phi_n(u) du$$

²Indices: po ... posterior; s ... sorted; r ... random; i ... threshold level counter;

With, $\phi_n(u) = \prod_{i=1}^n \phi(u_i)$ as the standard normal pdf and $G(u) = g(T^{-1}(u))$ as the limit state function in standard normal space. These integrals (3.36) denote the baseline for all reliability analyses. In civil engineering, one of the more common ways of solving these, is by applying the Taylor series approximations of the limit-state surface, called FORM or SORM, depending on the order of the Taylor series. Problems of higher order (more random variables) or strongly non-linear limit-state functions can lead to severe errors [18]. Another simple approach is to perform standard Monte Carlo simulation, due to its robustness. However, the computational demand is rather large when it comes to sampling small failure probabilities. Thus, many approaches try to preserve the robustness of Monte Carlo while increasing its efficiency, like Subset sampling. [18]

Original Metropolis-Hastings algorithm according to [18]

The variable $\phi_n(u|Z_j)$ denotes the distribution that is being sampled for. u represents θ , the random variable in transformed normal space. Z_j represents an intermediate failure domain of a subset in standard normal space.

The Markov chain is anticipated to become stationary at some point of the process. Once the Markov chain becomes stationary, the following samples will follow the posterior distribution. The following equations illustrate these properties.

$$Pr(U_{n+1} \in A | \cap_{t \leq n} U_t = u_t) = Pr(U_{n+1} \in A | U_n = u_n) \quad (3.37)$$

Within this notation, U_t describes a stationary discrete-time vector process, where A represents any event of its outcome space. $p(v|u)$ denotes the transitional density of U_n progressing to U_{n+1} with v being the candidate sample. Thus, equation 3.37 expresses two major characteristics. First, the equation's right side implies the main characteristic of a Markov chain, that the next state U_{n+1} is only dependent on the current state U_n . This means, if the sample gets accepted, the state U_{n+1} becomes v . The second characteristic is that the equation as a whole describes the conditions set for the chain to become stationary. The transition pdf has to satisfy the following condition.

$$\phi_n(v|F_j) = \int_{u \in R^n} p(v|u) \phi_n(u|F_j) du \quad (3.38)$$

Furthermore, inherent to the Markov chain, the reversibility condition needs to be fulfilled.

$$p(v|u) \phi_n(u|F_j) = p(u|v) \phi_n(v|F_j) \quad (3.39)$$

Usually, for general application of the Metropolis-Hastings algorithm, a certain burn-in period is required until the Markov chain reaches its steady-state and most of the follow-up samples will be accepted, since they share the same distribution as the posterior. However, for Subset sampling, this burn-in period is not necessary. When sampling for the first and broadest intermediate failure domain at $j = 0$, crude Monte-Carlo is applied until the boundaries for the conditional probability are satisfied. For the next step at $j + 1$, the samples of the previous subset are used as the seeds or starting points of the Markov chains and by definition they already lie in the posterior domain. Therefore, the Markov chain is from the start on stationary and all samples lie within the posterior. The transition pdf can be expressed as follows.

$$p(v|u) = a(u, v)q(v|u) + (1 - r(u))\delta_u(v) \quad (3.40)$$

With $q(v|u)$ as the proposal pdf, $\delta_u(v)$ as the Dirac mass at u and $a(u, v)$ as the probability to go from one

state to the next in the Markov chain, i.e. the acceptance probability.

$$\begin{aligned} a(u, v) &= \min\left(1, \frac{\phi_n(v|F_j)q(u|v)}{\phi_n(u|F_j)q(v|u)}\right) I_{F_j}(v) \\ a(u, v) &= \tilde{a}(u, v) I_{F_j} \end{aligned} \quad (3.41)$$

The indicator function I_{F_j} becomes 1 since the Markov chain starts already at its stationary state. The variable r_u can be expressed as,

$$r(u) = \int_{v \in R^n} a(u, v) q(v|u) dv \quad (3.42)$$

and the value of $1 - r(u)$ is basically the probability of the Markov chain to remain at the current state.

The Metropolis-Hastings algorithm is a two-step procedure. The first step is to generate a sample v from $\phi_n(\cdot)$, the second step is to either accept or reject v . This implies a pre-candidate state, a sample that first needs to pass the acceptance criteria of the Markov chain before it can be accepted or rejected based on its location within the nested failure domains F_j . In the appendix, a detailed illustration of the algorithm can be found.

Adaptive MCMC with optimal scaling according to [18]

The procedure proposed in [4], for the 'aBUS-SuS' method, utilizes an adapted version of the Metropolis-Hastings algorithm. The motivation for this is to eliminate some of the weaknesses that the original Metropolis-Hastings (MH) algorithm bears. One of the main issues of MCMC-MH is that the mean acceptance rate of a sample with independent normal distributions becomes lower than 10 % for problems with more than 8 random variables. Some procedures that increase these acceptance rates through various different methods can lead to a high correlation of the samples within the Markov chain.

One adaptation that targets the inherent acceptance rates related to the procedure of having a candidate state and a pre-candidate state is the introduction of a cross-correlation coefficient ρ_i . The main idea is that v and u_0 are normally distributed with zero means and that their cross-covariance matrix R is the identity matrix I with the correlation coefficient ρ_i as the diagonal component. This means that the candidate samples v are generated from $\phi_n(\cdot)$ with ϕ_n having the shape of a multivariate standard Gaussian distribution. For each v_i , (i is the counter of the random variables in n random variables in total), the mean and the standard deviation can be calculated as,

$$\begin{aligned} \mu_i &= \rho_i \cdot u_{0,i} \\ \sigma_i &= \sqrt{1 - \rho_i^2} \end{aligned} \quad (3.43)$$

A large ρ_i will lead to strong correlation between each state of the Markov chain, while a small ρ_i will lead to many rejected samples. The method that is proposed by the authors adjusts ρ_i during the calculation process for each subset level. The key idea is to perform the simulation stepwise.

The first step is to define an amount of Markov chains that is supposed to be considered for adaptation, N_a which is an integer fraction of the total amount of Markov chains N_s . A decent estimation is to assume $N_a = p_a \cdot N_s$, with $p_a \in [0.1, 0.2]$. Then, a starting value of the sample's standard deviation σ_{0i} is either chosen or calculated, depending on the problem. For higher dimensional problems a constant σ_{0i} is recommended, for problems where the influence of a few random variables have a large effect on the outcome the calculation procedure is recommended. Within that one, the mean and the standard deviation of i of the seeds of the

chains are computed like,

$$\begin{aligned}\hat{\mu}_i &= \frac{1}{N_s} \sum_{k=1}^{N_s} u_{ji}^{(k)} \\ \hat{\sigma}_i^2 &= \frac{1}{N_s - 1} \sum_{k=1}^{N_s} (u_{ji}^{(k)} - \hat{\mu}_i)^2\end{aligned}\tag{3.44}$$

Again, these quantities are calculated for all the samples that fell in the failure domain F_j at the previous subset j .

As a next step, N_a seeds from the previous subset are randomly selected as an input for the next subset level, here denoted as $\{u_{j-1}^{(k)} : k = 1, \dots, N_s\}$.

After this, another iteration is started, that has as its goal to calculate the correlation parameter ρ_i and finally sample from $\phi_n(u|F_j)$. The counter is named *iter* and ranges from 1 to $\frac{N_s}{N_a}$. For this process, the variable λ_{iter} is introduced, which is necessary to calculate the correlation parameter ρ_i .

$$\begin{aligned}\sigma_i &= \min(\lambda_{iter} \cdot \sigma_{0i}, 1) \\ \rho_i &= \sqrt{1 - \sigma_i^2} \\ \hat{a}_{iter} &= \frac{1}{N_a} \sum_{k=1}^{N_a} \hat{E}_\zeta[a(u_j^{(k)})] \\ \log(\lambda_{iter+1}) &= \log(\lambda_{iter}) + \zeta_{iter}[\hat{a}_{iter} - a^*]\end{aligned}\tag{3.45}$$

Within this step, first the correlation parameter ρ_i is calculated. Next, for $k = (iter - 1)/N_a + 1, \dots, iter \cdot N_a$, starting from $u_j^{(k-1)/p_0+1}$ a Markov chain is generated, that has $1/p_0 - 1$ states, that has its stationary pdf as $\phi_n(u|F_j)$. It is described as $\{u_j^{((k-1)/p_0+t)} : t = 2, \dots, 1/p_0\}$. The evaluation is done, applying the conditional sampling algorithm presented above.

After that the average acceptance rate \hat{a}_{iter} is calculated for the N_a chains and for the next subset the new scaling parameter λ_{iter+1} is calculated. Another explanation is found in the appendix, or can be directly obtained from the source, [18].

Final aBUS-SuS according to [4]

With these tools, the final 'aBUS-SuS' algorithm can be elaborated. As an input, the prior distribution, the likelihood function, the total number of samples K and the probability of intermediate subsets p_t are necessary.

1. Sampling K samples from $[\theta_{0,k}, \pi_{0,k}]$ from the prior distribution
2. Initializing the counter $i = 1$ and the threshold level $h_0 = \infty$
3. Setting ℓ as the maximum of the likelihood function, $\ell = \max(\{\ln L(\theta_{0,k}|D)\}_{k=1}^K)$
4. Loop, as long as the threshold level $h_i > 0$
 - (a) Increasing counter i by 1
 - (b) Selecting the threshold level h_i :
 - i. Sorting the samples $\{\theta_{(i-1,k)}, \pi_{(i-1,k)}\}_{k=1}^K$ regarding the value that they take in the limit state function $g_1(\theta_{(i-1,k)}, \pi_{(i-1,k)})$ in ascending order

- ii. Calculating the threshold level h_i as $h_i = \frac{g_1(\theta_{(i-1, p_t \cdot K)}, \pi_{(i-1, p_t \cdot K+1)})}{2}$ (should be always larger than 0)
 - iii. Selecting n as the amount of samples where the condition $g_1(\theta_{(i-1, k)}, \pi_{(i-1, k)}) \leq \max(h_i, 0)$ is fulfilled
 - iv. If the threshold level $h_i < 0$, h_i becomes 0, $p_i = \frac{n}{K}$ or $p_i = p_t$
- (c) Generation of conditional samples in the intermediate domain Z_i
- i. Randomization of the samples ordered in previous step, $\{[\theta_{(i-1, k)}, \pi_{(i-1, k)}]\}_{k=1}^n$
 - ii. Generation of samples $\{[\theta_{(i, k)}, \pi_{(i, k)}]\}$ using n Markov chains using adaptive conditional sampling
- (d) Updating the value of the scaling constant
- i. Setting $\ell_{new} = \max(\ell, \{\ln L(\theta_{(i, k)}|D)\}_{k=1}^K)$
 - ii. Modification of $h_i = h_i - \ell - \ell_{new}$
 - iii. Setting $\ell = \ell_{new}$
- (e) Decreasing the dependencies of the total K samples from one each other
- i. Drawing $\hat{\pi}$ as a sample of a uniform distribution with the bounds $[0, \min(1, \exp(\ln L(\theta_{i, k}|D) - \ell + h_i))]$
 - ii. Setting $[\theta_{(i, k)}, \pi_{(i, k)}]$ as $[\theta_{(i, k)}, \hat{\pi}]$
5. Setting $m = 1$
 6. Calculating $p_\Omega = \prod_{i=1}^m p_i$
 7. Calculating the evidence as $c_E = p_\Omega \cdot \exp \ell$

4. Practical elaboration

The anchor design procedures from the theoretical background are in this chapter assessed practically using the example of the 'HES Hartel Tank Terminal', HHTT-site at the port of Rotterdam. This is the same site and data basis that is used as a case study throughout this report. All forces that are calculated are characteristic forces to ensure an unbiased comparison between the methods.

4.1. Site description

The anchors were installed in a deep sea quay wall, thus, of large dimensions. For the chosen anchor, investigation and suitability test results are available. The figures below show the structure of the quay wall and the anchor

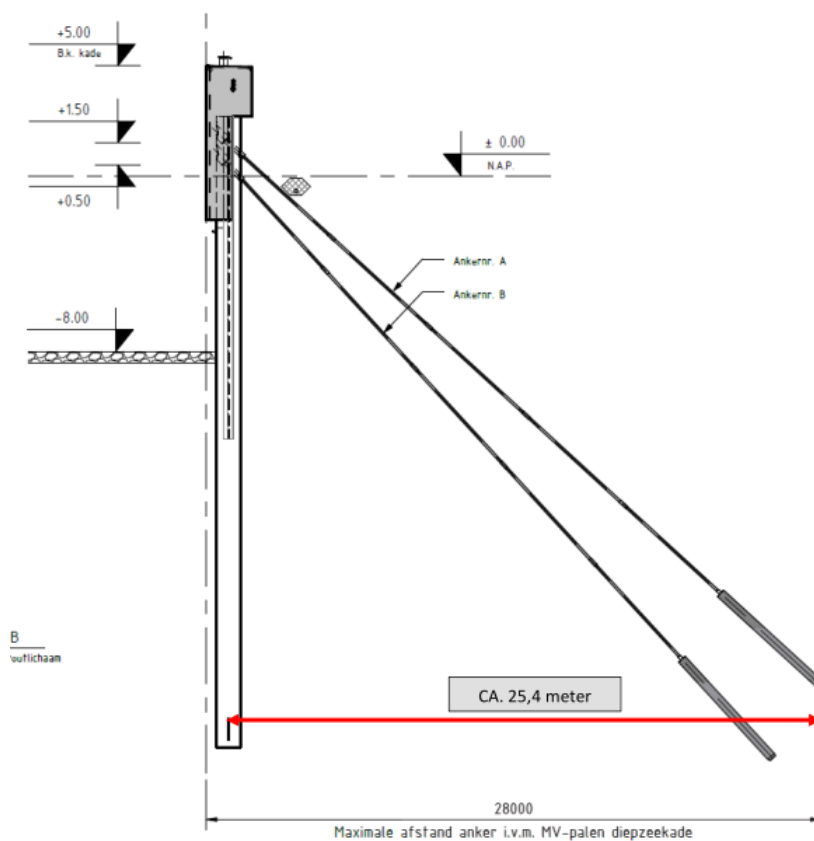


Figure 4.1: Deep sea quay structure, [22]

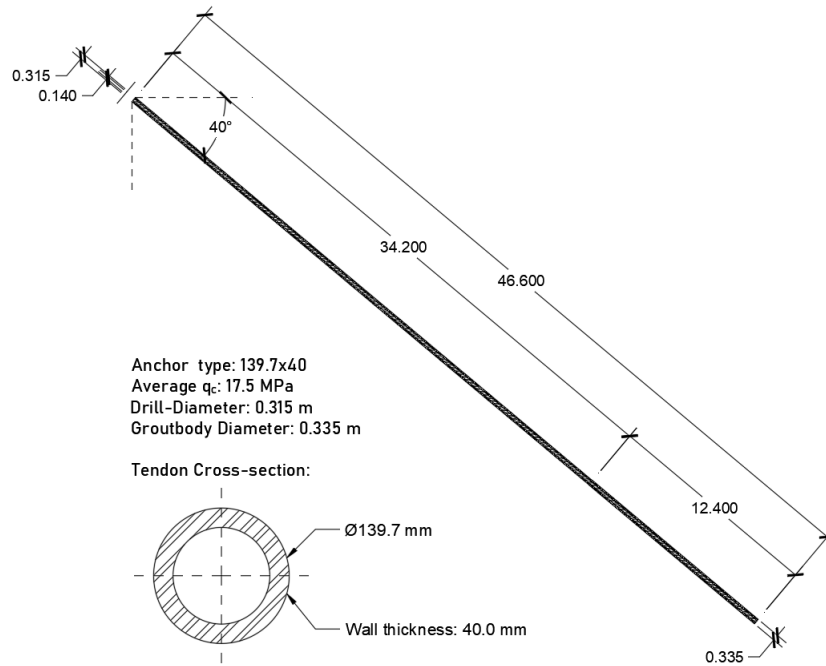


Figure 4.2: HHTT anchor

In the table below, the parameters and geometries are summarized.

| | |
|-------------------------------|-----------|
| Type wall | AZ-28-700 |
| H_{wall} [m] | 13.0 |
| L_{anchor} [m] | 46.6 |
| $L_{groutbody}$ [m] | 12.4 |
| $D_{groutbody}$ [m] | 0.335 |
| Anchor type | 139.7x40 |
| Tendon area [m ²] | 0.01253 |
| Inclination | 40° |
| $q_{c,avg}$ [MPa] | 17.5 |

Table 4.1: Model parameters, HHTT anchor

The corresponding CPT data can be found in the appendix, B.1. The average q_c value can conservatively be estimated as $q_{c,avg} = 27.5 \text{ MPa}$. However, while 20 MPa is still justifiable, the q_c value was limited to max. 17.5 MPa in the design documentation. Therefore, the following calculations make use of the cut-off value.

4.2. Ostermayer method

As described earlier, there is no design chart for CPT values, but CPT and SPT values can be empirically correlated to each other. For now, the more valuable information concerning the design charts at hand is the relative density of the soil. Assuming uniform soil conditions and a unit weight of 20 kN/m^2 , the average vertical stress on the grout body can be assumed to be approx. 310 kPa . The relative density is calculated with the Lunne & Christoffersen approach in the following equation.

$$D_r = \frac{1}{2.91} \cdot \ln \frac{q_c}{60 \cdot \sigma_v'^{0.7}}$$

$$D_r = \frac{1}{2.91} \cdot \ln \frac{17.5}{60 \cdot 310^{0.7}} \quad (4.1)$$

$$D_r = 0.57$$

With the result of 0.57, the soil can be classified as medium dense to dense. Using figure 3.4 and adjusting for the larger grout body with a factor of 2, the ultimate bearing capacity is estimated around **1800 kN**. It is obvious that this approach is less suitable for an anchor of these dimensions, since the graph is only made for smaller grout anchors. Thus, it can be concluded that the Ostermayer method shall be used only for anchors that fit into the geometrical boundaries for which the charts were developed.

4.3. CUR method

With the CUR-method, the bearing capacity can be calculated in a straight forward manner with the given information.

$$\begin{aligned}
 R_{min} &= \alpha_t \cdot \pi \cdot D \cdot L_A \cdot q_{c,avg} \\
 R_{min} &= 0.015 \cdot \pi \cdot 0.335 \cdot 12.4 \cdot 17500 \\
 R_{min} &= 3426kN
 \end{aligned} \tag{4.2}$$

4.4. Analytical model

The analytical model does not calculate a bearing capacity, but the initial displacements and the displacements over time.

The initial displacements are calculated, using equation 3.11, 3.12, 3.17 and 3.10. These equations yield only the force P_0 , the shear modulus G and the Poisson's ratio ν as unknowns. The Poisson's ratio is assumed to be 0.35 for medium dense sand. The corresponding force is chosen to be the one calculated with the CUR-method earlier. The shear modulus is calculated using an empirical correlation from [5].

$$\begin{aligned}
 G_{0,ref} &= 60000 + 68000RD/100 \\
 G_{0,ref} &= 98,760kPa
 \end{aligned} \tag{4.3}$$

With this, the initial displacement components can be calculated. The equations are not shown for all minor variables or the integrals.

$$\begin{aligned}
 \Delta L &= \frac{L}{EA} \cdot P_0 \\
 \Delta L &= \frac{46.6}{2.1E + 08 \cdot 0.01253} \cdot 3426 \\
 \Delta L &= 0.0607m \\
 u_{pc} &= \frac{1 - \nu}{(1 + \nu)G} \frac{P_0}{4b} \\
 u_{pc} &= \frac{1 - 0.35}{(1 + 0.35) \cdot 98760} \frac{3426}{4 \cdot 1.335} \\
 u_{pc} &= 0.0031m
 \end{aligned} \tag{4.4}$$

$$\begin{aligned}
u_{pt} &= P_0 \cdot \frac{1 - \nu}{\pi ab^2 G} \cdot \int \phi_{31} + \frac{1}{2\pi ab^2 G} \cdot \int \phi_{32} \\
u_{pt} &= 3426 \cdot \frac{1 - 0.35}{\pi \cdot 12.4 \cdot 1.335^2 \cdot 98760} \cdot 0.2756 + \frac{1}{2 \cdot \pi \cdot 12.4 \cdot 1.335^2 \cdot 98760} \cdot 0.2754 \\
u_{pt} &= 0.00009m \\
\\
u_A &= \frac{P_0}{2\pi D^2 G(1 - \nu)} \int [I'(r_e) - I'(r_i)] \tag{4.5} \\
u_A &= \frac{3426}{2\pi \cdot 0.335^2 \cdot 98760 \cdot (1 - 0.35)} \cdot 0.1967 \\
u_A &= 0.0149m \\
\\
u_{tot} &= 0.0787m \approx 7.9cm
\end{aligned}$$

In this context, the time dependent displacements are not calculated because the necessary parameters are not available and as a preliminary example the initial displacements suffice.

4.5. Comparison

It becomes clear that the Ostermayer method is not a suitable option if the model dimensions are not within the range of the design methodology. Here, a conservative factor of 2 has been applied, since the circumference in the case study is approximately twice as large as what the design charts are made for. However, the relationship between the grout body dimensions can also be non-linear, especially since the CUR-method estimates a minimum force twice as large as the Ostermayer method with a factor of 2 and 4 times as large without any additional factors to correct for the divergence in the grout body dimensions.

The resulting displacements from the analytical model are in a reasonable magnitude, but slightly too large compared to the test data. For forces of this magnitude, the governing displacement component is the tendon elongation of the anchor. The measured displacements, in the investigation tests, were 5.8 cm and 6.1 cm. These displacements correspond to 3570 kN loading - the 70 % loading increment, including the prestressing displacements ¹. For anchors of the same dimension from the suitability tests, anchor 1 and 2, the initial displacements were 8.0 cm and 8.9 cm for 3507 kN.

This deviation suggests that the shear modulus was chosen too small to fit the investigation tests and too large for the suitability tests. The main reason for this is that the average cone resistance $q_{c,avg}$ was chosen conservatively, since it is commonly cut-off between 15 MPa and 20 MPa. The calculated displacement is approximately in the middle of all measurements taken. One disadvantage is that the analytical model needs the force as an input, and it cannot be back-calculated without using measurement data. However, it is observed that the displacement model works well in combination with the CUR-method. Both methods could be used complementary to each other.

¹The prestressing displacements are a governing factor in the magnitude of the displacements and are further discussed in the following chapters.

5. Anchor Modelling Results

In the following chapter, the analytical model presented in section 3.2.3 is tested on its limitations, its predictive power and its suitability for Bayesian updating. The following flowchart gives an indication of what is discussed in this chapter.

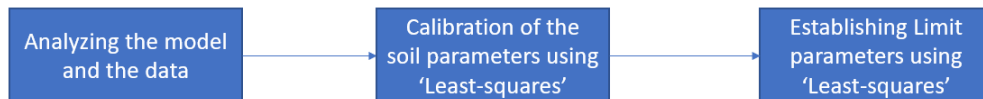


Figure 5.1: Procedure of the Anchor modelling chapter

Throughout this report, a specific set of colors and markers are used to show what kind of test is represented and especially what incremental loading can be seen. The markers are for readability purposes not always included, but the colors are used consistently.

- Orange with '+' marker for 40 % loading
- Green with 'x' marker for 55 % loading
- Blue with '|' marker for 70 % loading
- Purple with diamond marker for 80 % and 85 % loading
- Red with star marker for 90 % loading
- Grey with squared marker for 100 % loading
- Black with 'o' marker for the compared measurement

The investigated database was the HHTT database consisting of two investigation tests, 9 suitability tests and 82 acceptance tests. It needs to be mentioned that the data set is not fully complete to exactly investigate the application of the analytical model presented in 3.2.3 because standard practice is to reset the measured displacements at the pre-stressing level of 10 % loading. The 10% - level is usually the chosen zero point for the displacement measurements. Thus, the displacement that is reported is the net displacement of the anchor, while the model calculates the gross displacement. Therefore, assumptions had to be made about the displacement before pre-stressing.

The issue of the pre-stressing displacement cannot be ignored because it is a quantity that is missing in the measurements and necessary for proper modelling. A simple example to illustrate this problem:

The measured initial displacement of the first investigation test anchor at 40 % loading (2040 kN) was 0.01721 m. The anchor's rod stiffness k_L is ≈ 76930 kN/m. Therefore, in reference to equation 3.10, the displacement

just resulting of the rod elongation must be $\Delta_L = \frac{2040}{76930} = 0.02651 \text{ m}$. Therefore, it becomes evident, that some displacements are not captured in the conventional anchor measuring techniques.

The classical way to use this model is to calculate displacements with known soil parameters and known forcing. These three components (green) are necessary to calculate any physical quantity. Only one of those can be solved for if the others are known.

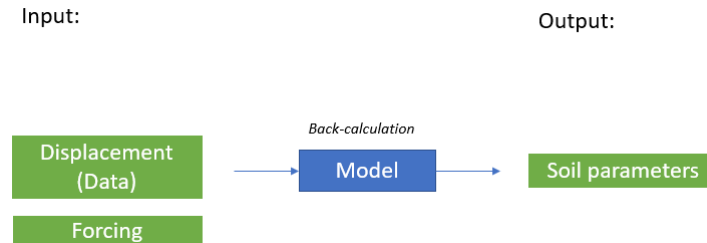


Figure 5.2: Application of the model

5.1. Limits

For the application of the model on real test data, caution is to be advised. First, usually only the net displacements are measured, which means that the pre-stressing displacements need to be added or subtracted accordingly. Otherwise, it occurs that the measured displacements are too small to account even for the tendon elongation of the anchor rod and a fit is not possible, as illustrated above.

Furthermore, it is important to keep the lower limit of the possible displacement in mind. Especially concerning lower incremental loading levels, it was observed that this condition does not always hold because the assumption of the initial displacement might not fit. This explained by analyzing Eq. 5.1.

$$k_s = \frac{1}{\frac{1}{k_L} + \frac{1}{k_{pc}} - \frac{1}{k_{pt}} + \frac{1}{k_A}} \quad (5.1)$$

The lower limit of Equation 5.1 is $k_s(t) = k_L$, because for large Burger parameters, the corresponding time dependent stiffness of each displacement component apart for the elongation stiffness tend to infinity. Thus, the total system's stiffness becomes the elongation stiffness and the minimum displacement is the one resulting only from the elastic elongation of the rod. Therefore, the pre-stressing displacements were chosen to fit this lower limit, where the value needs to be large enough to exceed this boundary. Since it only changes the general magnitude of the displacements, the only parameter that is affected by this uncertainty is the shear modulus G .

An upper limit was not observed. Depending on the parameters, if the stiffness becomes close to zero, the displacements tend towards infinity. However, this does not apply to a physically realistic range of parameters.

5.2. Calibration

The following shows the results of the calibration process. This was done utilizing the python library 'SciPy' and incorporating the 'least squares' solving algorithm. The boundary conditions were chosen in a way that ensures a physically realistic range of the results. This needs to be done with care since the model tends to 'overfit' the measurement data, meaning there is a larger range of parameter values possible that enables

the algorithm to stop because the anticipated error is small enough for stopping the procedure.

The purpose is to show that the analytical model is capable of reproducing the measured displacement of the tests. More importantly, these results provide a benchmark to which the effects of the Bayesian updating can be compared to, since the necessary soil parameters are not trivial to derive. However, the possible range for certain parameters was observed to be large also compared to which type of measurement (displacement or creep) the data was intended to fit. Therefore, for each test, 3 sets of parameters are calculated, all differing in the general approach of curve fitting.

The first one (Set 1) focused on **obtaining the best possible fit to the measured displacements**.

The second one (Set 2) on **the best possible fit to the observed creep behavior**

The third one (Set 3) to **the best possible fit to displacement and creep with a minimum amount of variables**. There, the viscous components of the mechanical model are assumed to be constant for each test frame.

This split into three sets was conducted because it was observed that a precise fit to the displacement and simultaneously a precise fit to the creep values is not possible. Therefore, the second set shows the soil parameters in context of the creep behavior, which gives insight about the model's sensitivities to the creep. For example, a divergence in the creep value for the different sets can be directly quantified and related to the soil parameters. With Set 3, it was investigated how the model can be reduced in its complexity while still being able to calibrate with decent concordance to the measurements. This was done because the follow-up investigations about Bayesian updating are computationally expensive, thus, the model shall be as simple as possible for decent efficiency.

The only parameter that was kept constant in all three sets is the Poisson's ratio at **0.35**.

For the procedure, the initial displacement (at $t=0$) is calculated with the initial and non-time dependent shear modulus G and the Poisson's ratio. Thus, the calibration of the shear modulus is done before the time dependent parameters are considered by solving the initial displacement for the shear modulus. The Poisson's ratio of 0.35 was basically observed to show the most reasonable fit for all anchors and loads. With these two values, the Bulk Modulus is calculated in the following fashion.

$$K = \frac{2G(1 + \nu)}{3(1 - 2\nu)} \quad (5.2)$$

The initial displacements are the first displacements occurring. They set the outline and the general magnitude of all the following displacements, especially through the close correlation of G to G_M , which is further elaborated in the sensitivity analysis. This means that the initial displacement can be calculated with only one uncertain soil parameter, which is the shear modulus G . The shear modulus can also be back-calculated with a measurement of the initial displacement by solving Equation 3.17, Equation 3.12 and Equation 3.11 for G .

The results are shown and discussed within this chapter. The necessary input parameters for all tests can be found in the appendix, as for the detailed results of the investigation tests. Due to the quantity, the test data of all the acceptance tests are not presented.

5.2.1 Sensitivities

Displacements

In the following, the sensitivities of the mechanical model’s soil parameters are described to gain an insight of the model’s behavior. As a basis, the ‘Set 1’ calibration parameters of Suitability Test Anchor 1 at 100 % were used. The observations are indicated within the figures, where the parameter that has been changed is also marked.

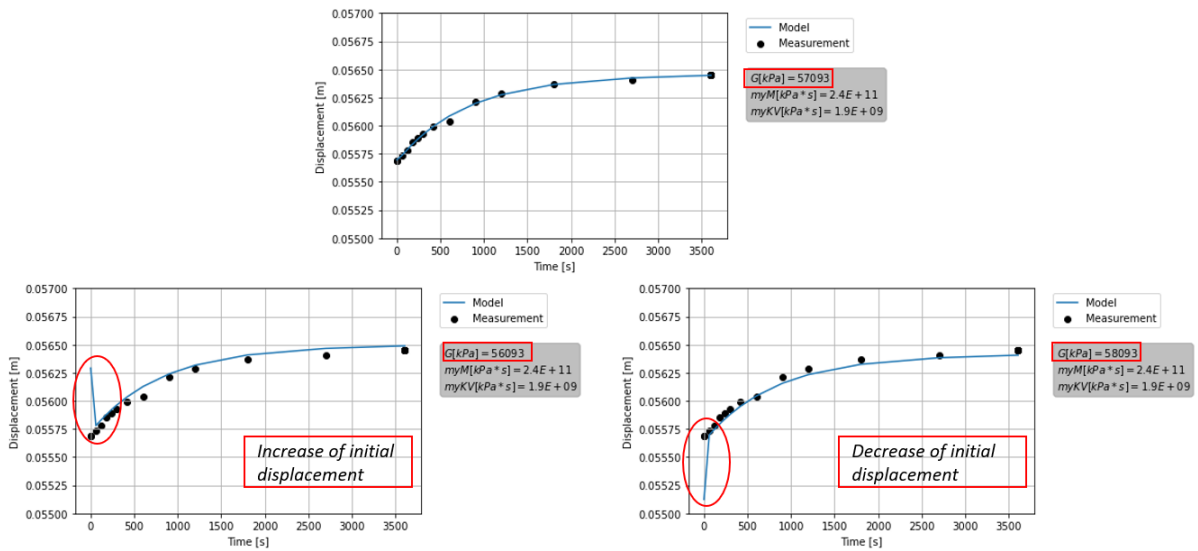


Figure 5.3: Sensitivity, Shear modulus G

As it can be observed in Fig. 5.3, the shear modulus is only affecting the initial displacements and with limited influence on the final displacements. The parameter has been changed by 1000 kPa but the observed divergence is quite large for an increase and decrease, which proves that the model is more sensitive to this parametric change.

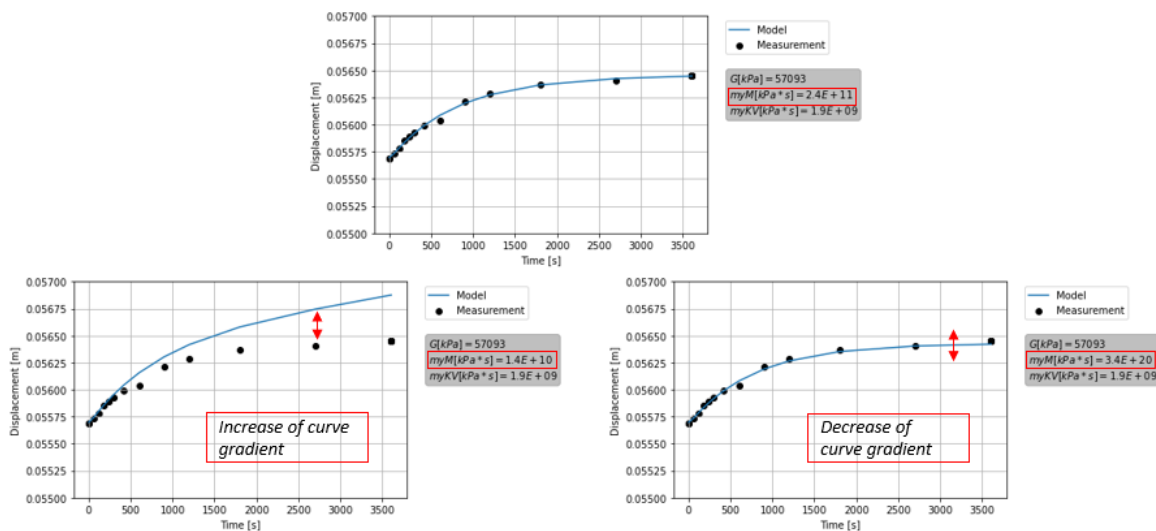


Figure 5.4: Sensitivity, Maxwell viscosity μ_M

It can be observed in Fig. 5.4 that this specific model is less sensitive upon increasing the viscosity. However,

this is problem specific. For other anchors, more sensitive behavior was observed. Generally an increase leads to a decreasing gradient of the curve, however, for these boundary conditions there is barely any change observable. In the other direction, upon decreasing the viscosity, the gradient quickly increases.

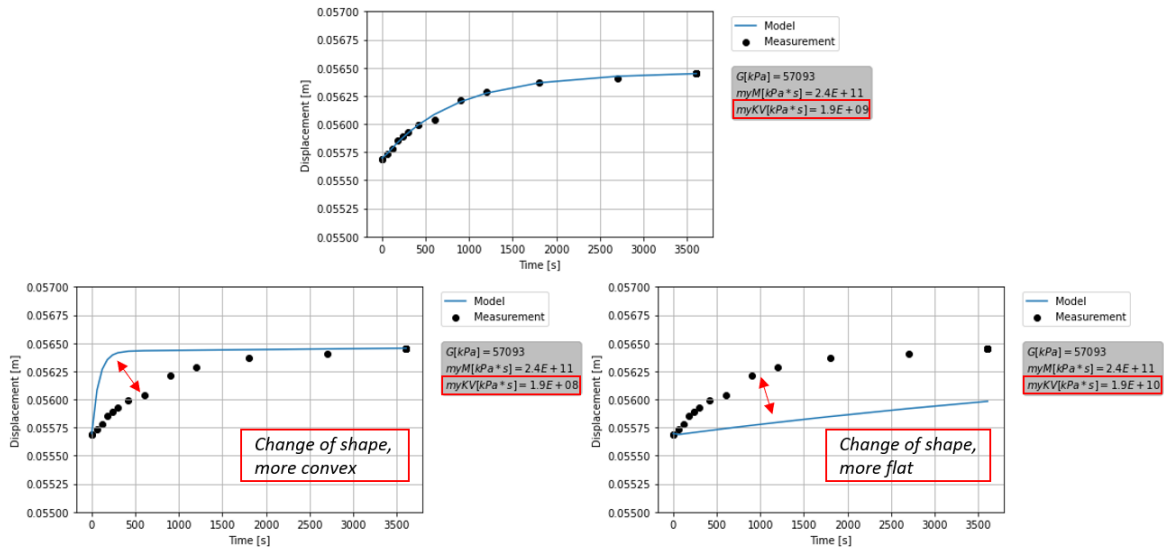


Figure 5.5: Sensitivity, Kelvin-Voigt viscosity μ_{KV}

The Kelvin-Voigt viscosity has a different influence on the model, as shown in Fig. 5.5. Its magnitude is governing in the determination of the curve’s shape. In this way it affects the displacements as it does the gradient. It basically sets the time after which the gradient becomes negligible.

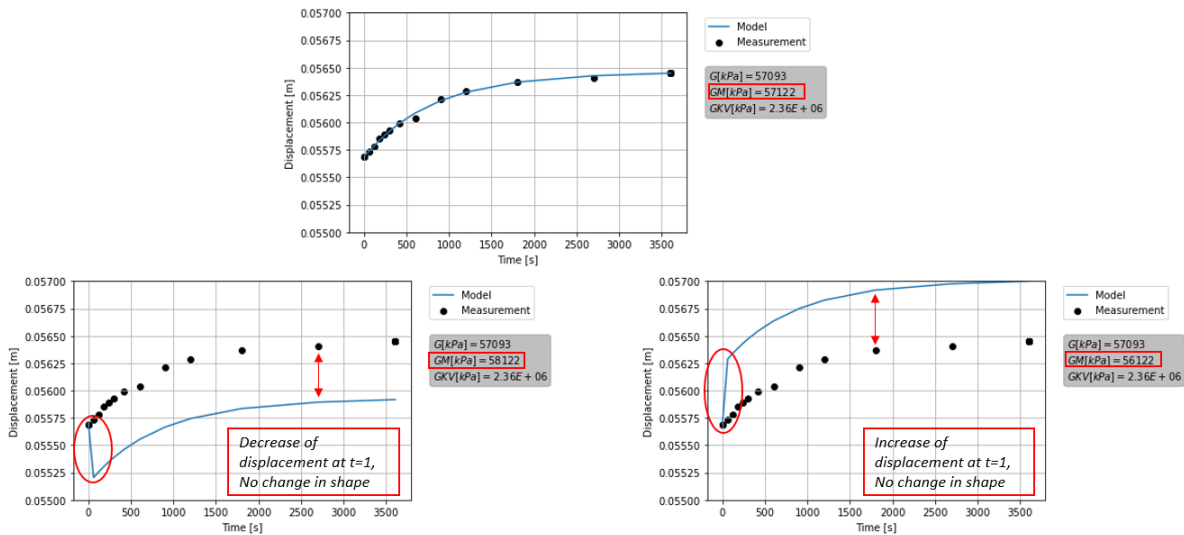


Figure 5.6: Sensitivity, Maxwell shear modulus G_M

The Maxwell shear modulus mainly governs the displacement at $t = 1$, Fig. 5.6. By doing so, the curve can be shifted and adapted, for example, to large displacements that occur within the first few seconds of the loading. The shape of the curve and the follow-up displacements remain largely unaffected.

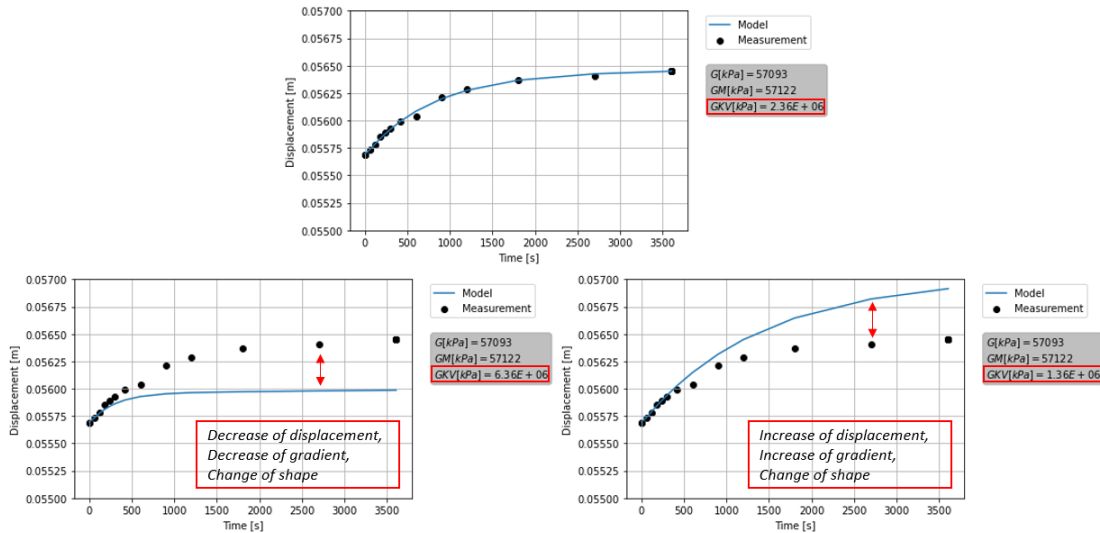


Figure 5.7: Sensitivity, Kelvin-Voigt shear modulus G_{KV}

The Kelvin-Voigt shear modulus influences the time and the magnitude of the anchor’s maximal displacement, Fig. 5.7. This means, a higher magnitude leads generally to lower time dependent displacements that are reached quicker, while a lower stiffness leads to higher time dependent displacements that are reached slower. Both Kelvin-Voigt components together influence the radius of the curve.

Creep

Here, the sensitivities of the mechanical model concerning the creep value are illustrated in a similar analysis as for the displacements. The factors that increase or decrease the parameters are changing and adjusted accordingly, depending on the sensitivity of the parameter towards change.

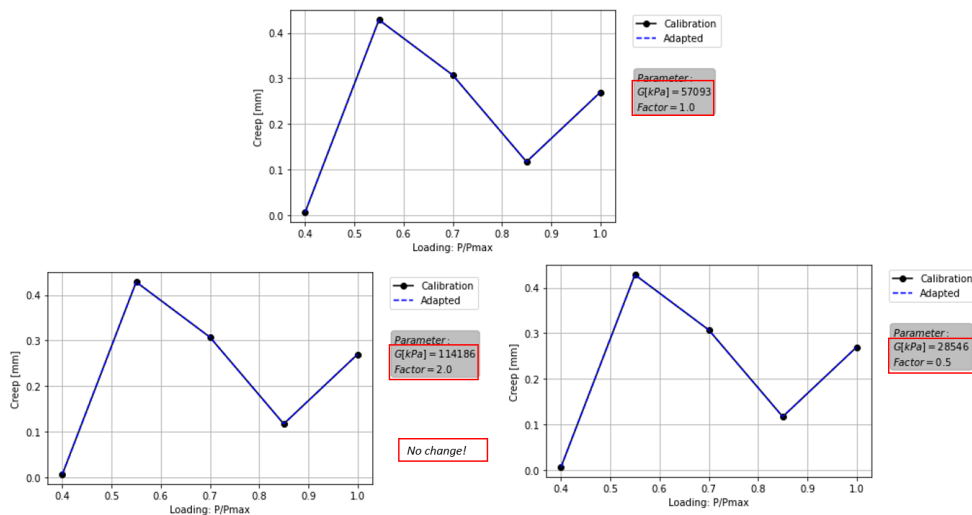


Figure 5.8: Sensitivity, shear modulus G

From Fig. 5.8, it can be observed that the creep is completely independent of the shear modulus. This is also expected, since all displacements at $t > 0$ are not calculated with the shear modulus.

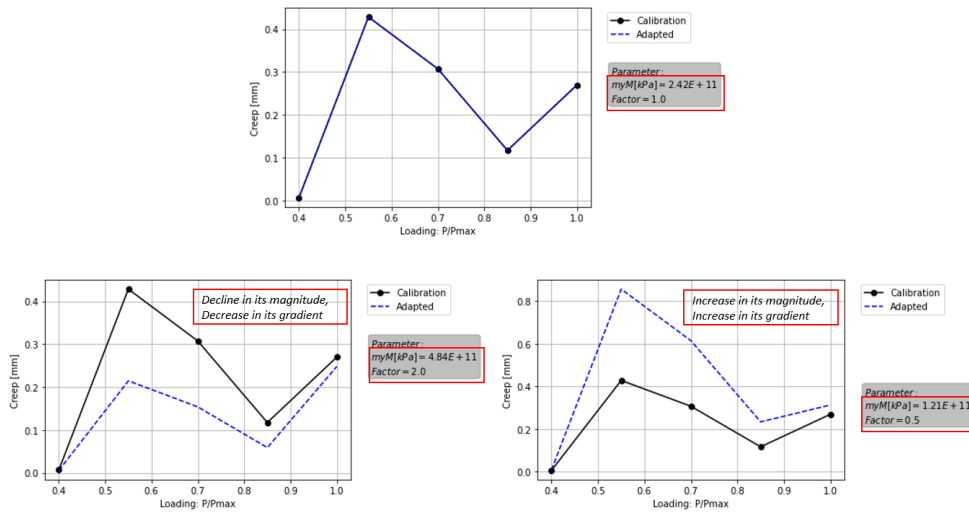


Figure 5.9: Sensitivity, Maxwell viscosity μ_M

The Maxwell viscosity is the main parameter governing the creep magnitude, Fig. 5.9. It is also the most sensitive one, slight changes have large effects on the magnitude of the curve.

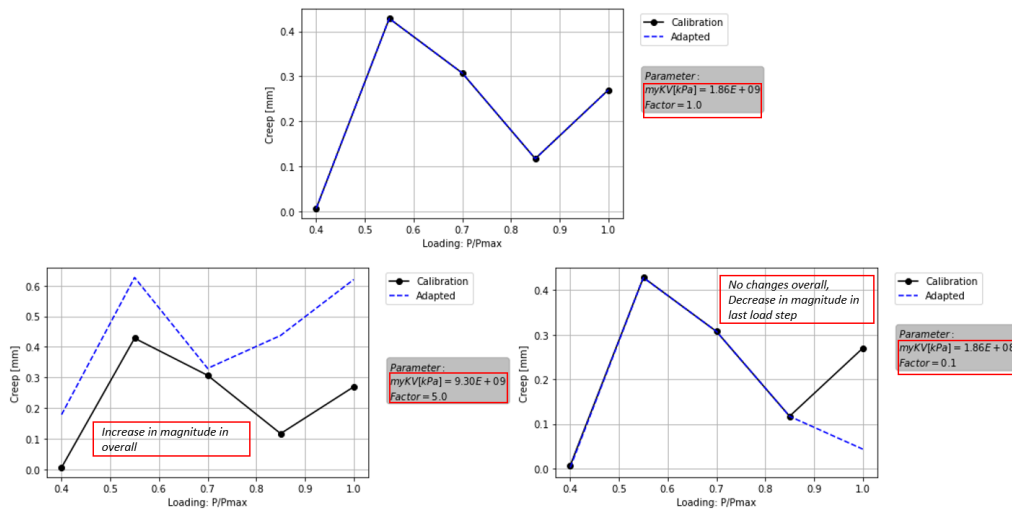


Figure 5.10: Sensitivity, Kelvin-Voigt viscosity μ_{KV}

The Kelvin-Voigt viscosity also has an impact on the magnitude of creep, but the model’s sensitivity to change is not as pronounced as for the Maxwell-viscosity or the Kelvin-Voigt shear modulus, Fig. 5.10.

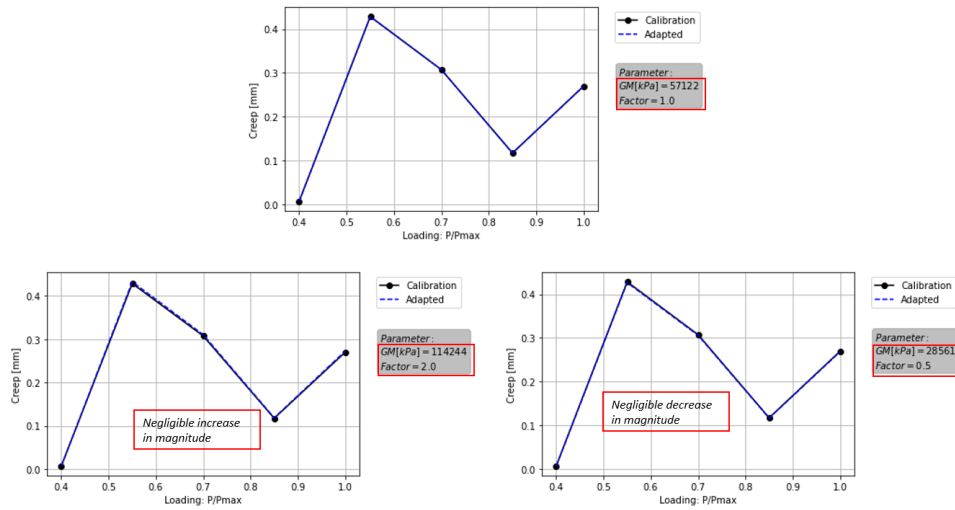


Figure 5.11: Sensitivity, Maxwell shear modulus G_M

As for the shear modulus, the influence of the Maxwell shear modulus in Fig. 5.11 is negligible on the creep in its common parametric ranges.

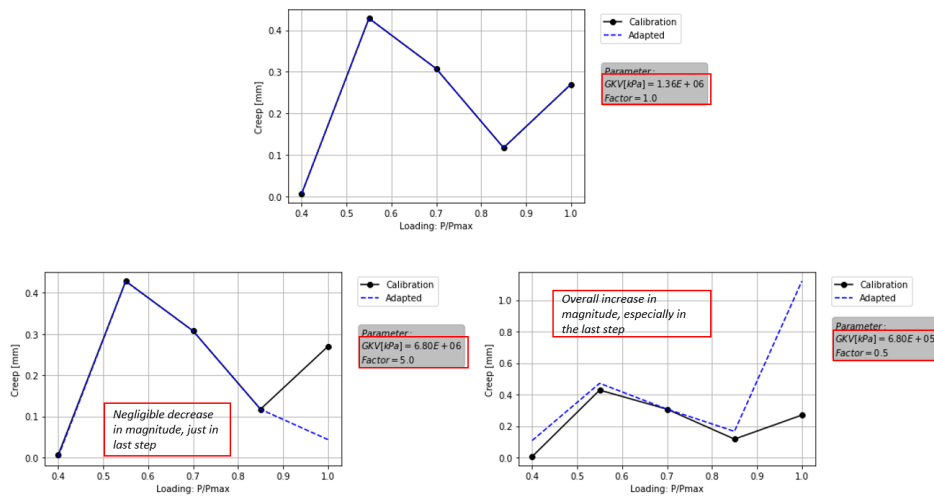


Figure 5.12: Sensitivity, Kelvin-Voigt shear modulus G_{KV}

The Kelvin-Voigt shear modulus has a major influence on the magnitude of the creep, Fig. 5.12. However, this component’s relationship to creep is complex and difficult to illustrate. Depending on the problem and the magnitude, slight parameter changes can have large or small consequences. Fig. 5.12 captures this behavior by depicting that the change is in this case most profound in the last load step. Generally, smaller values induce large changes in the creep’s magnitude.

5.2.2 Investigation Tests

Set 1: Displacements

This section shows the results of the calibration of the anchor model to the investigation test displacement data with all soil parameters involved. The following figures show the fit between the data and the model results.

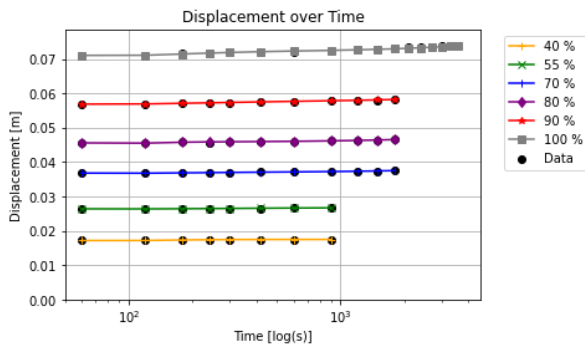


Figure 5.13: Inv. test calibration, Anchor 1

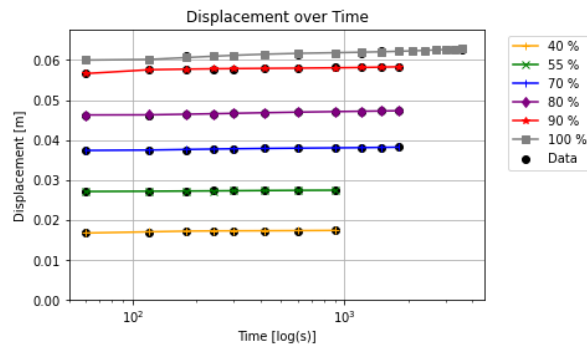


Figure 5.14: Inv. test calibration, Anchor 2

As it can be observed, precise fits are possible, only for the 100 % - loading increment it can be seen that the gradient of the calibrated curve is slightly too large to provide an exact fit. This also is noticeable in the following graph that depicts the creep characteristics of the entire test of the anchors.

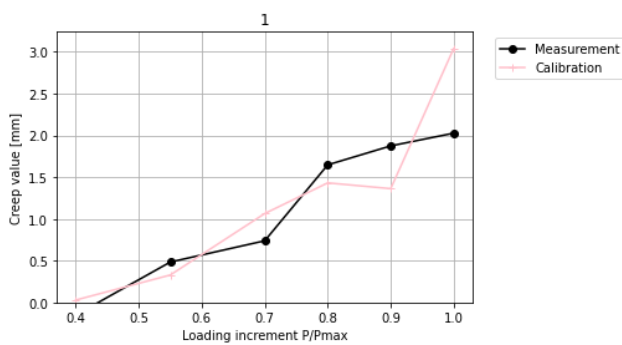


Figure 5.15: Inv. test creep, Anchor 1

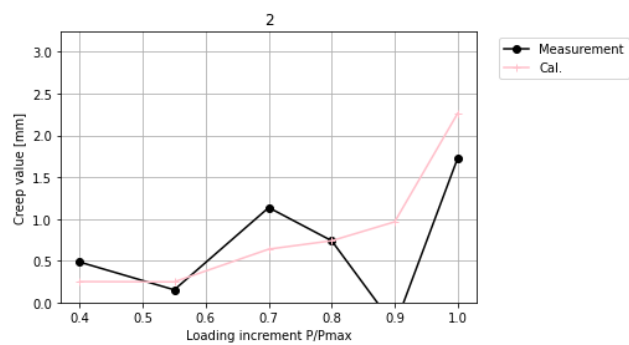


Figure 5.16: Inv. test creep, Anchor 2

Since the gradient of the calibration is slightly larger than the measurement at the 100 % loading increment, the resulting creep value is also larger compared to the measurements. The Maxwell viscosity component μ_M of the Burger mechanical model shows to have a major influence on the gradient of the model's curve. It can be observed that the curve of the calibrated model resembles the idealized behavior of an anchor with increasing load, which would be an exponentially increasing curve. However, it is also natural that this idealized behavior cannot be observed in the measurement data, which is prone to measurement error.

Set 2: Creep value

The calibration purely to the creep value yield mediocre concordance concerning the displacements, as it can be observed in the figures below.

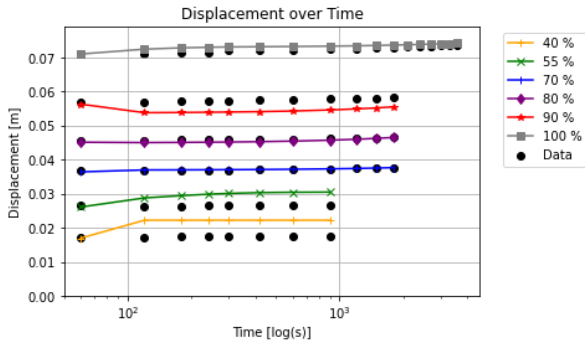


Figure 5.17: Inv. test calibration, Anchor 1

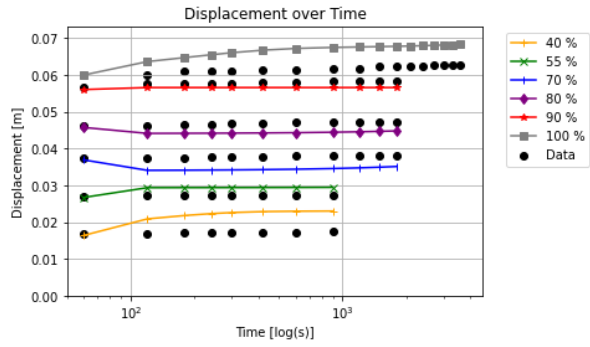


Figure 5.18: Inv. test calibration, Anchor 2

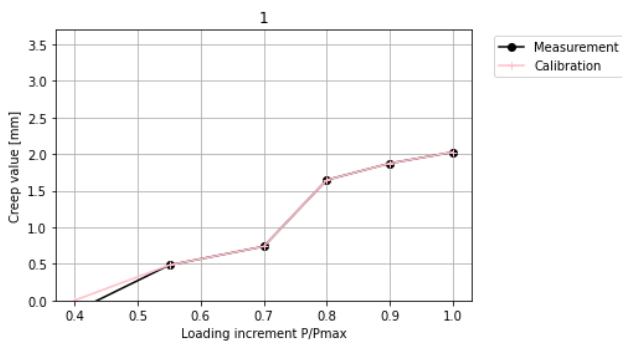


Figure 5.19: Inv. test creep, Anchor 1

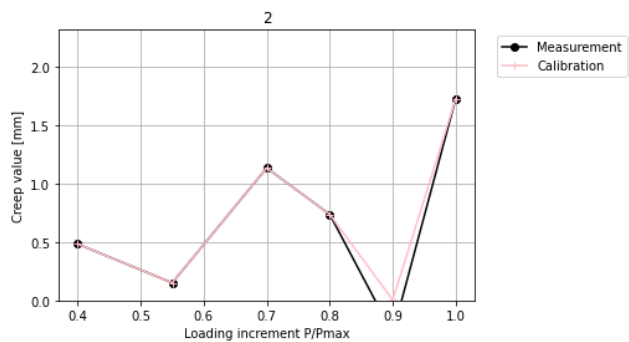


Figure 5.20: Inv. test creep, Anchor 2

The creep value curves show an exact concordance for the values larger than 0. But since the divergence within the displacements is rather large, the usefulness of this set is questionable. Especially the 90 % measurement of the second anchor suggests a negative creep value which distorts the calibration, as this way the algorithm assumes no time dependent displacements at all. However, the data has uncertainty inherent, thus, measurement errors need to be considered. This approach is not appropriate for Bayesian updating, but to obtain the 'true' parametric values to fit the anchor's creep characteristics.

Set 3: Least-variables

In this section, curve-fitting with the least amount of changing variables per anchor and loading cycle was anticipated. It has been managed to obtain a good concordance with constant viscosity of the Maxwell and Kelvin-Voigt components. Furthermore, the Maxwell shear modulus was assumed to be the same as the initial elastic shear modulus of the soil. Thus, for the investigation tests, the following table shows the constants that were determined.

| Poisson's ratio ν | Maxwell viscosity μ_M | Kelvin-Voigt viscosity μ_{KV} |
|-----------------------|---------------------------|-----------------------------------|
| - | kPa · s | kPa · s |
| 0.35 | 7.93E+9 | 6.1E+8 |

Table 5.1: Soil constants for Investigation Tests

The following figures show the obtained fit.

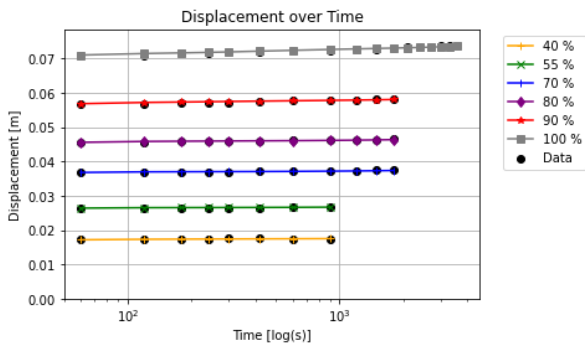


Figure 5.21: Inv. test calibration, Anchor 1

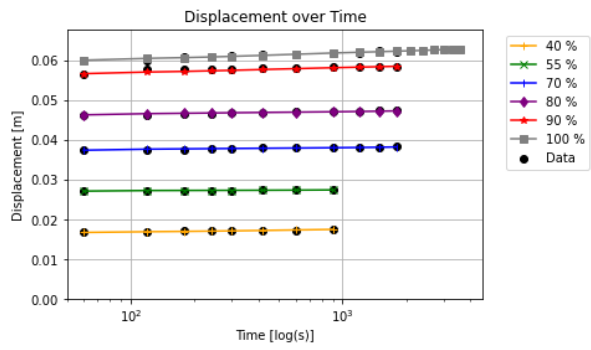


Figure 5.22: Inv. test calibration, Anchor 2

Fig. 5.13 and 5.22 suggest that the assumptions made are valid to model the displacements. The creep characteristics are depicted in the following graphs.

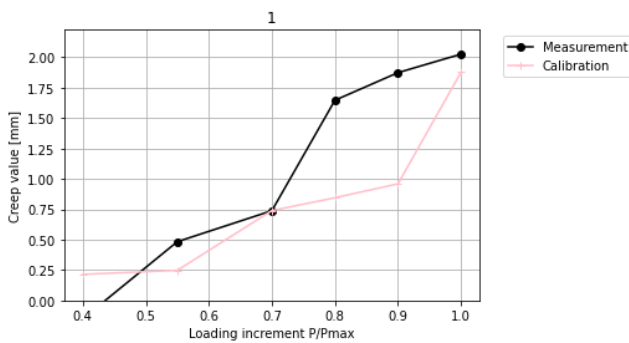


Figure 5.23: Inv. test creep, Anchor 1

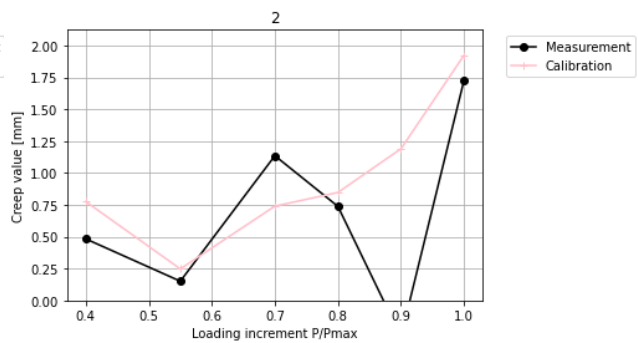


Figure 5.24: Inv. test creep, Anchor 2

Here the divergence to the measurements is larger than for the first set. As shown in the sensitivity analysis, the viscosity components of the model are governing in the magnitude of the anchor’s creep. The constants were chosen to fit the creep curves as close as possible, mainly focussed around the 100 % loading increment.

5.2.3 Suitability tests

For the suitability tests, it needs to be mentioned that the database consists of 3 different testing conditions. The first two anchors are designed for a working load of 3507 kN, the third and fourth anchor for a working load of 1465 kN, and the rest of the anchors for a working load of 2653 kN. Therefore, the geometries and the rod properties are deviating from each other as well. Due to this difference, certain peculiarities are observed concerning the range of the parameters, especially in Set 3, where uniform viscosity parameters are being used. All suitability test model properties can be found in Appendix C in table C.6.

Set 1: Displacements

Below, the results of the first set are shown.

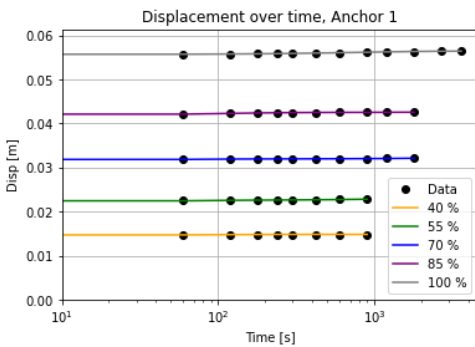


Figure 5.25: Suit. test calibration, Anchor 1

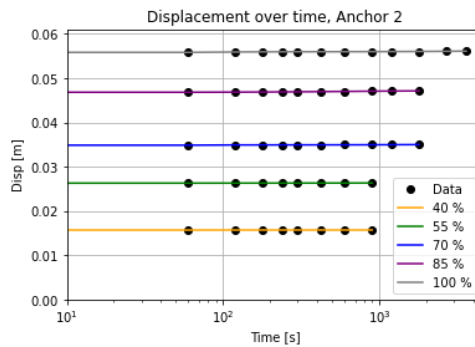


Figure 5.26: Suit. test calibration, Anchor 2

Fig. 5.25 and 5.26 show that, similar to investigation tests, the model is able to capture precisely the displacements of the measurements.

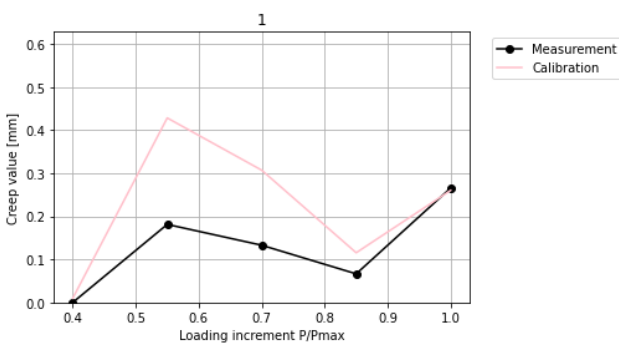


Figure 5.27: Suit. test creep, Anchor 1

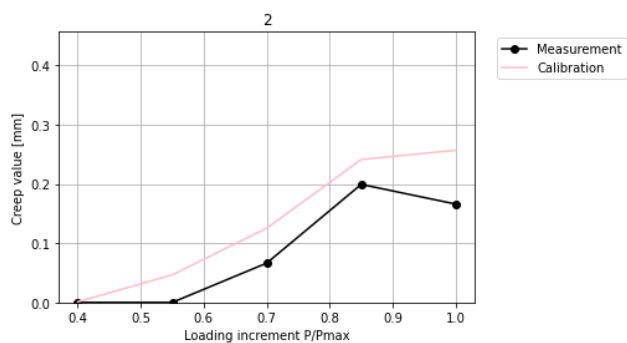


Figure 5.28: Suit. test creep, Anchor 2

The creep curve measurements have an unusual shape, five of the nine anchors show the opposite trend compared to what is expected from the idealized behavior. The creep value at the highest loading increment is lower than for the previous, lower loading conditions. Especially for anchor no. 2, Fig. 5.28, the model has problems to depict the measurements since they show a negative and noisy trend in the opposite direction. This is even more pronounced in Fig. C.9, which can be found in appendix C. Overall, the calibrated parameters capture the underlying trend that the data suggests. On average, the creep value is slightly overestimated by the calibration.

Set 2: Creep value

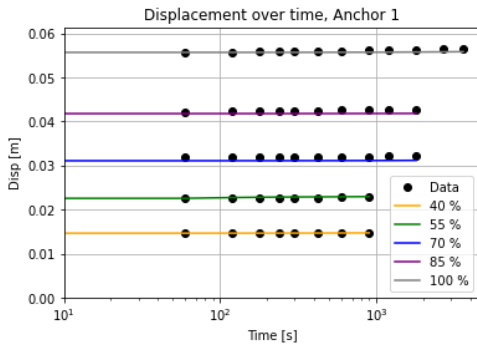


Figure 5.29: Suit. test calibration, Anchor 1

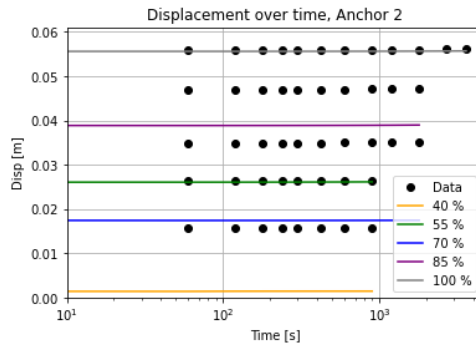


Figure 5.30: Suit. test calibration, Anchor 2

Compared to Set 1, the displacements of this calibration are further off. For some anchors there is a decent concordance observable, for others the deviation is larger. What cannot be observed on the logarithmic scales is, that for most anchors, even if the displacement is in a decent magnitude, the overall shape of the curve does not match the data, which suggests deviations in the Kelvin-Voigt components.

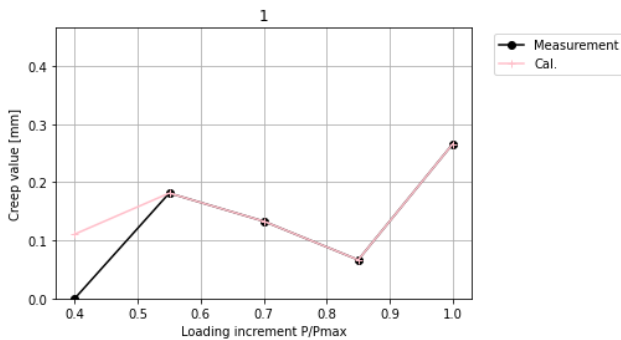


Figure 5.31: Suit. test creep, Anchor 1

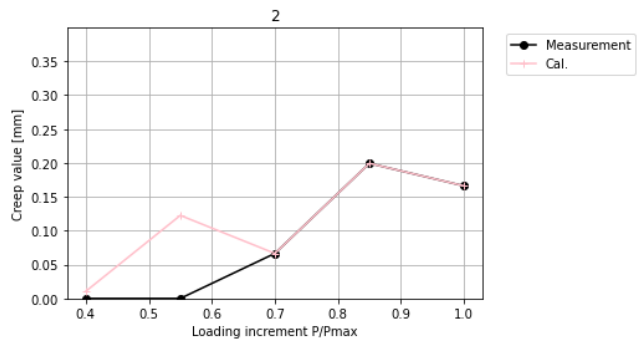


Figure 5.32: Suit. test creep, Anchor 2

As expected, the obtained parameters precisely capture the creep characteristics for values larger than zero. The displacement for creep values close to or equal to zero cannot be properly derived, which typically results in noise.

Set 3: Least variables

Due to the different properties of the anchors, a single Maxwell- or Kelvin-Voigt viscosity parameter for all anchors provided no decent fit to the data. Therefore, for each design, separate values have been determined and are shown in table 5.2.

| Anchor | Poisson's ratio ν | Maxwell viscosity μ_M kPa · s | Kelvin-Voigt viscosity μ_{KV} kPa · s |
|--------|-----------------------|--------------------------------------|--|
| 1 + 2 | 0.35 | 5.1E+10 | 6.1E+8 |
| 3 + 4 | 0.35 | 8.9E+9 | 9.5E+7 |
| 5 - 9 | 0.35 | 2.4E+10 | 3.1E+8 |

Table 5.2: Soil constants for Suitability Tests

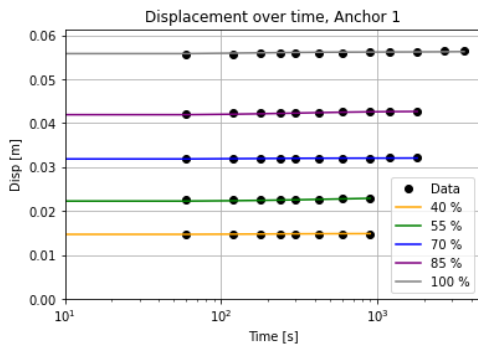


Figure 5.33: Suit. test calibration, Anchor 1

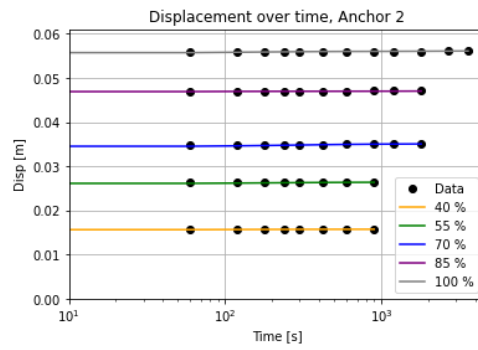


Figure 5.34: Suit. test calibration, Anchor 2

The figures 5.33 and 5.34 show that the derived parameters provide proper model fits comparable to the precision of Set 1.

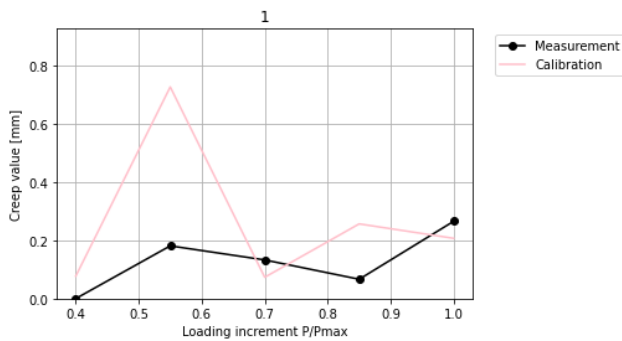


Figure 5.35: Suit. test creep, Anchor 1

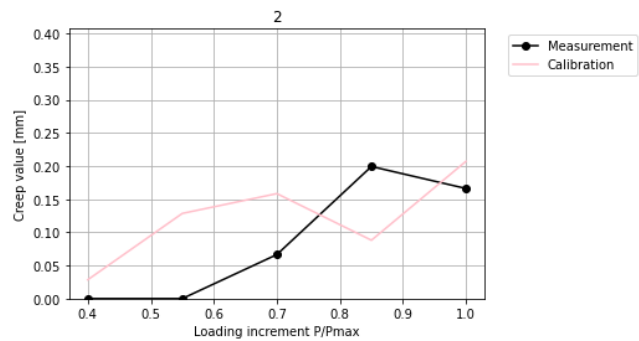


Figure 5.36: Suit. test creep, Anchor 2

As Fig. 5.35 and 5.36 prove, to fit the data closely, especially concerning the creep value, one single value for each loading step shows little concordance with the data. As the sensitivity analysis suggests, the creep value itself is largely governed by both, the Maxwell and Kelvin-Voigt viscosity. For anchor 1 and 2 at the 100 % loading increment, depicted in 5.31 and 5.32, the obtained values will be regarded as the 'true values' since the parameters show such a close alignment. Now, for this set, the Maxwell viscosity was determined to be approx. $5.1E+10$. The 'true values' for Anchor 1 and 2 are $3.98E+10$ and $6.36E+10$ respectively (determined in Set 2), which indicates that if the creep curve shows a too large value, deviating from the data, like for anchor 2 in Fig. 5.36 the cause is a too small Maxwell viscosity. It needs to be mentioned that this is not unconditionally valid due to the influences of other soil parameters, but the point that shall be stressed, is that the creep value itself is largely influenced by the Maxwell viscosity.

5.2.4 Acceptance Tests

The acceptance tests were investigated in the same fashion as the other tests. The main difference is that the acceptance tests' duration at 100 % loading is just 5 minutes, which allows limited statements about the actual time dependent behavior. For reasons of completeness, this investigation is also carried out, but it is not possible to obtain a creep curve when there are no time-displacement measurements. Thus, the precision of the creep calibration is investigated differently. However, the most valuable measurements are the initial displacements for such a large quantity of anchors at every loading cycle. To refer back to the beginning of this chapter, the shear modulus is derived only by the initial displacements. The quantity of measurements means that the data can be analyzed and checked for any underlying distributions of the calibrated parameters.

Set 1: Displacements

The first set shows the result of the calibration to the displacements with all soil parameters, similar to the calibrations in the previous sections. The results are shown in Fig. 5.37 and 5.38.

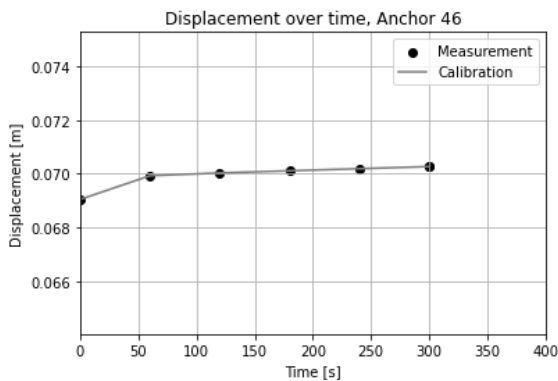


Figure 5.37: Acc. test calibration, Anchor 46

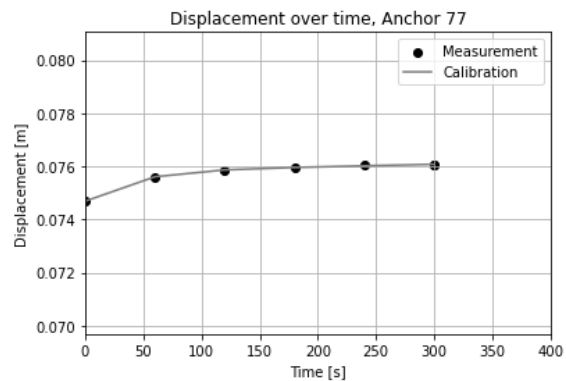


Figure 5.38: Acc. test calibration, Anchor 77

Again, the calibration delivers a precise fit to the data. Fig. 5.37 and 5.38 show just two anchors of the database, but the obtained results draw a clear picture. The creep value is now just a single value for every anchor, and the calibration is compared to the measurements in the following graph.

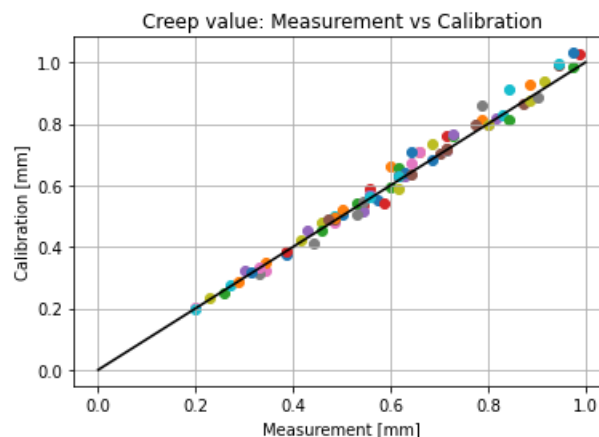


Figure 5.39: Creep value: Comparison measurement vs calibration

The parameters obtained through the calibration procedure enable precise fits to the data. There are no large divergences that distort the result.

Set 2: Least variables

For the 'least variables' approach, the viscosity parameters are kept as a constant while only the shear modulus parameters are varied. The following table shows the parameters that showed the highest concordance with the data.

| Poisson's ratio ν | Maxwell viscosity μ_M | Kelvin-Voigt viscosity μ_{KV} |
|-----------------------|---------------------------|-----------------------------------|
| - | kPa · s | kPa · s |
| 0.35 | 7.5E+8 | 2.5E+7 |

Table 5.3: Soil constants for Acceptance Tests

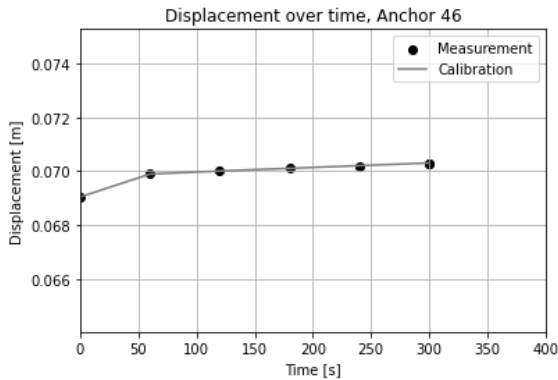


Figure 5.40: Acc. test calibration, Anchor 46

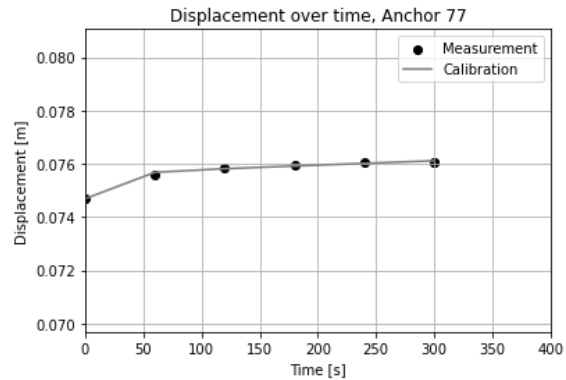


Figure 5.41: Acc. test calibration, Anchor 77

In Fig. 5.40 and 5.41 it can be observed that regarding the displacements, a decent concordance is obtained. The difference in the curves shape is negligible compared to the first set, (Fig. 5.37 and 5.38). However, there is a large difference in the creep values.

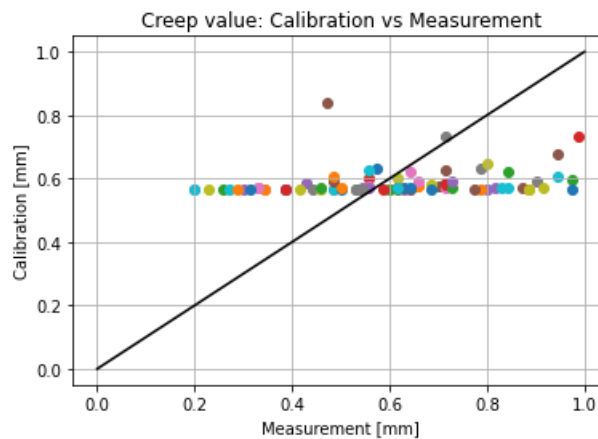


Figure 5.42: Creep value: comparison measurement vs calibration

The first observation goes in line with previous observations, the magnitude of the creep value is strongly dependent on the Maxwell viscosity. Since all anchors are given the same viscosity parameters, they also show a small range of different calculated creep values. For now, the Maxwell viscosity was chosen in such a fashion that the ratio of any overestimation to any underestimation is approximately 1. However, the creep value resulting from this calibration is therefore for all anchors around 0.58 mm.

As the Maxwell viscosity influences the magnitude of the creep value, the Kelvin-Voigt viscosity is mainly

influencing the shape of the curves and therefore, the spread of possible results. In the context of Fig. 5.42, the spread would be how close the data points are to each other on a vertical scale. For a small Kelvin-Voigt viscosity, the spread decreases as it increases for a larger value. The same result, as it is observed in Fig. 5.39, cannot be reproduced with uniform viscosity parameters.

5.2.5 Summary

In the previous sections (section 5.2.2, 5.2.3, 5.2.4), several sets of parameters were computed that each show a different advantage for calibration purposes. For all tests, the results allow the same conclusions because in each framework the same phenomena were observed. The first set with a full parameter set gives the most precise results concerning both, creep and displacements, but it has the longest calculation time. The second set returns precise parameters to fit the creep curves of the anchor, but the displacements are not correctly captured. The third set gives a good indication about the displacements and captures the trend of the creep curves. However, the divergence in each set for the comparison of the 'Least variables' with the creep characteristics curve is large, especially regarding the acceptance tests. It has the shortest calculation time, and is therefore attractive for large databases. Table 5.4 summarizes the constant parameters that were obtained for each test frame in set 3. From the comparison, it can be concluded that the parameters' magnitude is in similar ranges as long as the timeframes are comparable. The magnitude for the Maxwell viscosity for the acceptance tests is smaller because 5 minutes are considered, opposed to the 60 minutes from the investigation and suitability tests. The gradient of the displacement curve is in the first few minutes the largest.

It can be concluded that the model possibilities are large, and it is possible to fit the model to all types of test and also different types of measurement (displacement or creep). Upon reducing the amount of model variables, certain losses in accuracy have to be accepted.

| Anchor load 100 % kN | Maxwell viscosity μ_M kPa · s | Kelvin-Voigt viscosity μ_{KV} / kPa · s |
|-------------------------|--------------------------------------|--|
| 5100 | 7.93E+9 | 6.1E+8 |
| 3507 | 5.1E+10 | 6.1E+8 |
| 2653 (Suit.) | 2.4E+10 | 3.1E+8 |
| 1465 | 8.9E+9 | 9.5E+7 |
| 2653 (Acc.) | 7.5E+8 | 2.5E+7 |

Table 5.4: Comparison of viscosity parameters for varying test loads

5.3. Parameter distribution

Based on the quantity of the acceptance tests, the calibrated parameters are in this section investigated for underlying distributions. The first section discusses the shear modulus based on the acceptance test and suitability test calibration, the second section discusses the Kelvin-Voigt shear modulus of the acceptance test calibration.

5.3.1 Shear modulus

One of the main influences that has been observed is the variability of the shear modulus.

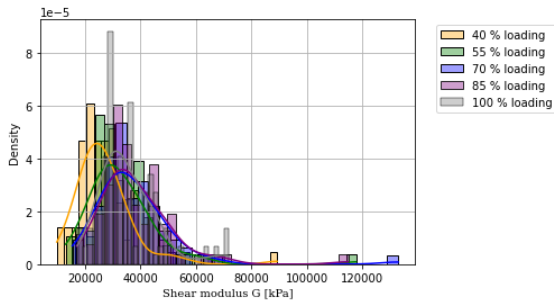


Figure 5.43: Distribution of the shear modulus for increasing loads

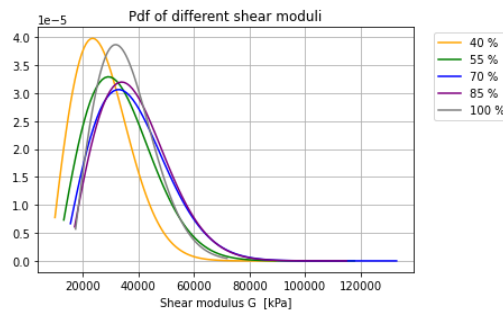


Figure 5.44: Probability density functions for G

Fig. 5.43 and 5.44 illustrate the results of the acceptance tests first, as a histogram and second depicted as probability density functions. As a distribution type, here a Rayleigh distribution was chosen, but other types like log-normal or Beta should also be suitable. Table 5.5 shows all the parameters necessary to build the pdfs using the Python library 'SciPy'.

| | μ [kPa] | σ [kPa] | location | scale |
|-------|-------------|----------------|----------|-------|
| 40 % | 27570 | 9986 | 8467 | 15242 |
| 55 % | 34178 | 12072 | 11081 | 18428 |
| 70 % | 38234 | 12969 | 13423 | 19796 |
| 85 % | 39034 | 12427 | 15260 | 18968 |
| 100 % | 35834 | 10279 | 16170 | 15690 |

Table 5.5: Statistical parameters: Shear Modulus, Rayleigh distribution

The results in Fig. 5.43 and 5.44 show that the mean shear modulus increases with the load until $\approx 85\%$ loading. After this threshold, the mean decreases again towards 100% loading. The stagnation of the means increase after 85% loading indicates that a residual value is reached, after which the shear modulus does not increase anymore.

Another observation is that the calibrated shear modulus are spread between $\approx 18,000$ kPa and 60,000 kPa. It must be noted that these anchors all share the same design and loading conditions. It is expected that the spread can be largely allocated to spacial variability in the soil.

The suitability tests suggest a similar trend as shown in Fig. 5.45.

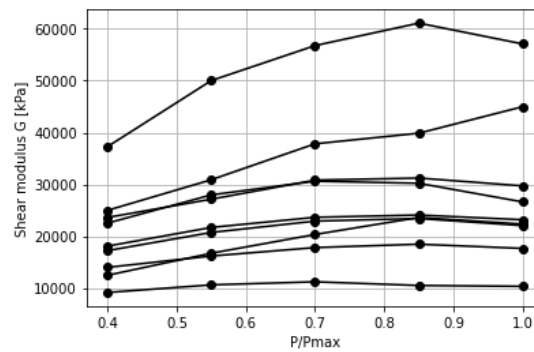


Figure 5.45: Evolution of G for increasing load, Suitability tests

Each line denotes one suitability test anchor. The difference for each loading step is small, but Fig. 5.3 illustrates how sensitive the model is to small deviations in the shear modulus. The calibration of all tests confirms this trend on how the shear modulus is behaving for increased loading. The trend that the shear modulus increases with the load is observed on most anchors. The trend that the shear modulus peaks earlier than the 100 % loading is observed on fewer anchors.

5.3.2 Kelvin-Voigt shear modulus

Generally, all the results of the time-dependent soil variables need to be carefully assessed, since the 5 data points of the acceptance tests are insufficient for clear conclusions. The distribution of the Kelvin-Voigt shear modulus provided the clearest picture compared to the distribution of the other soil parameters.

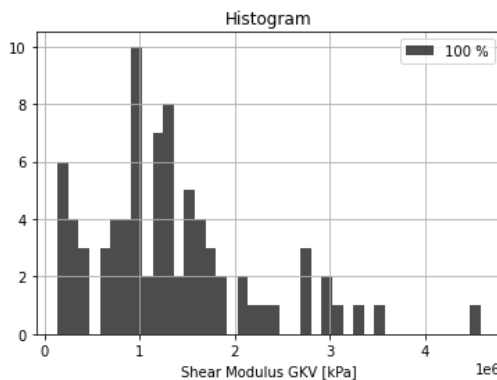
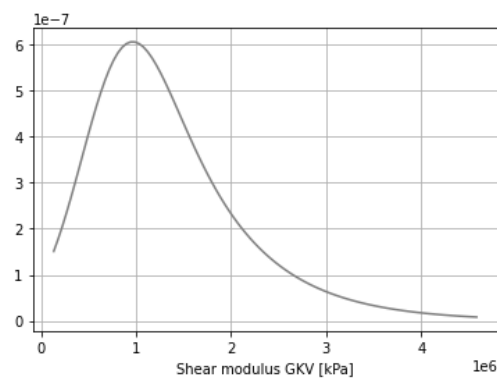
Figure 5.46: Histogram, Kelvin-Voigt shear modulus G_{KV} Figure 5.47: Probability density function G_{KV}

Fig. 5.46 and 5.47 show the histogram and the probability density function of the acceptance test calibration. It can be observed that the Kelvin-Voigt shear modulus shows a similar distribution as the elastic shear modulus G . Thus, the same type of distribution, the Rayleigh distribution, was picked to model the behavior.

All soil parameters to model the time dependent displacement components are stress and strain dependent. The evolution of these parameters can be observed in the parameters' magnitude, but the illustration of the trends is difficult. Generally, the Burger parameters decrease in magnitude for increased stiffness. This is most profound with the viscosity parameters. It is expected that the creep of an anchor increases with increased load. In section 5.2.1, it is illustrated that those parameters have the largest influence on the creep value. Therefore, the viscosity parameters must decrease for higher loads. It has been tried to establish empirical correlations to estimate this degradation, but no clear trend prevailed.

5.4. Parametric limits at failure

As a subsequent step, it was tried to derive the anchor’s failure conditions by increasing the load and then check for the parametric limits. The basis were the investigation and suitability tests, since it was established that the time-dependent information inherent to acceptance tests is of limited value for the application of this model. All the anchors within this database are designed according to the CUR 166 guidelines. This means that the failure load of the anchors is approximately 1.5 times the working load. At this failure load, the creep value should be ideally around 2 mm. Within the investigation tests it is observed that that is not always the case, the first anchor showed a creep value of ≈ 2.0 mm at its failure load, but the second anchor only had a creep of 1.75 mm. If it is assumed that the anchor is at failure for a creep value of 2 mm, the model can be solved for the parameters that influence the creep the largest for a limit value of 2 mm. The previous investigations showed that the Maxwell viscosity and the Kelvin-Voigt shear modulus have the largest contribution to the creep characteristics and were solved for. For this investigation, it is in the interest to keep as many variables as constants as possible to prevent interaction.

One disadvantage poses the creep value itself. It is a soft and ambiguous criterion, since different solutions are possible for the displacements to arrive at a creep value of 2 mm with this model at hand. Due to the lack of a better approximation, for this analysis only limit values in a similar range to the previously calibrated parameters are considered.

The solutions were obtained by using the ‘Least-squares’ method. However, especially for the Kelvin-Voigt shear modulus, it is important to establish proper bounds, to prevent physically unrealistic curve shapes of the output. If the Kelvin-Voigt components become too small, the displacements for $0 < t[s] < \approx 300$ are significantly smaller than the displacement at $t = 0$, which needs to be considered. The derived limit values provide a lower bound, because smaller stiffnesses and viscosity lead to larger displacement and creep.

| Anchor | μ_M [kPa·s] | μ_{KV} [kPa·s] | G_{KV} [kPa] |
|----------|-----------------|--------------------|----------------|
| Inv. 1. | 7.3E+9 | 7.9E+7 | 5.9E+5 |
| Inv. 2. | 7.3E+9 | 3.4E+7 | 3.8E+5 |
| Suit. 1. | 9.4E+9 | 1.8E+9 | 2.4E+6 |
| Suit. 2. | 7.9E+9 | 2.9E+8 | 2.4E+6 |
| Suit. 3. | 2.8E+9 | 7.9E+7 | 3.8E+5 |
| Suit. 4. | 2.8E+9 | 1.9E+8 | 1.6E+6 |
| Suit. 5. | 5.5E+9 | 3.5E+8 | 1.9E+6 |
| Suit. 6. | 5.6E+9 | 3.8E+8 | 1.1E+6 |
| Suit. 7. | 5.5E+9 | 8.0E+8 | 3.6E+6 |
| Suit. 8. | 5.5E+9 | 2.4E+7 | 6.2E+5 |
| Suit. 9. | 5.5E+9 | 1.3E+8 | 6.9E+5 |

Table 5.6: Limit Parameters corresponding to failure

It is observed from table 5.6, that the limit parameters are mostly in similar ranges for the considered tests. The limit Maxwell viscosity is for all anchors between 3E+9 and 9E+9. Also, the Kelvin-Voigt shear modulus shows a similar range for the limits. This procedure is rather imprecise. For the same anchor, different limit values can be found. This is because the soil parameters that need to be kept constant do not correspond to this limit load, and mainly because the model allows for multiple solutions.

An alternative computational approach that has not been investigated because it is not the primary scope of this research would be to impose strict boundaries to the resulting parameters curve shape. The strongest influence on the curve’s shape have the Kelvin-Voigt parameters. Based on the calibrated values, one could establish upper and lower bounds not only based on physically realistic shapes but also on physically realistic

curve progression. The latter can prevent that the derived limit parameters' displacement curve's magnitude is too large compared to what is expected. This would be an iterative approach, that could be reflected upon in further research.

To establish understanding of the anchor's utilization, either the limit load or the limit soil parameters need to be known. The database that was used in this context did not allow a proper estimation of the soil parameters at a set failure load because no site investigation for the parameters in question was carried out. Another alternative would be to investigate the soil parameters experimentally for certain stress and strain levels. Then, more accurate predictions about the anchor's behavior at failure and possibly limit loads can be made. In the following chapter, it is anticipated to relate these limit values to the anchor's reliability.

6. Bayesian Updating Results

In this chapter, the influence of Bayesian updating is investigated on the soil parameters. The general concept of this chapter is shown in the flow chart in Fig 6.1.

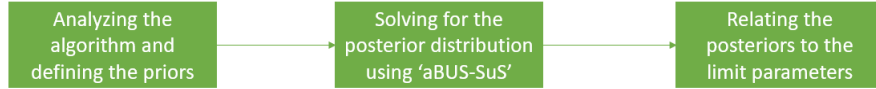


Figure 6.1: Procedure of the Bayesian updating chapter

The procedure on how the Bayesian updating is carried out is explained in the following. It was observed that for the parameters that govern the time-dependent displacements, weak prior distributions yield no proper results. Therefore, strong and informed priors are introduced. The investigation test's prior distributions are derived using the information from the calibration. Each set of investigated parameters used different types of prior distributions. Parts of the conclusions about the updating and its results can be related to the choice of the priors. The following tables provide an overview over the assumed prior distributions and their input parameters.

| | G | μ_M | μ_{KV} | G_M | G_{KV} |
|--------------|----------------------------------|--|--|---------------------------------|--------------------|
| Distribution | Uniform | Log-normal | Log-normal | uniform | Rayleigh |
| Parameters | $min = 10000;$ $max = 200000$ | $\mu = \mu_{M,Cal};$ $\sigma = \mu_{M,Cal}$ | $\mu = \mu_{KV,Cal};$ $\sigma = \mu_{KV,Cal}$ | $min = 10000$ $max = 200000$ | $\mu = G_{KV,Cal}$ |

Table 6.1: Set 1 - 5 Parameter, Prior distributions

| | G | μ_M | μ_{KV} | G_M | G_{KV} |
|--------------|----------------------------------|----------------------|-----------------------|-----------|--------------------|
| Distribution | Uniform | constant | constant | $G_M = G$ | Rayleigh |
| Parameters | $min = 10000;$ $max = 200000$ | $\mu = \mu_{M,Cal};$ | $\mu = \mu_{KV,Cal};$ | | $\mu = G_{KV,Cal}$ |

Table 6.2: Set 3 - 2 Parameter, Prior distributions

Set 4 is a new parameter set that was not introduced in the calibration analyses. This set is similar to set 3 but here, the Maxwell viscosity is included as well because of its major influence on the creep value.

| | G | μ_M | μ_{KV} | G_M | G_{KV} |
|--------------|----------------------------------|---|-----------------------|-----------|---|
| Distribution | Uniform | truncated-normal | constant | $G_M = G$ | truncated-normal |
| Parameters | $min = 10000;$ $max = 200000$ | $\mu = \mu_{M,Cal};$ $\sigma = 5 \cdot \mu_{M,Cal}$ $min = 1E + 9$ $max = 1E + 12$ | $\mu = \mu_{KV,Cal};$ | | $\mu = G_{KV,Cal}$ $\sigma = 5 \cdot G_{KV,Cal}$ $min = 1E + 5$ $max = \text{upper limit}$ |

Table 6.3: Set 4 - 3 Parameter, Prior distributions

The 'upper limit' referred to in table 6.3 is the physical upper bound chosen in a way that the shape is still

realistic. Both Kelvin-Voigt parameters should be limited in such a fashion because from a certain magnitude on the displacements curve shape becomes physically unrealistic.

The aBUS-SuS algorithm needs 4 quantities as an input: the amount of samples that is generated in each subset, the prior distribution, the likelihood function and the probability of intermediate failure domains p_0 . Now the investigation focused mainly on variations of the amount of updated parameters, different prior distributions and different sample amounts. The intermediate failure probability and the definition of the likelihood function were not altered and chosen according to the recommendations of the authors of the algorithm ($p_0 = 0.1$)[4].

The algorithm calculates different threshold levels, where each level has a nested failure domain and the samples within approach the final posterior distribution. With each level, the posterior is better approximated and the domain becomes smaller. The following figure shows how this convergence towards the posterior distribution can look like. The algorithm stops once this threshold level becomes 0 for two consecutive times. This is illustrated in Fig. 6.2.

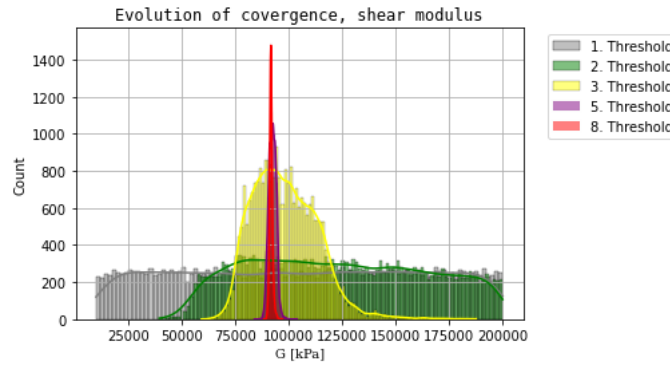


Figure 6.2: Convergence of each threshold level towards final posterior

6.1. Artificial Case

To understand how the algorithm and the analytical model work together, an artificial case is investigated for the 5 parameter set. Table 6.4 shows the true parameters.

| | $G[kPa]$ | $\mu_M[kPa \cdot s]$ | $\mu_{KV}[kPa \cdot s]$ | $G_M[kPa]$ | $G_{KV}[kPa]$ |
|------------|-----------------------------------|---|--|-----------------------------------|---------------|
| True value | 80000 | $5E+9$ | $1E+8$ | 85000 | $3E+6$ |
| Prior type | uniform | truncated-normal | truncated-normal | uniform | Rayleigh |
| Parameters | $min = 10,000$ $max = 100,000$ | $\mu = 5E+09$ $\sigma = 0.5 \cdot 5E+09$ $min = 1E+08$ $max = 1E+12$ | $\mu = 1E+08$ $\sigma = 0.5 \cdot 1E+08$ $min = 1E+7$ $max = 1E+10$ | $min = 10,000$ $max = 100,000$ | $\mu = 3E+06$ |

Table 6.4: Artificial analysis true parameters

The figure 6.3 shows the results of the updating algorithm. To show all values in the same graph, each parameter has been normalized by its initial value and the ratio is shown. The closer to the black indicator line, the better the concordance.

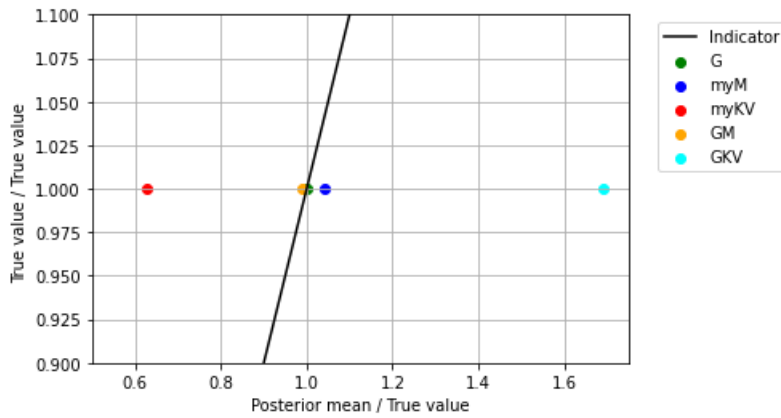


Figure 6.3: Artificial Data case, 5 parameters

It can be observed, that for some parameters there is a large deviation, for the Kelvin-Voigt viscosity, and for the Kelvin-Voigt shear modulus. The shear modulus and the Maxwell parameters provide quite a decent fit. Therefore, these posteriors need to be assessed with care, since the accuracy is compromised.

6.2. Investigation Test Results

Three sets of parameters are investigated, similar to the calibration. The first set, 'Set 1', is the full set, where all soil parameters are updated, the second one, 'Set 3', is the reduced set with only two variable soil parameters. The original 'Set 2' investigation is no longer considered for the Bayesian updating due to the quality of the results. For reasons of consistency, the Sets' names remain the same. In reference to the Maxwell viscosity's strong influence on the creep value and the precision of the posteriors that can be generated, another set - Set 4, is introduced. This set is a 3 Parameter set, shear modulus G , Maxwell viscosity μ_M and Kelvin-Voigt shear modulus G_{KV} .

6.2.1 Set 1 - 5 Parameters

The primary reason to choose strong priors for the time influential parameters is the quality of the results. It was observed that the posteriors for the Maxwell viscosity, the Kelvin-Voigt viscosity and the Kelvin-Voigt shear modulus are always located around the upper limits of the uniform distribution, no matter how physically unrealistic those might be.

For both viscosity parameters, a wide normal distribution with its location at the value from the calibration has been tried, but the algorithm returns negative values as a result, even though the probability of those occurring is very low. Thus, a distribution that does not allow negative values had to be chosen. Therefore, the log-normal distribution had been introduced for those two parameters.

For the Kelvin-Voigt shear modulus prior distribution, the information from the acceptance test calibration was utilized. There, it has been determined that a Rayleigh distribution fits the distribution reasonably well (Fig. 5.47). In another investigation, the prior distributions were changed to truncated normal distributions for the viscosity parameters and the Kelvin-Voigt shear modulus. The results were not largely deviating from the results of the other sets, examples are in appendix D.1.4.

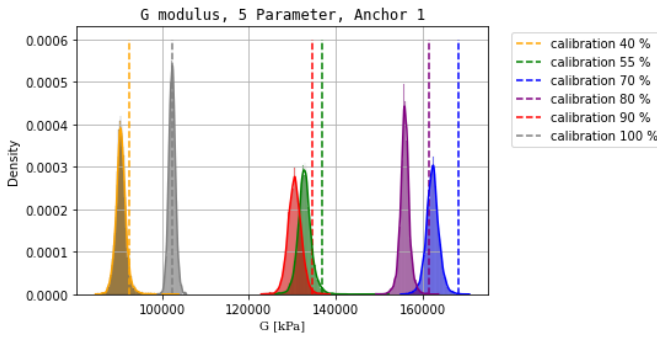


Figure 6.4: Posterior distributions, Shear modulus

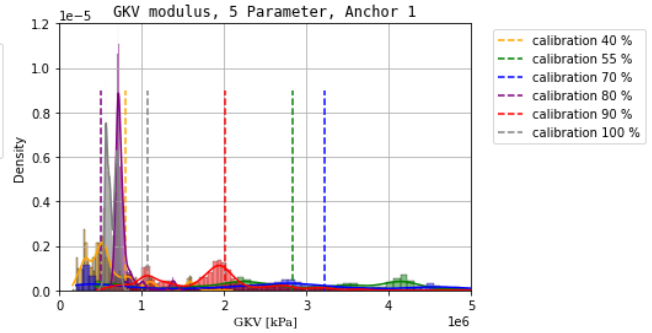


Figure 6.5: Posterior distributions, Kelvin-Voigt shear modulus

The posterior of the shear modulus shows profound peaks, all around the calibrated values. However, the means of the posterior distributions are all smaller than the calibrated value. This suggests a slight overestimation from the calibration or an underestimation by the Bayesian updating.

The Kelvin-Voigt shear modulus shows noisy, multimodal behavior. This means that several peaks are observed, especially in the posterior of the 90 % load step. The posteriors are very noisy, but the trend can still be determined. Another observation is that the posterior distributions, for the 40 % and 55 % loading, are wider with less pronounced peaks. This is also observed for the other time-dependent parameters. Concerning both viscosity parameters, the 40 % and 55 % load steps are not included due to their flat posteriors. The reason for this is the amount of measurement points within the 40 % and 55 % loading. There, the displacement measurements consist only of 8 data points opposing to the 17 at 100 %, with which 5 soil parameters and the covariance are supposed to be updated.

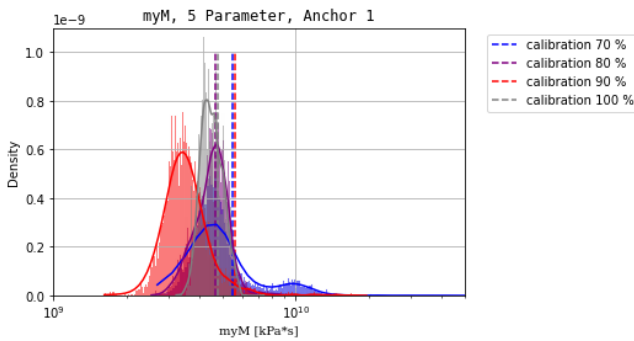


Figure 6.6: Posterior distributions, Maxwell viscosity

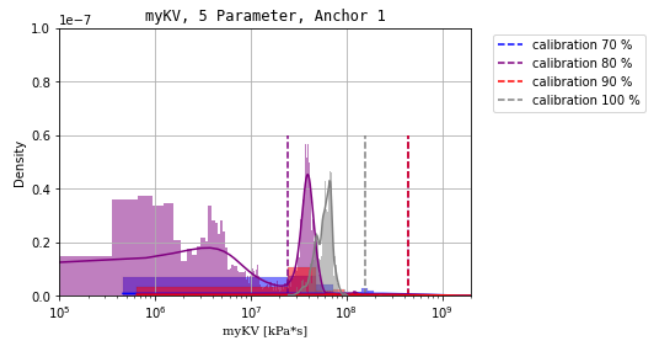


Figure 6.7: Posterior distributions, Kelvin-Voigt viscosity

For the Maxwell viscosity, satisfactory posteriors could be calculated for the 70 % - 100 % loading. Their mean values are all close around the calibrated values, and within a reasonable magnitude. The Kelvin-Voigt viscosity has diffuse posterior distributions. It can be observed that a lot of samples fall into the lower magnitudes of the domain. Based on the artificial analysis, it was expected that the quality of the Kelvin-Voigt viscosity posterior distribution could be insufficient. One explanation is that the lower bounds are not properly limited within the prior distribution, which leads to a weak prior. Therefore, no result can be found, since it was determined that the procedure works only for strong priors.

Below, the calculated credible intervals for 80 % and 100 % loading are shown.

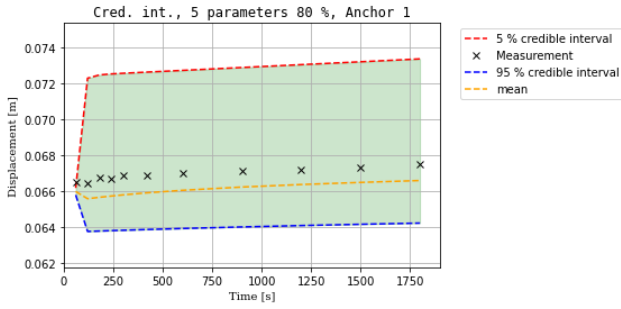


Figure 6.8: Credible intervals, Anchor 1, 80 % loading

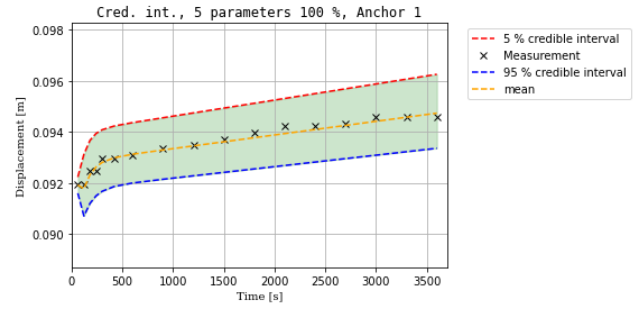


Figure 6.9: Credible intervals, Anchor 1, 100 % loading

For Fig. 6.8, it is clear, the main source of the spread is the wide posterior of the Kelvin-Voigt viscosity in Fig. 6.7. One major observation for anchor 1 is that the uncertainty given by the credible intervals decreases for larger load steps. The further the anchor is loaded, the narrower the bounds are lying. However, this is not always the case. The results from the second anchor in Fig 6.10, 6.11, which are shown below, indicate the opposite. Another contribution to the wide credible intervals is the fact that the Maxwell shear modulus is an updated parameter. It is clearly visible, in reference to the sensitivity analysis, 5.2.1, Figure 5.6, that this parameter majorly contributes to the spread that is observed.

It is important to note that this set is not underlying the same type of prior distributions as for some of the other sets. Since both Kelvin-Voigt components have no underlying lower limit that is bound to the curve’s shape, the lower credible intervals and the lower boundary is not precise. The wide spread of the posterior of the Kelvin-Voigt component can be observed in Figure 6.7 at 80 %, which explains this irregularity.

For the second anchor, just the credible intervals are shown, since the general trends of the posterior distributions are similar as for the first anchor.

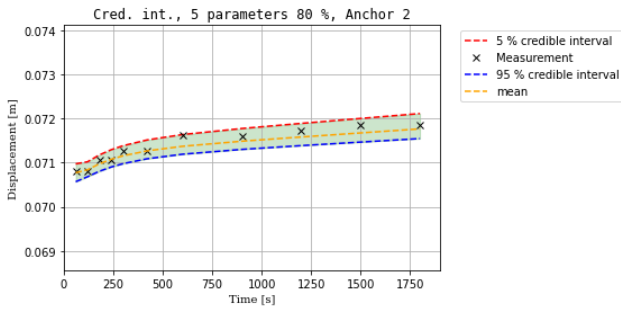


Figure 6.10: Credible intervals, Anchor 2, 80 % loading

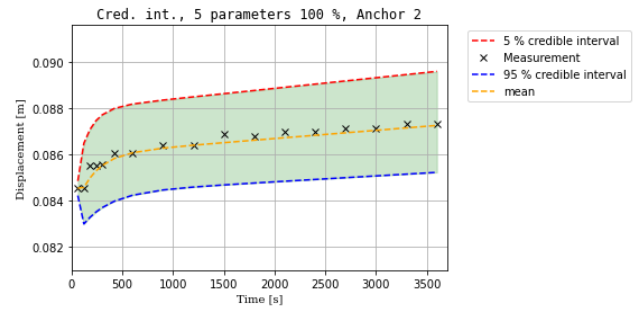


Figure 6.11: Credible intervals, Anchor 2, 100 % loading

Figure 6.10 shows how irregular the observations and trends are, especially concerning the Kelvin-Voigt viscosity. In this case, the spread is small, since the Kelvin-Voigt viscosity posterior is a dense distribution (Fig D.4). From the plots of the credible intervals and the sensitivity analysis 5.2.1, the spread of each of the parameters can be observed. Where, the posterior distributions of the shear modulus are dense, the initial displacement’s divergence is small. Where the spread is large, for this set this is mainly due to the lower bounds and larger spread of the Kelvin-Voigt viscosity. It is clear that the definition of the prior distribution plays the most governing factor in the quality and density of the results.

6.2.2 Set 3 - 2 Parameters

The 2 Parameter set offers, due to its amount of variables, a two-dimensional range. Therefore, it is possible to evaluate the likelihood function and illustrate the results with common 2D graphs. For higher dimensional problems, this illustration would be very complex. Thus, the following likelihood analysis is only carried out for this parameter set. The log-likelihood function is evaluated for anchor 1 based on random values of the prior distribution, here with 10000 samples. Each dot represents a sample with a positive likelihood. The colors and the legend denote the magnitude of the likelihood.

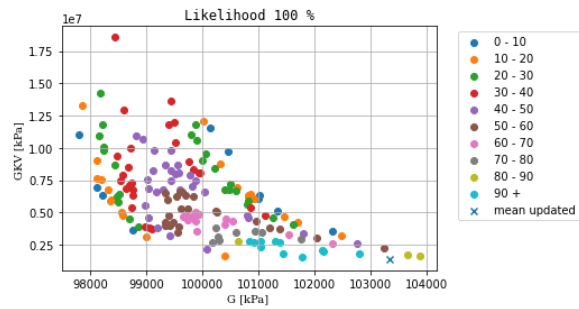
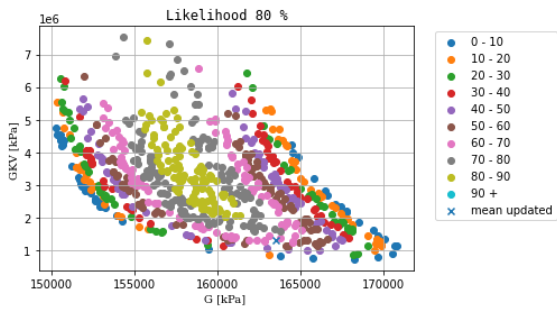


Figure 6.12: Log-Likelihood convergence, 80 % loading Figure 6.13: Log-Likelihood convergence, 100 % loading

In Fig. 6.12 and 6.13, it can be observed that for a higher likelihood, the limits become smaller. Here, the maximum likelihood converges overtime towards the mean of the updated samples. Furthermore, a negative correlation can be observed. For a higher shear modulus, the Kelvin-Voigt shear modulus becomes smaller. Overall, just a plot of the evaluated likelihood function gives already a good insight in which range the updated parameters are going to lie. The likelihood function has for all load steps a specific 'banana-like' shape, and its location can be estimated without evaluating the algorithm. This is interesting because, it gives insight about the expected range of the posterior distributions. The typical result would be that the likelihood converges towards a circular range of values, but here, especially regarding the Kelvin-Voigt shear modulus, a 'corridor' is the result. This shows clearly that for this parameter set, the main uncertainty revolves around the Kelvin-Voigt shear modulus.

Another observation is the amount of positive likelihood results. The figures 6.12 and 6.13 show, for the 10,000 samples, all data point in the graph. The observed trend is that the amount of possible results (samples that have a positive likelihood) is decreasing over increased loading. An explanation for this is that the amount of measurement data points increases with the loading, and the likelihood must become overall smaller, because possible fits are more seldom.

After this analysis, the Bayesian updating algorithm is applied to the problem. The posterior samples distributions are shown below.

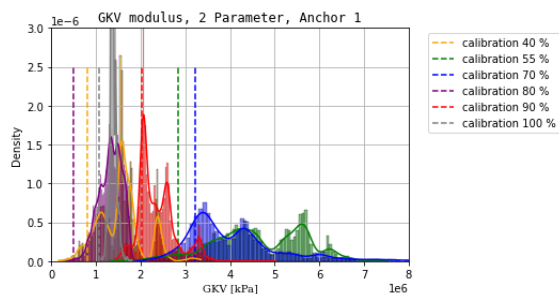
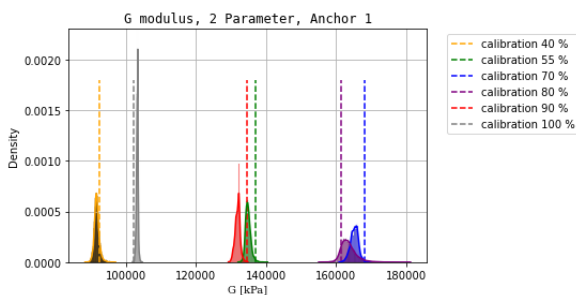


Figure 6.14: Posterior distributions, Shear modulus

Figure 6.15: Posterior distributions, Kelvin-Voigt shear modulus

For the third set, with just 2 parameters involved, the posterior shear modulus develops strongly pronounced peaks. For all load steps, the updated mean value lies below the value from the calibration. The Kelvin-Voigt shear modulus shows a more complex posterior distribution. The trend of the calibration, which load step has smaller or larger magnitudes inherent, is observable in a similar way. However, the divergence between the calibration and the posteriors is more profound than for the shear modulus. The means of the posterior distributions are observed to be larger than the calibrated values.

The calculation of the credible intervals are shown in the following figures.

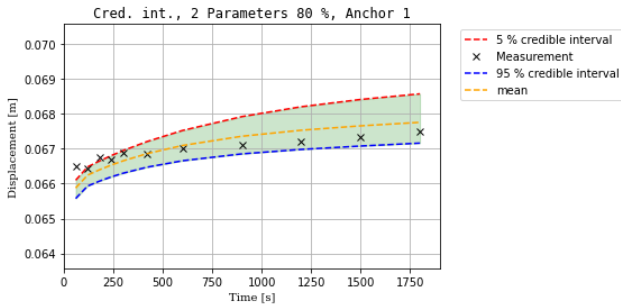


Figure 6.16: Credible intervals, Anchor 1, 80 % loading

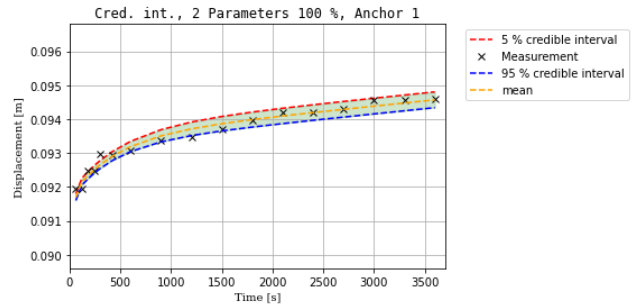


Figure 6.17: Credible intervals, Anchor 1, 100 % loading

It can be observed that for the 2 parameter set, the spread decreases with increased loading. At 100 % loading, the credible intervals are only marginally larger or smaller than the spread of the measurements. Within the updating process, the measurement uncertainty is not quantified, but here the remaining uncertainty in the posteriors is limited to this measurement uncertainty. Again, the small divergence can be related to the dense posteriors shown in figure 6.14 and 6.15 for both parameters.

The second anchor shows similar behavior as the first anchor. The results are not included here, but can be found in the appendix D.7, D.8.

6.2.3 Set 4 - 3 Parameters

In the following, the results for the 3 parameter investigation are presented. Here, different estimations for prior distributions are chosen. The shear modulus prior was kept uniform, but the Maxwell viscosity and the Kelvin-Voigt shear modulus are truncated normal distributions. The limits were chosen based on the physical boundaries of the shape of the displacement curve.

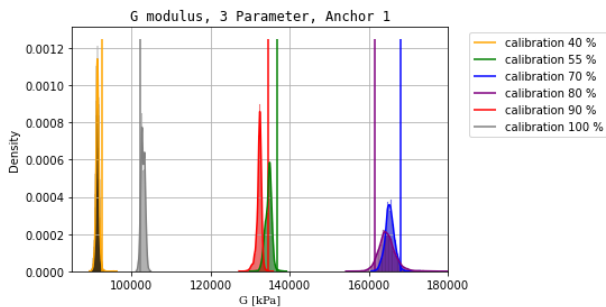


Figure 6.18: Posterior distributions, Shear modulus

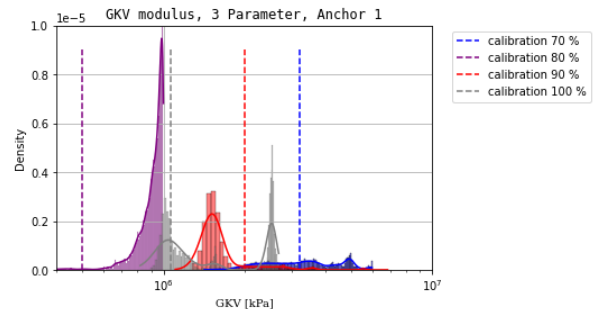


Figure 6.19: Posterior distributions, Kelvin-Voigt shear modulus

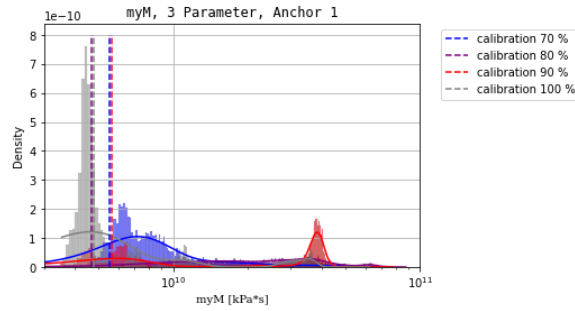


Figure 6.20: Posterior distributions, Maxwell viscosity

The difference in the posteriors of the shear modulus compared to the ones from Set 1 and 3 is only small. There are slight variances in the shape and in standard deviation, but nearly negligible, Fig. 6.18. It can be observed that the posterior distribution of the Kelvin-Voigt shear modulus, Fig. 6.19, is more clear and less noisy compared to the other sets, but still multimodal at 100 % loading. The results of the Maxwell viscosity posteriors, Fig. 6.20, are not as dense as for example of the first set, Fig. 6.6, but the posteriors are nevertheless regarded as useful. The two lower load steps were again not included in the plots.

The benefit of this set shows itself in the calculation of the credible intervals.

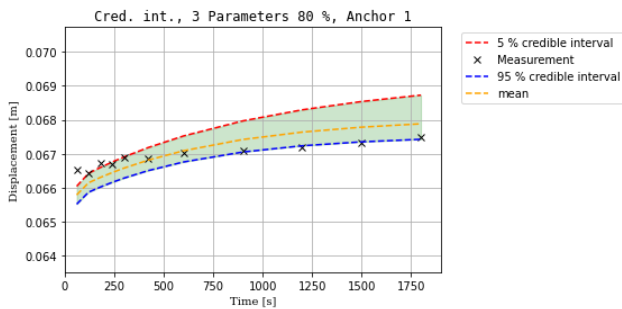


Figure 6.21: Credible intervals, 80 % loading

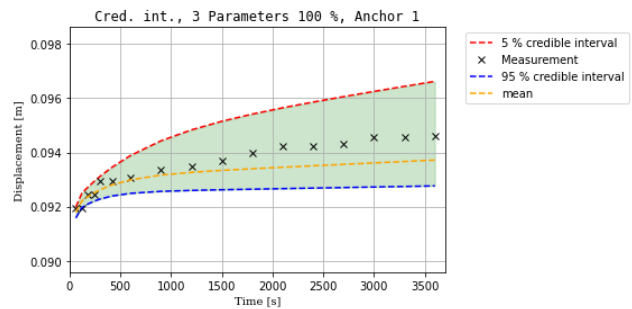


Figure 6.22: Credible intervals, 100 % loading

For Set 3, the Maxwell viscosity is regarded as a constant. Therefore, the gradients of the credible bounds are the same. Here, the Maxwell viscosity is an updated parameter and at the upper load steps, the gradients are not as stationary as for the 2 Parameter set. These credible intervals, Fig. 6.21, 6.22 capture more realistic anchor behavior compared to Set 3 and higher quality posteriors compared to Set 1. Furthermore, the spread of the credible bounds becomes larger and not smaller with increased loading. This characteristic is expected to capture the behavior of the anchor in a more realistic manner. However, compared to Set 1, in this set, the mean of the posteriors does not have the same quality of concordance to the measurements. The results of the second anchor show the same trends, and are in the appendix, Fig. D.12, D.13.

6.2.4 Large Sample Size Investigation

For two sets, the calculation was once executed with large sample sizes of 100,000 to check on the effect on the results. In advance, the effect is quite pronounced. Generally, the noise is reduced, and the posteriors could peak at locations where previously there was just a minor peak. Another phenomenon is that the whole distributions slightly shift. This could be a phenomenon due to larger sample amounts or just due to inherent uncertainty of the procedure, which shows itself in slightly different results upon re-evaluation of the algorithm. For Set 1 and Set 4, the opposite phenomena are observed. While the 5 Parameter set

develops more multimodal distributions and larger standard deviations, are the posteriors of the 3 Parameter set narrowed down by a larger sample amount. The observations are summarized within the figures 6.23 and 6.24 in red.

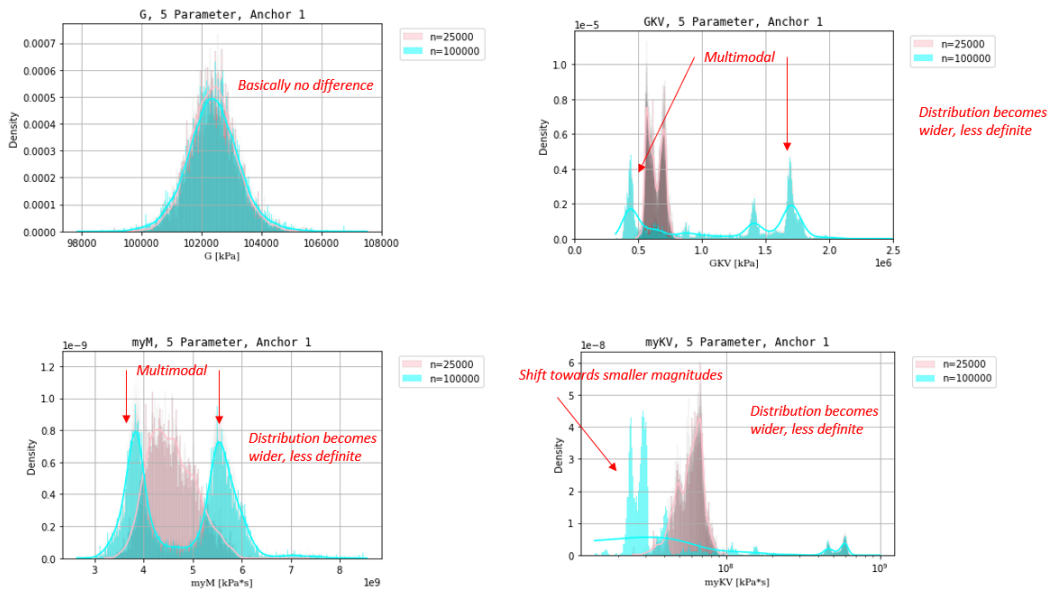


Figure 6.23: Comparison of larger samples sizes, 5 Parameters

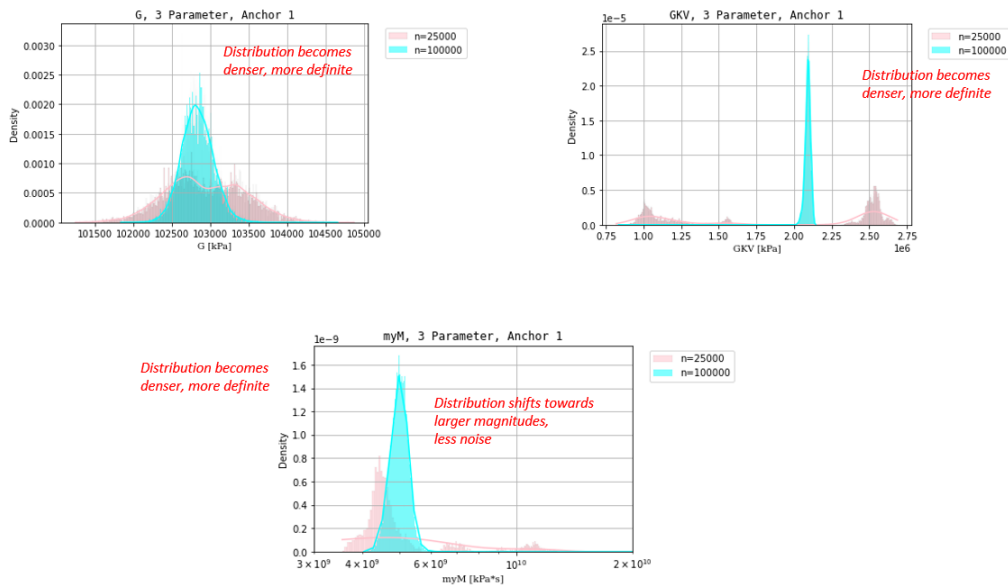


Figure 6.24: Comparison of larger samples sizes, 3 Parameters

It was expected that more samples lead to larger certainty in the form of larger densities and less noise. However, for the 5 Parameter investigation, the opposite is the case. Furthermore, the Kelvin-Voigt viscosity shifts to the left side of the scale and becomes smaller. Smaller parameters mean larger displacements in the design and more safety. At this point, it is not possible to give a reasonable explanation for this behavior. For the 3 Parameter investigation, the expected result holds and the posteriors, especially of the GKV modulus, are far more definite. The mean value of the Maxwell viscosity becomes larger and represents smaller displacement curve gradients. This shift means that the large sample distribution shifts closer to the less conservative

domain.

6.3. Suitability Test Results

The same analyses of the previous sections have been carried out for the suitability tests. This means the suitability calibration results were used as mean values for different types of distributions within and varying numbers of updated parameters for reasons of consistency. Conceptually, an alternative would be to use the calibration results of the investigation test. However, the suitability tests and the investigation test frameworks are not the same. Anchor dimensions and test loads vary and therefore, the stress and strain conditions as well. Therefore, the most logical approach in the scope of this analysis is to update each anchor individually. For this investigation, only the data from the full loading at 100 % was considered. The reason is that the amount of measurement points is smaller for the suitability tests, and the previous investigations proved that this leads to results of low quality. For each set, 15000 samples were generated for each parameter and anchor.

6.3.1 Set 1 - 5 Parameters

The shapes of the distributions, the magnitude of the parameters and of the magnitudes of the densities were all in a similar range as calculated for the investigation tests.

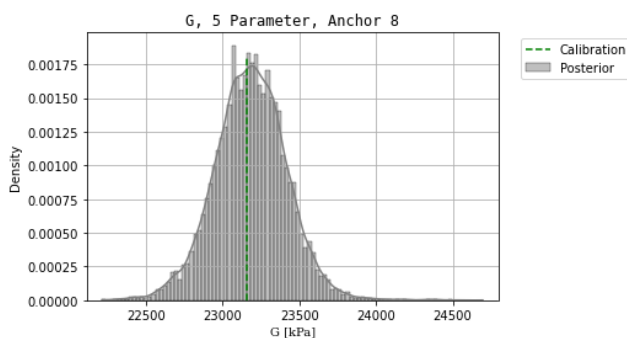


Figure 6.25: Posterior distribution, Shear modulus

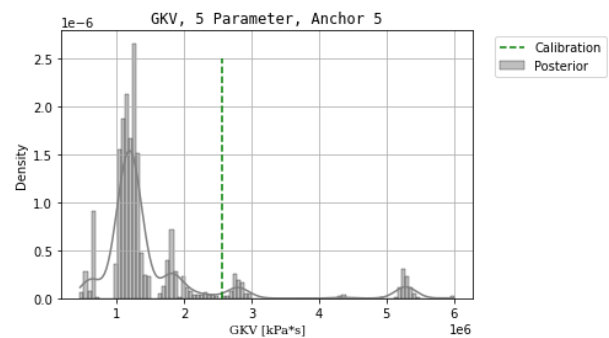


Figure 6.26: Posterior distribution, Kelvin-Voigt shear modulus

Concerning the shear modulus, the same resemblance to the typical Gaussian 'bell' shape as previously observed can be found. Interestingly, here, the calibration values do very closely coincide with the mean values of the posterior distribution. The Kelvin-Voigt shear modulus shows an equally noisy and slightly multimodal posterior as in the investigation tests.

The viscosity parameters also resemble in their posterior shapes the posterior shapes of the investigation tests.

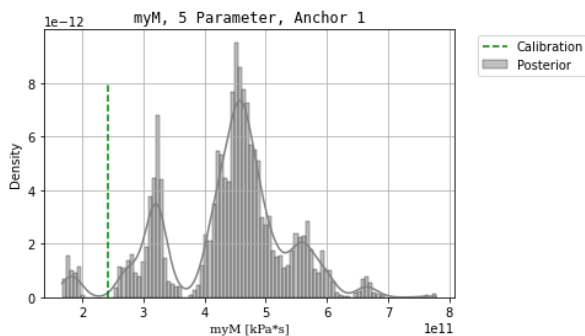


Figure 6.27: Posterior distribution, Maxwell viscosity

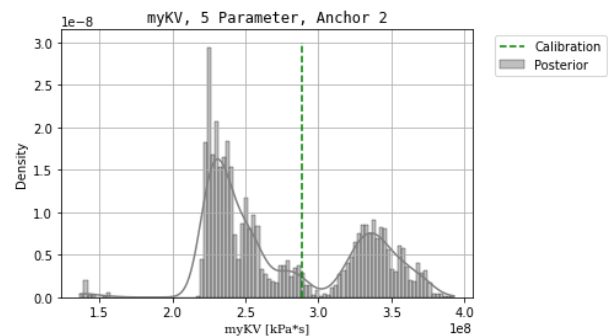


Figure 6.28: Posterior distribution, Kelvin-Voigt viscosity

Again, the viscosity posteriors, Fig. 6.27, 6.28, are slightly multimodal. Often, when the posteriors show multi-modality, a 'wave-like' shape can be observed. There is a main peak and then typically to the right-hand side, so in the direction of larger parameter values, there are more peaks gradually decreasing in their density. This can be observed in all time-dependent parameters presented here (Fig. 6.26, 6.27, 6.28).

Another observation is a consistent trend concerning the calibration values compared to the posteriors. For a distinct majority of the anchors, the posterior mean of the Kelvin-Voigt shear modulus and of the Kelvin-Voigt viscosity is smaller than the calibration, for the Maxwell viscosity the posterior mean is larger.

6.3.2 Set 3 - 2 Parameters

The figures 6.29 and 6.30 show the posterior distributions of the 2 parameter investigation.

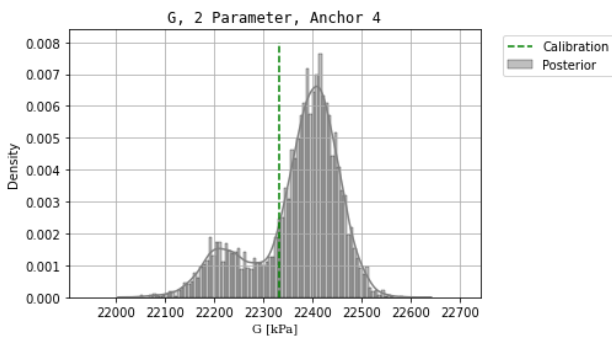


Figure 6.29: Posterior distribution, Shear modulus

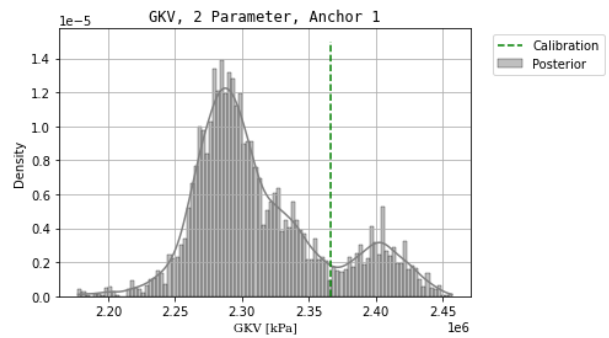


Figure 6.30: Posterior distribution, Kelvin-Voigt shear modulus

The shear modulus distribution illustrated in Fig. 6.29 does not show the same single modal shape as in the 5 Parameter investigation. Also, the density is larger. The Kelvin-Voigt shear modulus posteriors are similar to the other parameter sets, in their shape and magnitude of the density. Opposing to Set 1, no major trend has been observed for both parameters, concerning the posterior mean and its location compared to the calibration value.

6.3.3 Set 4 - 3 Parameters

The figures 6.31, 6.32 and 6.33 show the posteriors of the 3 Parameter investigation.

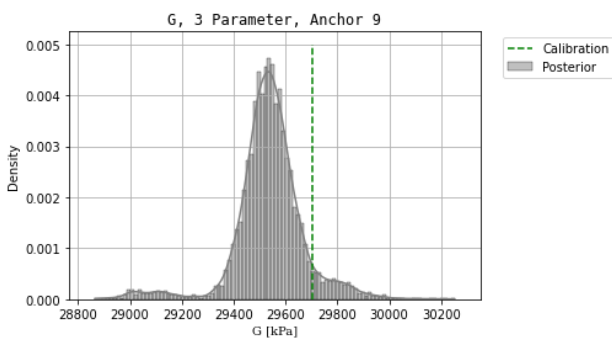


Figure 6.31: Posterior distribution, Shear modulus

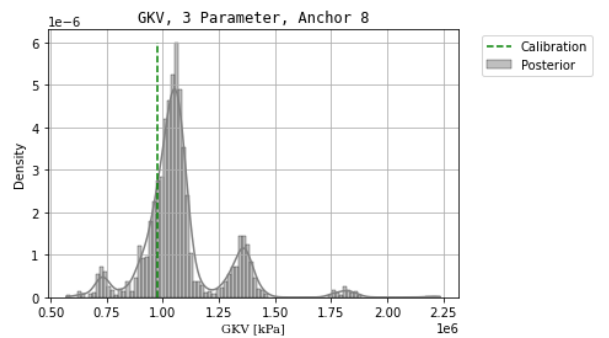


Figure 6.32: Posterior distribution, Kelvin-Voigt shear modulus

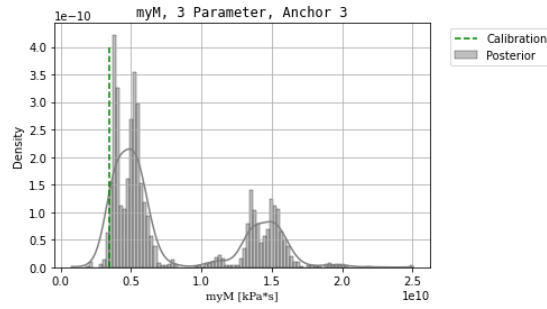


Figure 6.33: Posterior distribution, Maxwell viscosity

Again, the shear modulus exhibits a Gaussian-shaped distribution. Sometimes, as shown in Fig. 6.31, minor variations from the ideal shape are observed. The shape and densities of the Kelvin-Voigt shear modulus and the Maxwell viscosity are as previously described for the other sets. Important to note here, is the clear trend concerning the posteriors' relation towards the calibration value. For the shear modulus, the posterior mean was uniformly smaller than the calibration value, while it was larger for the Maxwell viscosity and for the Kelvin-Voigt shear modulus.

6.3.4 Credible Intervals

The following figures present the calculated credible intervals of each set.

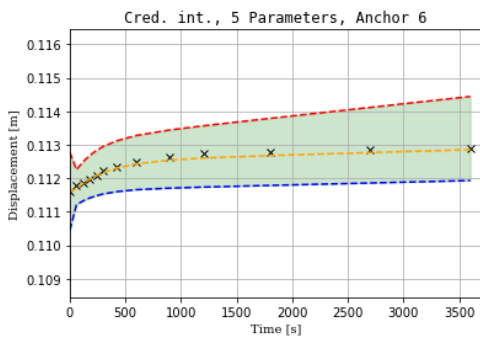


Figure 6.34: Credible intervals, Set 1

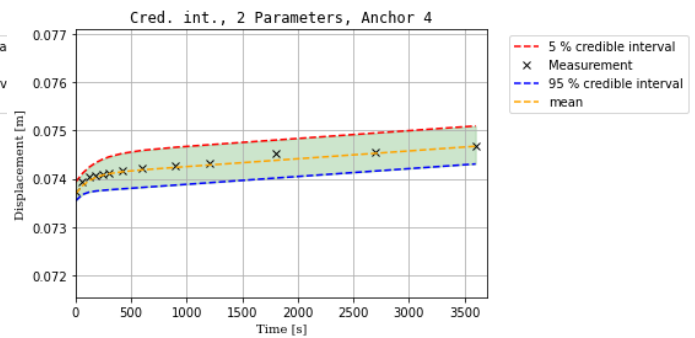


Figure 6.35: Credible intervals, Set 3

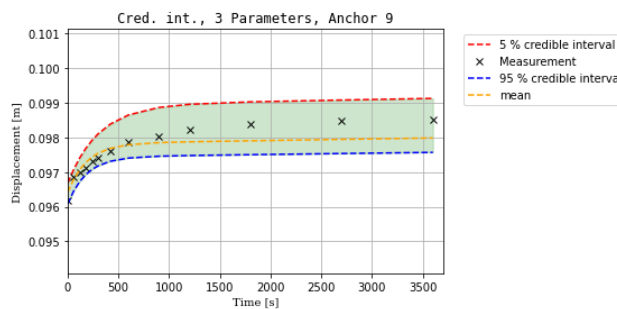


Figure 6.36: Credible intervals, Set 4

The underlying uncertainty and the distance of the bounds of the credible intervals follow the same patterns as for the investigation tests. This means, the more parameters are updated, the larger the uncertainty is since the uncertainty underlying the constant parameters is not captured by the algorithm. This means that even though the spread is the largest for the 5 Parameter investigation, the certainty that those bounds hold

is the largest. The 5 Parameter and the 3 Parameter sets' mean displacements are for most anchors below the measurements in their magnitude. For the 2 Parameter set, this fit is the "best" one. There, the bounds around the measurements are again the narrowest, because the viscosity parameters are not accounted for in the updating procedure and the values are understood as 'certain'.

6.4. Reliability analysis

In the following, the results of the preliminary reliability analysis are shown. The parametric limits that were calculated in chapter 5.4 are now related to the posterior distributions to make a statement about the anchor's reliability towards failure. The investigation tests provide a baseline of the accuracy of the procedure. Despite the satisfactory fits to the displacements and narrow credible intervals, Set 3 (2 Parameters) is not considered for the reliability analysis as the Set 3 results and corresponding limit parameter are judged to lack sufficient accuracy. For Set 3 only a single parameter governs the time dependent displacements. With the limit parameters used, the expected results that are presented in the next section could not be confirmed. One explanation for this is that under the assumption of a constant viscosity, no proper limit parameters could be calculated and furthermore, no precise estimations about the anchor's reliability can be made from the resulting posterior distributions. For such an analysis, further research is necessary.

6.4.1 Investigation Tests

At 100 % loading, for the first anchor a creep value of 2.0 mm was measured, which is the defined failure condition. This means that the posterior samples are expected all to be below the limit parameter. Generally, the limit parameters correspond to a lower bound, because smaller stiffness and viscosity lead to larger displacement and creep. The figures 6.37, 6.38 and 6.39 show this for the first anchor and 'Set 1 - 5 Parameters'.

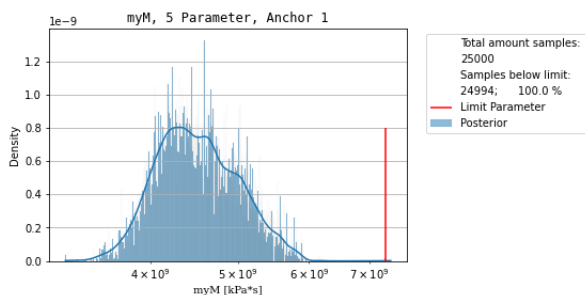


Figure 6.37: Maxwell viscosity posterior vs. Limit Parameter

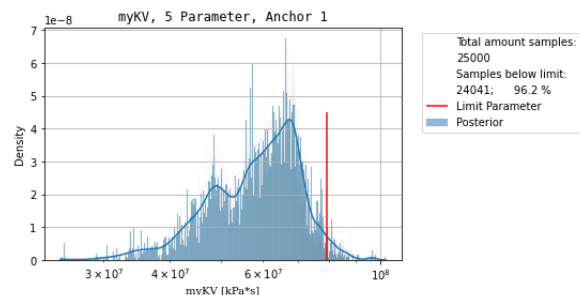


Figure 6.38: Kelvin-Voigt viscosity posterior vs. Limit Parameter

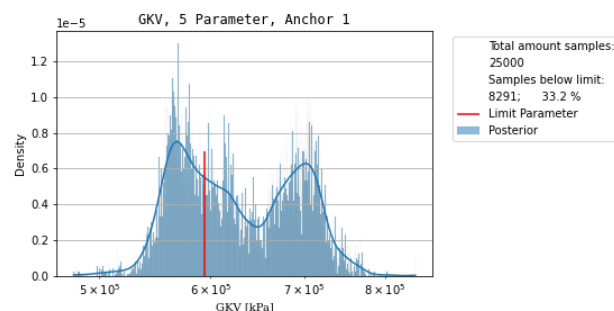


Figure 6.39: Kelvin-Voigt shear modulus posterior vs. Limit Parameter

The Maxwell viscosity, has the largest influence on the creep and shows clear results. The majority of the

samples are below the critical limit, which suggests anchor failure. The Kelvin-Voigt viscosity follows the same trend, the majority of the samples are below the limit value. For the Kelvin-Voigt shear modulus, this is not the case. Here, the majority of the samples are above the failure limit, indicating reserves in the anchor’s capacity.

The second anchor measured a creep value of 1.75 mm at 100 % loading. Following this, the posteriors are expected to show a form of a transition state, close before failure.

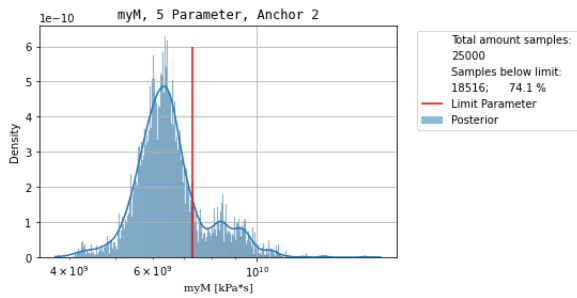


Figure 6.40: Maxwell viscosity posterior vs. Limit Parameter

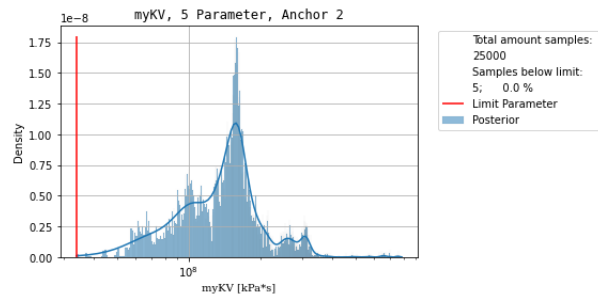


Figure 6.41: Kelvin-Voigt viscosity posterior vs. Limit Parameter

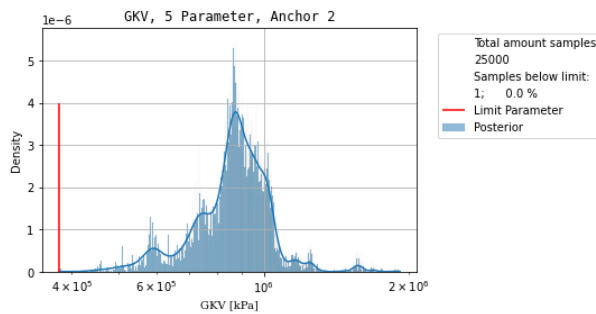


Figure 6.42: Kelvin-Voigt shear modulus posterior vs. Limit Parameter

The majority of the Maxwell viscosity samples are below the limit value, which indicates failure. The other parameters show the opposite, the majority of samples are above the limit value. From the second anchor, it becomes evident that the Maxwell viscosity posterior is a proper failure indication because it shows that the anchor is close to failure but also that there are still some reserves. Both Kelvin-Voigt parameters seem to be more sensitive, and failure conditions must not be indicated by large percentages below the limit value.

The results of the 3 Parameter set are shown below.

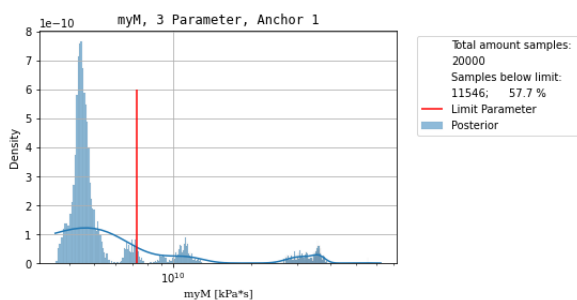


Figure 6.43: Maxwell viscosity posterior vs. Limit Parameter

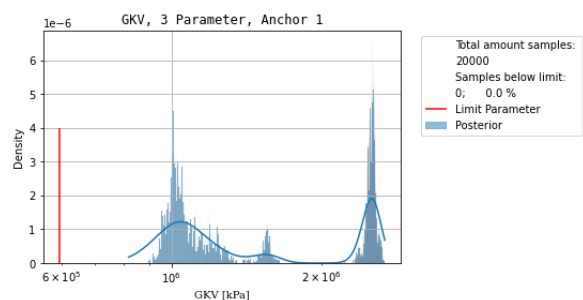


Figure 6.44: Kelvin-Voigt shear modulus posterior vs. Limit Parameter

In figure 6.43 it can be observed that for the Maxwell viscosity, a close majority of the posterior samples is below the failure limit, indicating failure conditions. However, the upper tail of the posterior is spreads long, which means that the actual amount below the limit is just $\approx 60\%$. The Kelvin-Voigt shear modulus posterior is further away from the limit and therefore not as precise.

The second anchor draws a similar picture.

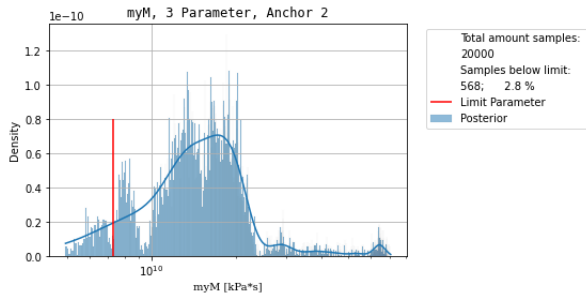


Figure 6.45: Maxwell viscosity posterior vs. Limit parameter

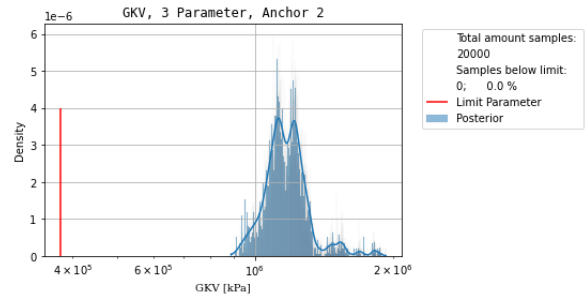


Figure 6.46: Kelvin-Voigt shear modulus posterior vs. Limit parameter

Here, the percentage of samples depicting failure is just 2.8 % for the Maxwell viscosity in Fig. 6.43. The Kelvin-Voigt shear modulus posterior is now even further away of the failure limit.

For the 3 Parameter set, it was observed that fewer samples are located in the failure domain compared to Set 1. This means that for Set 4, the percentage below the failure limit must be interpreted differently than for Set 1.

The graphs 6.47 and 6.48 show the evolution of the percentage of samples in the failure domain.

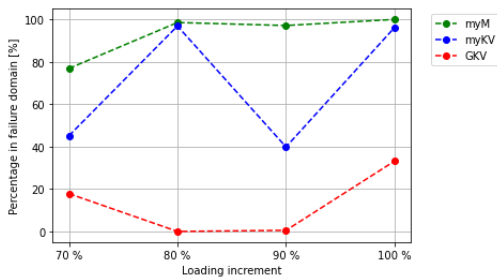


Figure 6.47: Samples in failure domain, 5 Par., Anchor 1

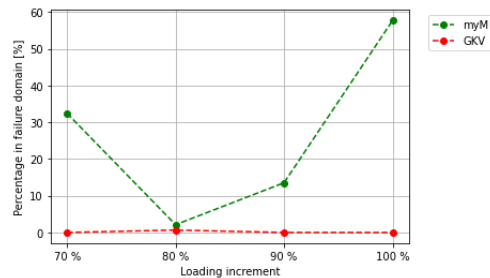


Figure 6.48: Samples in failure domain, 3 Par., Anchor 1

From the graphs, a trend can be observed that the amount of samples in the failure domain increases with increased loading. It is noted that the load steps 40 % and 55 % were not included in the figures, since the percentage in the failure domain is zero for those load steps.

The graphs for the second anchor draw an unclear picture because they show large percentages of samples in the failure domain for the earlier load steps. However, from 90 % loading to 100 % loading, a gradual increase of the failure percentages is observed, which supports the observations of the first anchor.

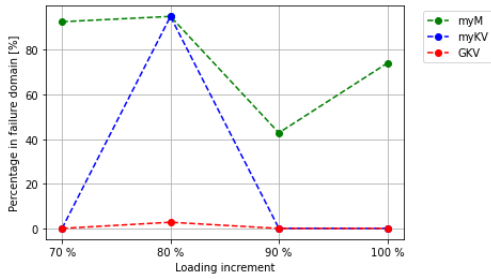


Figure 6.49: Samples in failure domain, 5 Par., Anchor 2

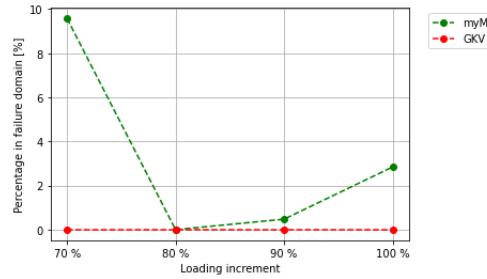


Figure 6.50: Samples in failure domain, 3 Par., Anchor 2

The second anchor shows an indication of failure around load step 80 %. However, after that, the posteriors seem to shift away from this boundary. Interestingly, at the same loading increment, the first anchor also exhibits large percentages of samples in the failure domain. Another observation is that the 3 Parameter set seems to have more inertia inherent in its posteriors. The overall magnitudes of the percentages are lower, and the increase or decrease are less profound. The lower magnitude either means that the 3 parameter set appoints larger safety reserves to each anchor, or that the values need to be interpreted differently compared to the 5 parameter set.

All in all, this procedure gives an indication on how close the anchor is to failure. The percentages of anchors in the failure domain confirm the failure indications set by the creep value. It is difficult to put the numbers of the posteriors into context to define a proper reliability index. For this, the procedure would need to be tested on a larger database. Nevertheless, the failure limits seem to give a valid indication of the actual anchor failure, at least for most of the parameters, even if it is more of a qualitative criterion at this point.

6.4.2 Suitability Tests

In the following, the same analysis is carried out with the suitability test posteriors. The limit parameters relate to total failure (2.0 mm creep) underneath maximum loading ($1.5 \cdot P_0$). This procedure is slightly inconsistent because those limit parameters were calculated with the rest of the soil parameters belonging to 100 % loading, while the considered loading would be 150 %. That discrepancy is accepted because of the lack of an approximation of the parametric evolution over increased loading. All results cannot be shown here, only the most relevant ones are presented. For the 5 parameter set, the majority of the anchors' posteriors have small percentages of samples in the failure domain (6 out of 9 below 3 %) for the Maxwell viscosity. Those results are summarized in table 6.5 below.

| Anchor | μ_M | μ_{KV} | G_{KV} | creep [mm] |
|--------|---------|------------|----------|------------|
| 1 | 0 % | 24.8 % | 26.8 % | 0.27 |
| 2 | 0 % | 63.7 % | 0.9 % | 0.17 |
| 3 | 2.6 % | 0 % | 39.4 % | 0.63 |
| 4 | 66.0 % | 99.9 % | 98.2 % | 0.50 |
| 5 | 0 % | 89.5 % | 86.6 % | 0.30 |
| 6 | 12.0 % | 66.4 % | 55.5 % | 0.43 |
| 7 | 0 % | 99.9 % | 0 % | 0.43 |
| 8 | 39.6 % | 60.6 % | 0 % | 0.33 |
| 9 | 0 % | 1.7 % | 8.3 % | 0.50 |

Table 6.5: Suitability test results, Limits, 5 Parameter

One of the more unexpected results is anchor 4. According to the posteriors and the corresponding limits, the

anchor should be clearly failing, while this is not the case judging from the creep value.

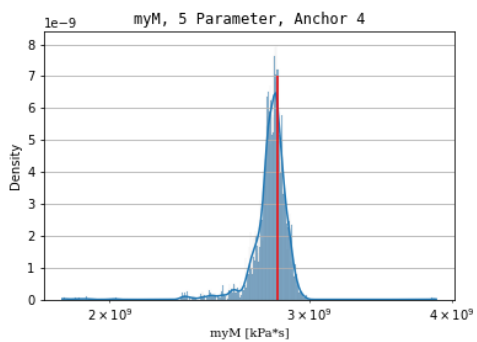


Figure 6.51: Maxwell viscosity posterior vs. Limit Parameter

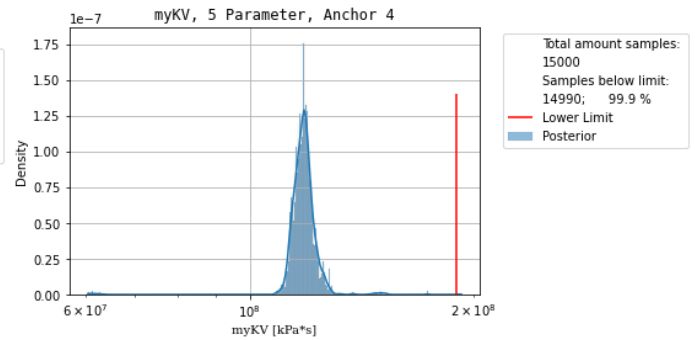


Figure 6.52: Kelvin-Voigt viscosity posterior vs. Limit Parameter

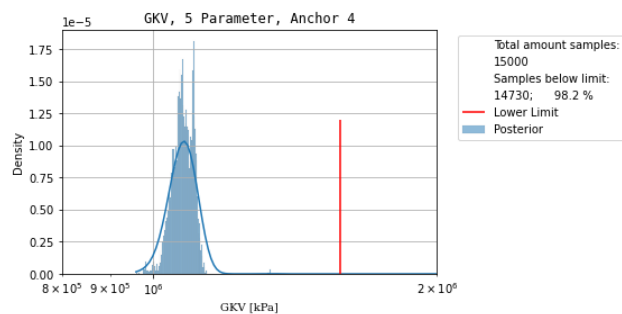


Figure 6.53: Kelvin-Voigt shear modulus posterior vs. Limit Parameter

One explanation, why this procedure does not properly work for this specific anchor 4 is because the densities of the posteriors are too profound. The magnitude of the density is for all parameters one power larger compared to the other suitability anchors. Looking at the credible intervals, due to the dense distributions, this anchor also has the narrowest bounds between the credible intervals. Apart from that, anchor 8 also shows high indicators of failure. The result is not shown here due to skewed, noisy and multimodal posterior distributions and can be found in appendix D.2. Overall, the results of the 5 parameter set make the impression of being more absolute than for the other set. For 6 out of 9 anchors, the majority of the Kelvin-Voigt viscosity posterior samples are in the failure domain, for anchor 2 even for a creep value of 0.17 mm. Based on this, it must be concluded that the predictions that are made with this parameter set are probably unreliable. Apart from the parametric inconsistencies or measurement errors mentioned before, no other reasonable explanation for this behavior could be found.

A better result is given by the 3 Parameter investigation. The following table shows the overall outcome.

| Anchor | μ_M | G_{KV} | creep [mm] |
|--------|---------|----------|------------|
| 1 | 0 % | 0.1 % | 0.27 |
| 2 | 0 % | 0 % | 0.17 |
| 3 | 0.32 % | 0.24 % | 0.63 |
| 4 | 1.53 % | 0 % | 0.50 |
| 5 | 0 % | 0.96 % | 0.30 |
| 6 | 0 % | 0 % | 0.43 |
| 7 | 0 % | 0.15 % | 0.43 |
| 8 | 0 % | 0.1 % | 0.33 |
| 9 | 1.95 % | 7.63 % | 0.50 |

Table 6.6: Suitability test results, Limits, 3 Parameter

The results of the 3 Parameter investigation correspond much better to the measurements. Here, a correlation between higher creep measurements and higher percentages of samples in the failure domain is observed. This means that the percentages could be potentially interpreted as actual probabilities of failure. A careful assessment of this final step is very important because within this research, a proper validation would lead to a larger scope with more data. Therefore, the author is reserved with calling those percentages actual failure probabilities.

7. Discussion

The calibration procedure is a basic technique to estimate 'true' parameter values for the model based on the best fit to the data. The Bayesian updating technique presented in chapter 6 is a statistically sound concept, that does not only give an indication of the 'true' values but also its distribution and therefore the probability to reach extreme values. These extreme values could then be further used for a reliability analysis if the underlying model allows this last step.

7.1. Calibration Comparison

Independent of the set or the quality of the calculated posterior distributions, certain trends could be observed concerning the relationship of the calibrated values towards the means of the posterior distributions. The trends were parameter dependent.

For the shear modulus and the Maxwell viscosity, the main trend was that the posterior means are slightly lower in magnitude, thus corresponding to higher initial displacements and larger displacement curve gradients than for the calibration. The Kelvin-Voigt shear modulus showed the opposite trend. There, the magnitude of the posterior means became on average larger, thus, corresponding to smaller displacements.

If the calibration and its parameters are regarded as an initial design result, it can be concluded that the Bayesian updating procedure results in higher safety because the re-evaluated parameters on average lead to larger displacements and higher creep magnitudes.

7.2. Parameter Evolution

One of the most pronounced patterns that have been observed is the evolution of the shear modulus over increased loads. This trend is observed on all anchors, independent of the sets. The shear modulus is mostly increasing until approx. the 70 % or 80 % loading increment and is then decreasing again to some sort of residual level. Figure 7.1 puts this into context for both investigation test anchors.

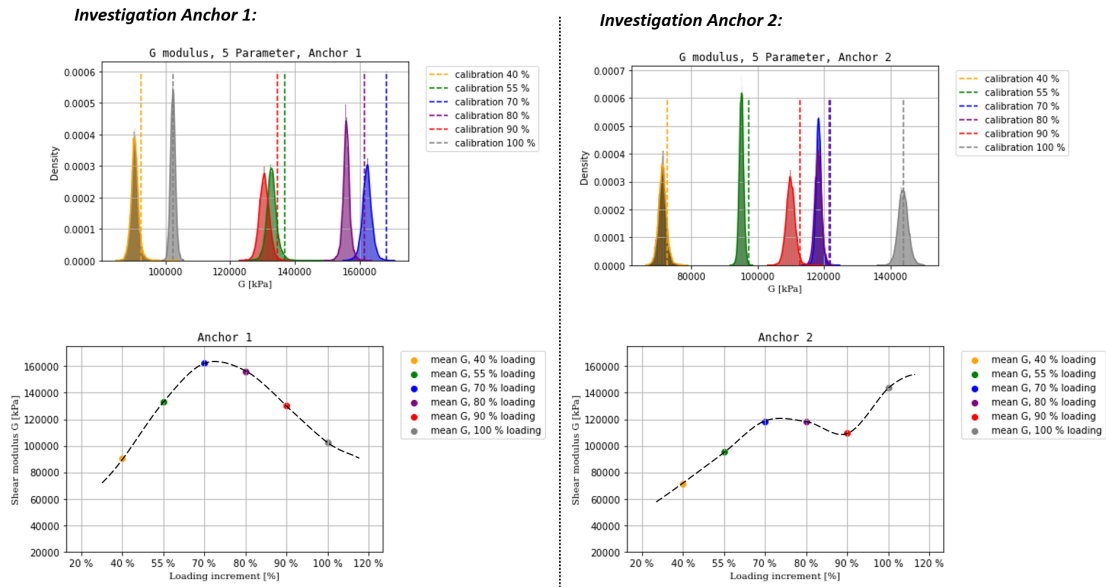


Figure 7.1: Shear modulus over increased loading

For the first anchor, the shear stiffness consistently increases until 70-80 % loading and then decreases towards 100 % loading. This also corresponds with the creep measurements. The first anchor measures creep of 2.0 mm and is per definition at failure, therefore, the 100 % loading shows a shear modulus closer to an expected residual value. The curve’s shape is similar to shear stress and shear strain graphs, which is why it is suspected that the same phenomenon is the underlying cause.

The second anchor exhibits different behavior, the 100 % loading is not a residual value but the peak. This shows concordance with the measurements, where the creep value is 1.75 mm, which indicates some reserve. However, based on this, it is difficult to estimate where the actual residual value might lie or how much reserve there is.

Similar behavior is also observed for other soil parameters. Below, the same type of graph is shown for the Kelvin-Voigt shear modulus.

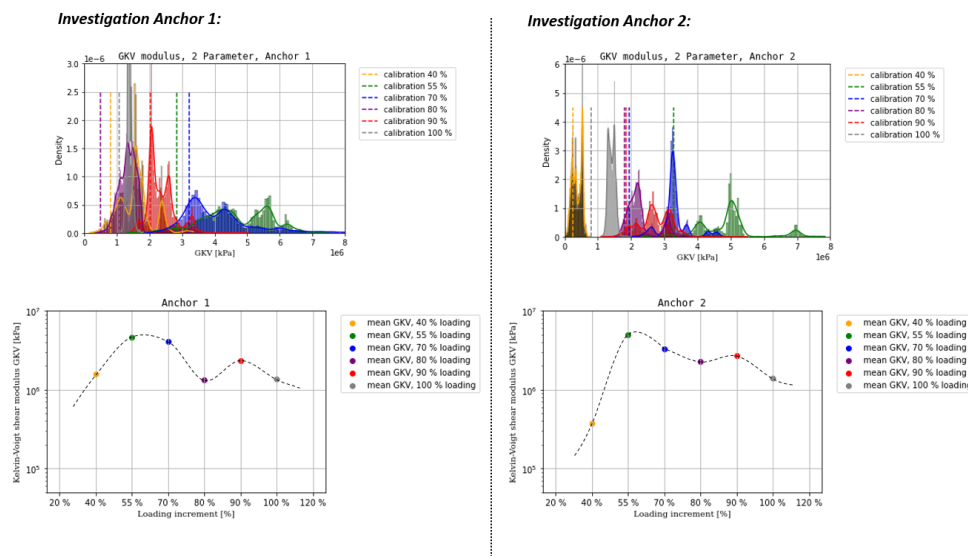


Figure 7.2: Kelvin-Voigt shear modulus over increased loading

In Fig. 7.2, the curves even have the same shapes from one to the next anchor, with a similar trend. The parameters increase in their magnitude first until $\approx 55\%$ and then decrease again, with the 100% increment being of smaller magnitude. The viscosity parameters were observed to consistently decrease in their magnitude with increasing loads. Viscosity is known to exhibit stress and strain dependent behavior, which too became visible in the parametric analysis in chapter 5. Nevertheless, the trends were not as clear as they were for the shear modulus. The Maxwell viscosity showed a clear decreasing trend in the investigation tests, but within this research, no quantifiable estimation could be established to capture this behavior. Again, this could be used for an estimation of the maximum bearing capacity. The concept of limit soil parameters functions given the scope of this research, but the target should be a limit bearing capacity comparable to the output of the existing methods. The model's components to calculate this quantity are summarized in the following sketch.

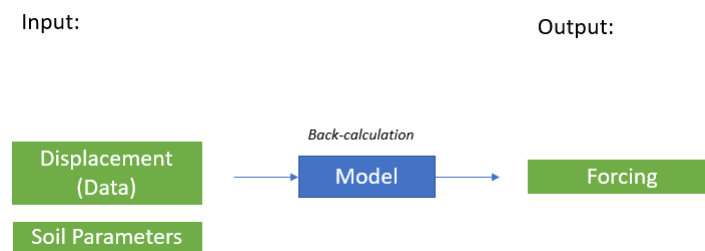


Figure 7.3: Components for bearing capacity estimation

This shows that the soil parameters at failure need to be known to calculate a maximum bearing capacity. A larger database is necessary to establish this relationship.

7.3. Non-time dependent Failure Criterion

Based on the parameter evolution curves shown in Fig. 7.1, it can be observed which anchor is closer to failure. The shear modulus of the second anchor peaks at 100% which indicates that there is some reserve to its capacity. This is interesting because failure is defined by creep, and the shear modulus has no influence on the calculation of the creep value itself within the analytical model. There, the shear modulus is only governing the initial displacements (see 5.2.1). Nevertheless, it shows that the shear modulus could be related to a failure criterion, which would make the analysis and the failure testing of anchors much simpler because no time-dependent, only cyclic loading would be required.

A similar observation is made for the calibration results of the suitability tests. Fig. 7.4 shows the measured creep values vs. the calibrated shear moduli and an estimated correlation curve.

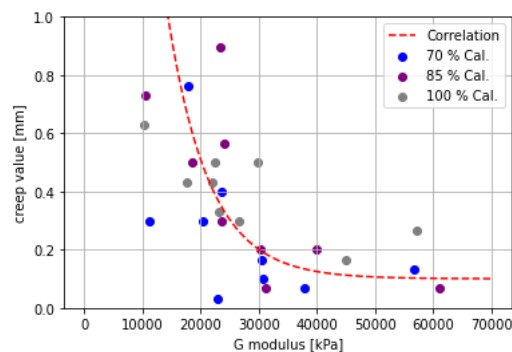


Figure 7.4: Creep value vs. shear modulus

The higher the measured creep values are, the lower are the resulting shear modulus values. In terms of the displacement components of the analytical model, if the initial displacement is large, the grout body displacement component has to be large and therefore the shear modulus small.

7.4. Multimodality, Post-processing

The shapes of the posteriors draw no clear picture. Even though larger amounts of samples are used, the necessary amount could not be finally determined since it depends on the quality of the anchor measurements. For some load steps, most likely the ones with the least measurement error, 20000 or fewer samples gave a decent indication of the posteriors. However, if more parameters are updated and the anchor behavior becomes increasingly nonlinear (towards 100 % failure load), more samples should be used.

Larger amounts of samples lead to longer calculation times. To give an idea, for the 5 Parameter set with 100,000 samples the calculation time was ≈ 10 days and for the 3 Parameter set it was ≈ 9 days, for all load steps computed 'parallel'. Obviously, there is optimization potential in the code to make it more efficient, but considering the scope of this research, the current implementation was deemed to be sufficient.

Now, to illustrate how the posteriors are sensitive to the measurement input, two examples are presented.

7.4.1 Example 1

The first example shows the bimodal posterior distribution of the Kelvin-Voigt shear modulus of the first investigation test anchor with the 5 Parameter set. The graph below shows the actual displacements corresponding to values close to the peaks.

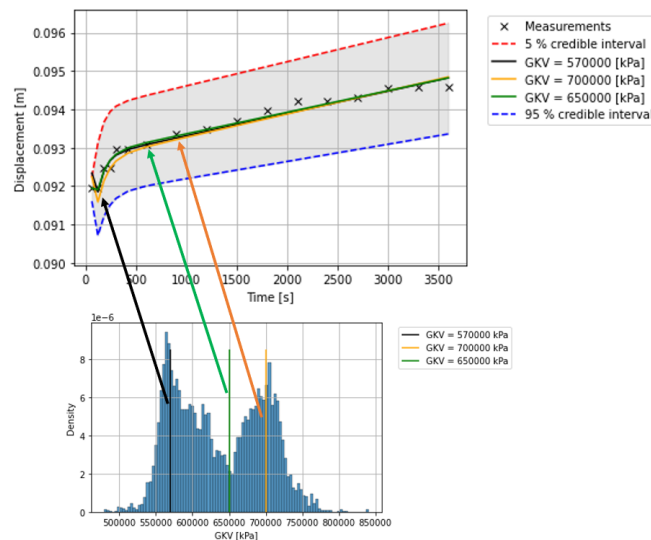


Figure 7.5: Illustration of multiple modes to the displacements

The difference between the different curves is slight but distinct. The displacements corresponding to the first mode are closer but not entirely associated to the displacements that are slightly larger than the average. The first mode captures the 'mean' of the displacements more precise. The second mode is closer associated with displacements slightly lower than the average. The difference between displacements of the dip and the first mode (black and green lines) is negligible.

7.4.2 Example 2

The second example shows the suitability anchor 8 of the 5 Parameter set. In Fig. 7.6 both Kelvin-Voigt parameters and their modes are shown in comparison.

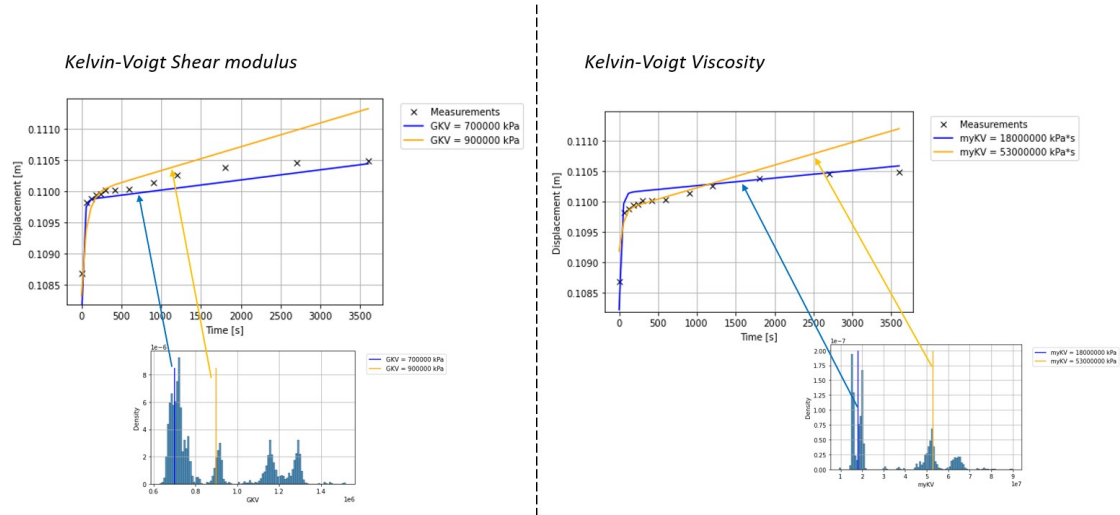


Figure 7.6: Illustration of multiple modes to the displacements, Kelvin-Voigt Parameters

Both parameters show similar trends. The first and major mode shows the better fit over the entire range of displacements. It captures the overall behavior of the anchor with appropriate accuracy, while some single measurements have larger deviations to the calculated displacement curve. The second mode shows a closer concordance with single measurements than with the entire trend of the displacements. This is most profound for the Kelvin-Voigt viscosity (right graph). There, the two modes represent essentially two different curves, one fitting to the earlier measurements and the other to the later measurements. The possibility of adding weights to certain measurements was not investigated.

Based on this, another step can be taken to achieve higher accuracy and confidence in the posterior distributions. As already discussed in the Bayesian updating chapter, the boundaries of the posteriors can be influenced with specific prior distributions like truncated-normal distributions. Another way of identifying possibly unimodal posterior distributions is by limiting certain curve shapes and filtering out samples that provide either physically unrealistic displacement curves or samples that are not sufficiently accurate for one's purposes.

The first example shall be the first investigation test anchor, with the 3 Parameter set.

Fig. 7.7 shows in red 2000 realizations of the calculated posterior samples. The green lines correspond to filtered samples, those samples that pass the criteria in terms of a realistic accuracy and shape that are imposed on them. The left histogram shows the Maxwell viscosity and the right one the Kelvin-Voigt shear modulus. The result of this analysis is that a clearer picture is drawn about each mode, and it's resulting displacements. For the Maxwell viscosity, most of the larger ranges and 'outcast' samples are filtered out, which results in a larger density of a specific value. For the Kelvin-Voigt shear modulus, the entire lower mode is filtered out because the divergence to the measurements in the earlier time steps is too large to be considered realistic. The criteria for which this filtering here was performed are arbitrary, and they can be redefined for specific applications. This investigation is only supposed to illustrate that post-processing can reduce uncertainties in the shape of posterior distributions.

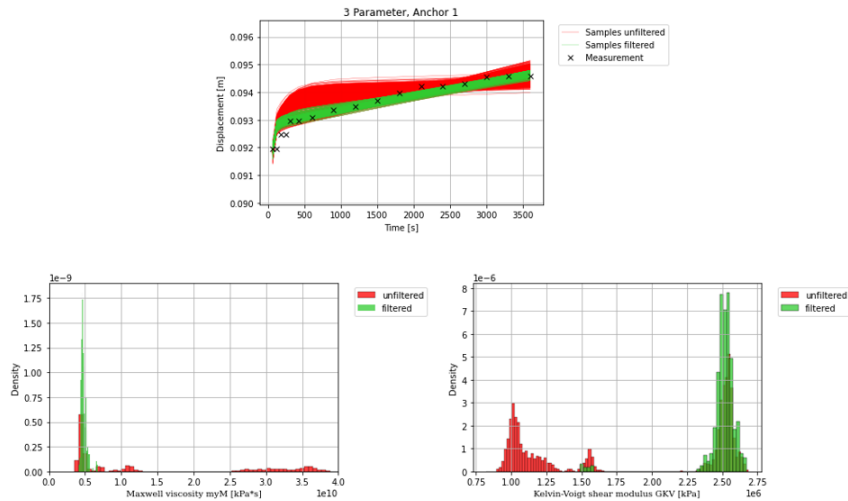


Figure 7.7: 3 Parameter set, Filtered comparison

In the case of denser distributions, the gain of the filtering is limited. The filtered distributions have similar shapes and bounds, like for the 5 Parameter set shown below.

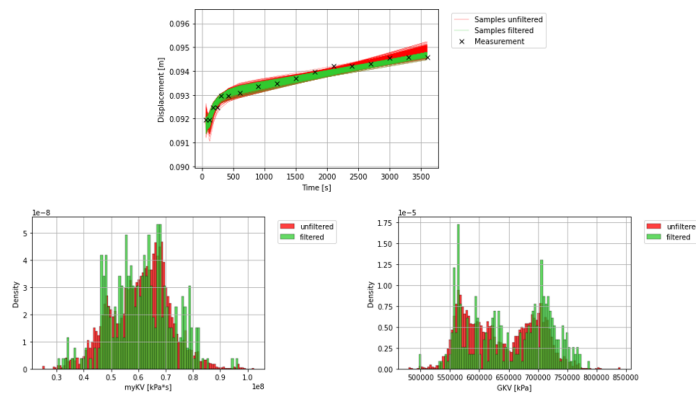


Figure 7.8: 3 Parameter set, Filtered comparison

In this case, Fig. 7.8, the posterior bounds are already narrow. Therefore, the filtering is of limited use, but especially with wide credible intervals, filtering can prove to be beneficial. The main point, that this investigation proves, is that not all modes represent the complete anchor behavior. These minor modes are some byproduct of the procedure caused by measurement errors and other non-capturable inaccuracies that illustrate the sensitivity of the algorithm to slight variances in the measurement input with this underlying model. Therefore, all modes are valid and mathematically correct, but not necessarily in a physical sense because often they do not represent the anchor behavior over its entire time frame.

Another aspect that needs to be discussed is the shape of the shear modulus posterior distributions. Even though, wide uniform distributions are given as a prior estimation, dense, 'bell-shaped' posteriors are the result. The shear modulus can be easily back-calculated and leaves less room for interpretation compared to the other parameters because only the first displacement measurement plays a role in its determination. Thus, the shape can be expected because the likelihood function is a multivariate normal distribution. Therefore, it is clear that nearly deterministic parameters like the shear modulus have the shape of a normal distribution, with the bounds reflecting the covariance.

Likelihood and covariance have rarely been discussed in this report because the scope did not allow investi-

gations in this direction. The multivariate normal distributions for the likelihood function and an updated covariance with the shape of an identity matrix with no correlation between measurements has been regarded as a given.

7.5. Reliability - Parametric Limits

The relation of the posteriors towards the limit parameters yielded mediocre results. The limit parameters showed certain validity and can potentially be used as failure criterion. Naturally, this relationship is largely dependent on the quality of the posterior distributions. If the posteriors are not deemed accurate, the results of this investigation should be interpreted carefully.

The results provide indications on how close the anchor might be towards failure. Reserves that are observed, for example, in the second investigation test anchor are existing and quantifiable to a certain extent. However, the most useful relation would be to correlate these reserves towards the bearing capacity. This translation is more complex. The main issue that comes up is the fact that the anchor behavior must be extrapolated into a stress/strain domain where no measurements are available. To do so, one needs to know how the soil parameters change under increased loading. In other words, a proper constitutive model must be able to capture these changing loading conditions for the soil parameters.

The different parameters that influence the creep also give insight about the behavior of the anchor. For example, in table 6.6 anchor 9 shows one of the highest indications towards failure. The fourth anchor has the same creep value as the 9th anchor, and the magnitude of the percentages of samples in the failure domain concerning the Maxwell viscosity are similar. The percentages of samples in the failure domain concerning the Kelvin-Voigt viscosity are largely different. One explanation is that both parameters draw a different picture on what displacement behavior might be expected towards failure. Based on the measured creep values and their evolution, the first investigation test anchor shows rather 'soft failure' while the second anchor exhibits more 'brittle failure' (creep figures, 5.15, 5.16). The posterior distributions indicate this 'soft failure' of the first anchor by showing larger sample percentages in the failure domain for both Kelvin-Voigt parameters. The second anchor shows a rather high Maxwell viscosity indication (74.1 %) with low Kelvin-Voigt components (0.0 % & 0.0 %).

An alternative explanation for this phenomenon could be also linked to the sensitivities of the parameters itself, meaning that the smaller changes in the parameters' magnitude lead to more severe outcomes of the displacement and creep. But to confirm this, more data would need to be investigated.

7.6. Practical Suitability

The presented procedures and analysis are yet of limited use in a practical environment. The uncertainties are still large, the models are new, and further validation is not covered in this research. The necessary soil parameters are seldom used and cannot be derived on site without additional research. The indication of failure on suitability test results could be of use, to estimate which anchor has the highest utilization. The model itself could be used as a tool to validate estimates from a finite element calculation. However, not until there is more experience with the model and especially its parameters, its application is conceivable. To summarize, the presented procedures yield potential but are not ready for imminent practical application.

In the following, a procedure is proposed on how this research can be reproduced in a practical environment.

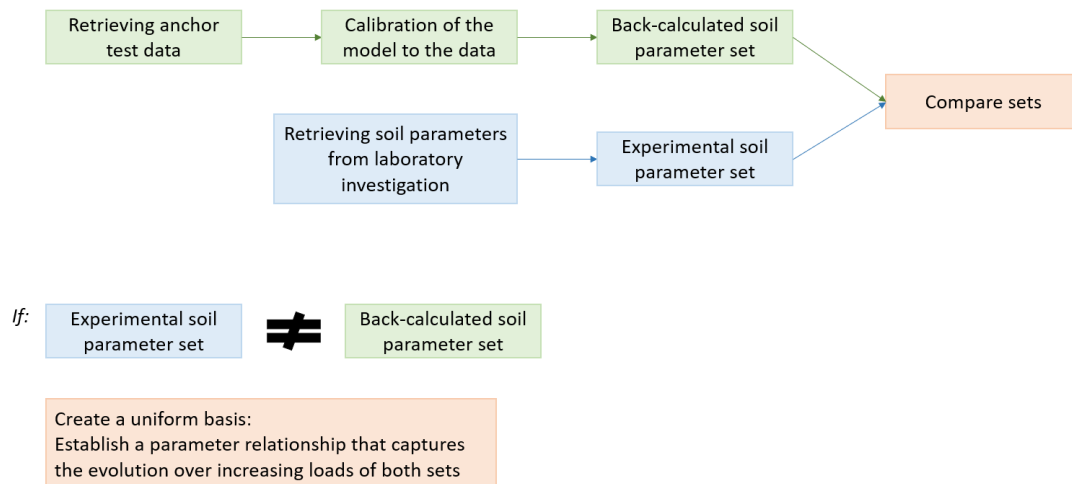


Figure 7.9: Practical application, Flowchart 1

A sufficient data basis is presumed. Assuming the back-calculated soil parameters are valid, the experimental soil tests should focus on establishing values for stress and strain levels that are outside the scope of common anchor testing. Especially for these boundary levels, it is important to retrieve soil parameters.

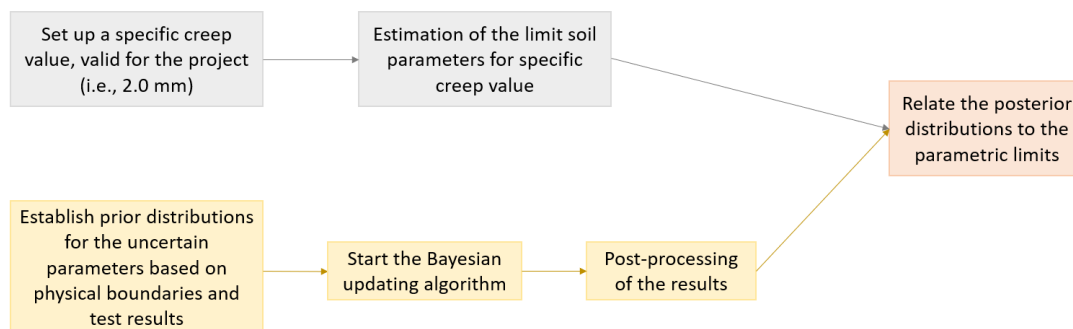


Figure 7.10: Practical application, Flowchart 2

The next step is to establish the limit soil parameters. Depending on a site specific creep value, the limit parameters can be either back-calculated or established based on the experimental data. Parallel to this, the Bayesian updating algorithm can be applied to derive posterior distributions of the uncertain parameters. As a last step, the posteriors and limit parameters can then be related to each other to make a statement about the anchor’s utilization or its bearing capacity. The posteriors might be used for more purposes that are not the scope of this research.

This procedure represents in a simplified way how this model can be applied accompanying the design process. If the experimental data of the soil parameters should fit the soil parameters of the back-calculation, which is rather unlikely, initial predictions of the creep magnitudes could be made.

8. Conclusions

This research combines two novelty approaches in a fashion that has not been performed before. The used anchor model is one of the few research models that is able to capture grout anchor displacements. Bayesian updating in the construction sector has been a topic of research for several centuries, but barely developed into practical applications. The Bayesian updating algorithm that was used is a reliability-based algorithm that just recently has been introduced and whose possibilities just begin to materialize.

The procedures and analyses presented here, are initial investigations that aim to answer fundamental questions. The overall approach to the topic does not change for different underlying models or algorithms, but stays the same. Furthermore, the analytical model is put into the context of a practical case study, which gives opportunities to better understand and further develop the model. Lastly, benefits are shown of deriving distributions of parameters in the context of uncertainty.

How can anchor measurement data be used for reliability-based updating of anchor bearing capacity?

This can be accomplished by applying the aBUS-SuS algorithm in the way it was presented. This reliability-based approach for Bayesian updating is robust, and its application is straight-forward. It is necessary to provide the algorithm with a suitable mechanical model where the output fits to the measurements and the input parameters can be related to the bearing capacity. With the model that was chosen, the latter showed to be more problematic. The last step, relating the posterior distribution to the bearing capacity of the anchor, was not fully achieved. In addition to spacial variability between the anchors, the strong stress and strain dependency of the main soil parameters led to variations from one load step to the next. Therefore, the calculated posterior distributions are only valid for the specific anchor and the loading that was applied, corresponding to the measurement.

An attempt has been made to solve this issue by deriving limit soil parameters using the CUR 166-method to obtain the anchor's limit force. However, within the scope of this research, verification and optimization with additional measurement data, could not be conducted. The analyses show that the limit parameters can be used as an indication to the anchors' failure and the type of failure that can be expected, which are in line with investigation test data. Nevertheless, the derived percentages of samples in the failure domain do not necessarily translate into actual probability of failure. For such a statement, further verification with more data is necessary.

- How can analytical models be used to predict anchor failure?

Industry practice defines anchor failure by a specific magnitude of creep. The investigation showed that the investigated analytical model is capable of capturing this kind of anchor displacements. However, the common failure criterion is vague, both in practice and in the context of the model output. Since the model output are displacements, several different parameter combinations are possible solutions to obtain a specific creep value. The analysis demonstrated how the model can provide limit soil parameters at failure condition by solving for them specifically. If the soil

parameters at failure condition are known, one can also solve for the limit load.

- What is the effect of Bayesian updating on the anchor capacity?

Applying Bayesian updating results in posterior distributions of uncertain parameters instead of single values resulting from a classic calibration. With these posterior distributions of critical variables, an alternative approach is presented on how anchor failure is indicated. This is achieved by relating the posteriors to the derived parametric limit values that correspond to failure. Furthermore, uncertainties are pointed out and conclusions about the brittleness of the failure mechanism can be drawn. Compared to the calibrated parameters, the majority of the means of the updated parameters were lower, resulting in larger instantaneous displacements and larger displacement curve gradients.

- What are the limitations of Bayesian updating using analytical models?

The first major limitation is the quality and amount of measurements. Depending on the underlying model, a certain amount of data points is necessary for the convergence of the algorithm. If the amount of data points is insufficient, the posteriors do not change and resemble closely the prior distributions, with the result that no new information is obtained.

The second limitation is the estimation of the prior distributions with a reasonable shape and more importantly proper bounds. If these are defined poorly, the algorithm can converge towards physically unrealistic values. The bounds can be established by pre-processing of possible model realizations and filtering. The availability of site investigation data or lab data helps in setting up boundaries.

The last limitation revolves around measurement error. Depending on the sensitivities of the analytical model, measurement error can strongly influence the shape and the amount of modes of the posterior distributions. With appropriate physical constraints on the posterior models and post-processing, the quality of the results can be improved.

9. Limitations and Recommendations

9.1. Limitations

The following lists the limitations of the procedures that have been encountered during this research. The first section focuses on the limitations of the general suitability of the analytical model and the algorithm, while the second section focuses around more detailed aspects of their application. To overcome the latter, assumptions have been made or procedures to evade these issues have been developed.

9.1.1 General Limitations

- More parameters lead to higher uncertainty in the results, which can be observed in the width of the bounds of the credible interval plots in chapter 6. Therefore, it is important to define in the beginning which parameters need updating and which can be regarded as constants.
- The analytical model used in the context of this research is mainly limited by the potential of its underlying equations. It can only capture the anchor systems that are in their shape similar to the idealized system.
- Another limitation is the amount of unusual soil parameters necessary to model the time dependent anchor displacements at $t > 0$. The soil's Maxwell or Kelvin-Voigt viscosity and shear modulus are highly stress and strain dependent, and their estimation is not trivial.
- One limitation of the Bayesian updating is that a certain amount of measurements must be available, otherwise no proper posterior distributions can be calculated, and the results are similar distributions as the priors. This was mainly an issue for the lower load steps, where fewer measurements were available. To give an example, for the lower load steps 8 data points were available, and the algorithm was not functioning properly to calculate the time dependent parameter posteriors. This quantity is purely dependent on the underlying model and the problem.

9.1.2 Detailed Limitations

- One of the biggest disadvantage of the application of the model is the characteristic that several parameters influence the curve's shape. This can lead to multimodal posterior distributions or different results in the calibration procedure, because different parameter combinations can lead to similar fits. Measurement error amplifies this phenomenon.
- Another limitation in a more conceptual sense is the fact that this model requires considerable input data. It is better suited to model and verify displacements rather than using it for back-calculation of maximum bearing capacities, whilst still being one of the most advanced analytical anchor models in research. Nevertheless, for grout anchors, the bearing capacity is directly related to the anchor's creep, which is displacement over time. Thus, the relationship of the model's output towards the measurements and back to the maximum bearing capacity is existing but rather complex. No model exists that has

anchor creep as a direct output.

- For the calibration procedure, the parametric bounds need to be fixed, otherwise the parameters become physically unrealistic. This is also the case in the context of the Bayesian updating in the estimation of prior distributions and processing of the posterior results.

9.2. Recommendations

In the following, the recommendations are listed. They shall serve to overcome most of the limitations that are mentioned above.

- The analytical model is able to capture a vast range of possible shapes of anchor displacement. Some shapes are physically unrealistic, like a decline of the displacements after the initial displacement. It is recommended to filter out these parametric boundaries for better efficiency in the calibration or Bayesian updating calculations. With simple criteria depicting a realistic shape of the displacement curve, this problem can be solved, i.e. excluding values that would result in negative gradients. This is important because the latter can happen even though the parameters are technically in a physically realistic range. To provide an example, one condition is that the Maxwell shear modulus cannot be larger than the elastic shear modulus.
- For practical application, it is recommended to test for the soil parameters in the laboratory or on site on stress and strain levels beyond the working load. The main benefit of this is having a proper benchmark for verification of the results. Back-calculation is possible, but lacks accuracy, as shown in the previous chapters. The calibration and also the updating within this research mainly focussed upon obtaining these parameters computationally. With the means of experimental tests, more accurate distributions can be obtained from the Bayesian updating. Furthermore, statements about anchor loading surpassing the test conditions can be made.
- Closely related to the previous point of attention is the importance of obtaining decent estimates of the limit parameters. Within this research, the limit parameters could just be crudely estimated, while small divergences make a large difference. The parameters underlying the model are not commonly used to quantify mechanical properties of soil. With a better understanding of how these parameters behave and change for increased stress or strain, many uncertainties of this procedure would be marginalized, and more precise estimates could be made.
- Measurement error plays a large role in the shape of the posterior distributions. Options of quantifying this error and treating it as a variable within the analyses were not closer investigated, but can be regarded as an opportunity to overcome this problem. Here, the post-processing of the posterior distributions proved to be a functioning method to identify the influences on results.
- Some displacement components of the analytical model only show small contributions to the overall displacements. For reasons of completeness, they were all included in the calculation but if more efficiency is required, the displacements can be limited only to the tendon elongation and the grout body displacements.

9.3. Further research

Based on the magnitude of the calculated shear modulus in the calibration and the Bayesian updating chapter and on the general testing procedures, it is suspected that the shear modulus is in the context of this application actually the un- and reloading shear modulus. Within the test, the anchor is loaded in several cycles, which justifies this hypothesis. This could be further researched. In this research, the concept of using limit parameters was developed in order to make a relation towards the anchors' reliability and utilization. An additional point of focus can be to develop an alternative approach to get a better approximation of either the limit parameters or possibly a completely different quantity that captures anchor failure.

Another aspect is the shear modulus and its magnitude as an indicator of failure. With a larger database of failure tests, this relationship can be further investigated, and a proper correlation curve with the creep value could be defined. Based on these findings, the failure criterion could be redefined as a function of the shear modulus. Then, using the model, the magnitude of displacements would be known from earlier design stages on and the site investigation can be adjusted to better estimations of the shear modulus, i.e. shear wave measurements.

The concepts and ideas presented above based on the test results of a single database. To verify those concepts, further investigations on more data is necessary. This way, a better understanding of the anchor model's capabilities and limitations in a more practical environment can be seized.

For future application, it could be investigated if the test procedure and test times could be related to the relative change of displacements for the higher load steps instead of fixed time frames for soil types. The displacement of the anchor from one measurement point to the next is large in the beginning of the test and becomes less towards the end of the test. Instead of using a fixed time frame one could end the test once i.e. a certain amount of consecutive measurement exhibit the same amount of change in displacement towards the last measurement. The motivation is to ensure that the testing procedure ends once the anchor's displacement over time is constantly changing from that point on. This raises the question if anchor displacement over time, thus anchor creep, becomes linear after a certain loading time.

References

- [1] G.B. Baecher and J.T. Christian. *Reliability and statistics in geotechnical engineering*. John Wiley and Sons Ltd., 2003.
- [2] K J Bakker. *Backanalysis of Sheetpile Wall Test Karlsruhe (1993) Applying Inverse Analysis*. Springer Vienna, Vienna, 1998.
- [3] James L. Beck and Siu-Kui Au. Bayesian Updating of Structural Models and Reliability using Markov Chain Monte Carlo Simulation. *Journal of Engineering Mechanics*, 128(4):380–391, 2002.
- [4] Wolfgang Betz, Iason Papaioannou, James L. Beck, and Daniel Straub. Bayesian inference with Subset Simulation: Strategies and improvements. *Computer Methods in Applied Mechanics and Engineering*, 331:72–93, 2018.
- [5] R.B.J. Brinkgreve, E. Engin, and H.K. Engin. Validation of empirical formulas to derive model parameters for sands. *Numerical methods in Geotechnical Engineering*, pages 137–142, 2010.
- [6] J.M. Büller. Reliability updating sheet pile walls. Master’s thesis, Delft University of Technology, 2019.
- [7] Technical committee: ISO/TC 182 Geotechnics. *ISO 22477-5: 2018, Geotechnical investigation and testing - Testing of geotechnical structures - Part 5: Testing of grouted anchors*. International Organisation for Standardization, 2018.
- [8] CURNET. *CUR 166 Damwandconstucties*, volume 1. CUR Bouw en infra, 6 edition, 2011.
- [9] B.H. Fellenius. From strain measurements to load in an instrumented pile. *Geotechnical News Magazine*, 19(1):35–38, 2001.
- [10] Wolfgang Fellin, Heimo Lessmann, Michael Oberguggenberger, and Robert Vieider. *Analyzing Uncertainty in Civil Engineering*. Springer, 2005 edition, 2004.
- [11] Normcomissie 351006 ”Geotechniek”. *NEN-EN 1537, Execution of special geotechnical works - Ground anchors*. European Committee For Standardization, 2013.
- [12] Masaru Kitahara, Sifeng Bi, Matteo Broggi, and Michael Beer. Bayesian Model Updating in Time Domain with Metamodel-Based Reliability Method. *ASCE-ASME Journal of Risk and Uncertainty in Engineering Systems, Part A: Civil Engineering*, 7(3), 2021.
- [13] K. Laghmouchi. Reliability updating of existing quay walls based on the effects of past performance. Master’s thesis, Delft University of Technology, 2021.
- [14] Natalia S. Montero-Cubillo, Rubén A. Galindo-Aires, Alcibiades Serrano-González, Claudio Olalla-Marañón, and Francisco D. Simic-Sureda. Analytical Model of an Anchored Wall in Creep Soils. *International Journal of Geomechanics*, 20(4):04020027, 2020.
- [15] H. Ostermayer. Construction, carrying behaviour and creep characteristics of ground anchors. In *Diaphragm walls and anchorages*, pages 141–151. Thomas Telford, London, England, May 1975.

- [16] H. Ostermayer. Das Verhalten des Systems Bauwerk-Anker-Boden als Grundlage für den Entwurf verankerter Konstruktionen. *Bauingenieur*, 70(1):371–380, 1995.
- [17] H. Ostermayer and Barley T. Ground anchors. In U. Smoltzyk, editor, *Geotechnical Engineering Handbook, Volumes 1-3*, volume 2. Ernst and Sohn, 1 edition, 2003.
- [18] Iason Papaioannou, Wolfgang Betz, Kilian Zwirgmaier, and Daniel Straub. MCMC algorithms for Subset Simulation. *Probabilistic Engineering Mechanics*, 41:89–103, 2015.
- [19] A. A. Roubos, T. Schweckendiek, R. B. Brinkgreve, R. D. Steenbergen, and S. N. Jonkman. Finite element-based reliability assessment of quay walls. *Georisk: Assessment and Management of Risk for Engineered Systems and Geohazards*, 15(3):165–181, 2020.
- [20] Hans-Henning Schmidt, Roland Fritz Buchmaier, and Carola Vogt-Breyer. *Grundlagen der Geotechnik: Geotechnik nach Eurocode (German Edition)*. Springer Vieweg, 5 edition, 2017.
- [21] H.F. Schweiger, Thurner R., and R. Pöttler. Reliability analysis in geotechnics with deterministic finite elements. *Int. J. Geomech.*, 1(4):389–413, 2001.
- [22] High5 Solutions. Berekening groutankers. Verankering HES Hartel Tank Terminal Rotterdam, June 2018.
- [23] Daniel Straub. Reliability updating with equality information. *Probabilistic Engineering Mechanics*, 26(2):254–258, 2011.
- [24] Daniel Straub. Efficient Algorithms and Models for Bayesian Updating in Structural Reliability. *Proceedings of the 5th Asian-Pacific Symposium on Structural Reliability and its Applications*, 2012.
- [25] Daniel Straub and Iason Papaioannou. Bayesian Updating with Structural Reliability Methods. *Journal of Engineering Mechanics*, 141(3), 2015.
- [26] T.J. van der Well. Reliability based assessment of quay walls. Master’s thesis, Delft University of Technology, 2018.
- [27] Volker Staal en Funderingen. Screw injection anchors. <https://en.vsf.nl/en/foundations/anchors/screw-injection-anchors>, 2022. Accessed: 2022-05-24.
- [28] L. Watzlik. Numerical studies on progressive failure of ground anchors. Master’s thesis, Graz University of Technology, 2015.
- [29] Herm-Jan Wolters. Reliability of quay walls. Master’s thesis, Delft University of Technology, 2012.

A. Appendix - Theoretical Background

A.1. Anchor design

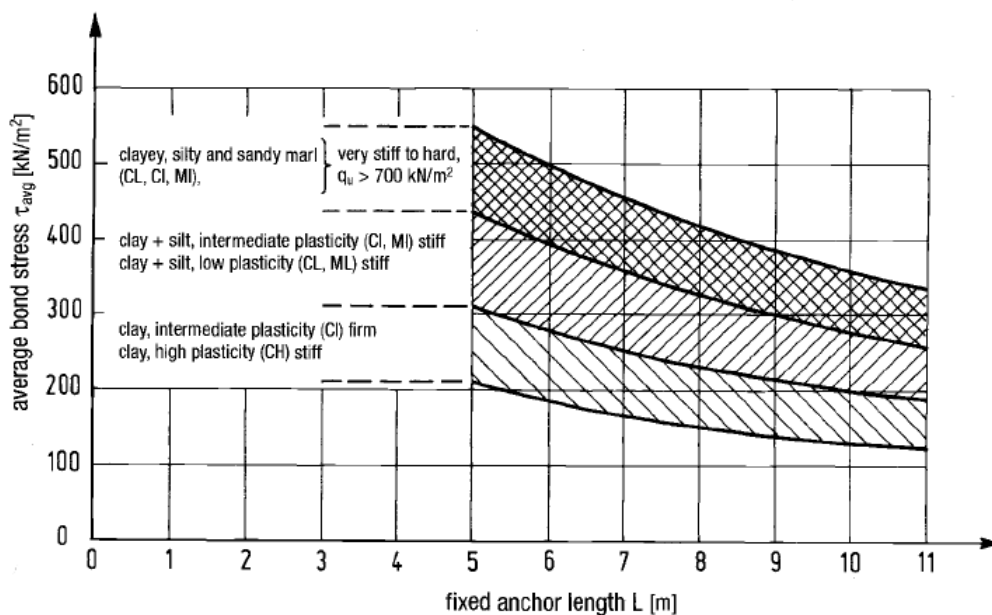


Figure A.1: Ultimate bearing capacity for cohesive soils 1 [17]

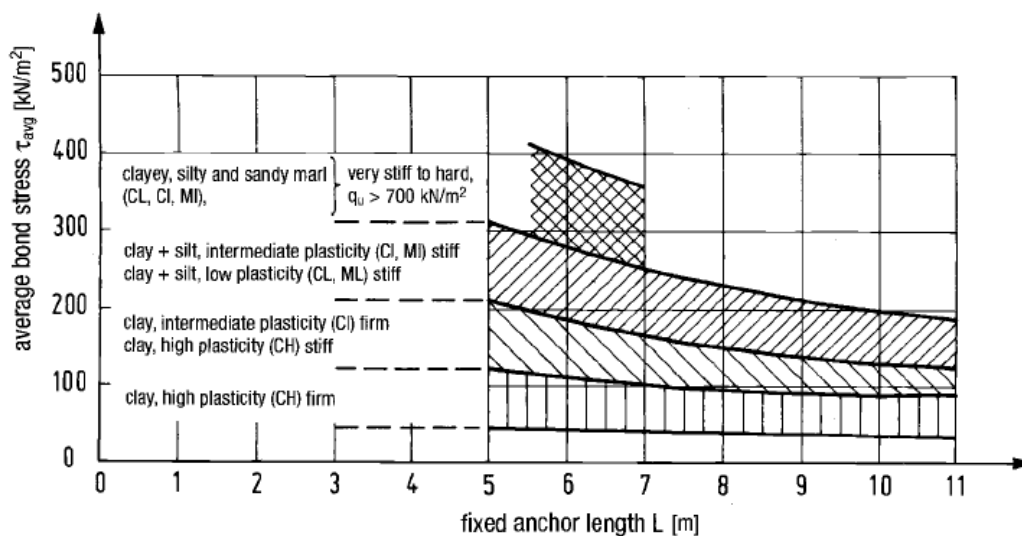


Figure A.2: Ultimate bearing capacity for cohesive soils 2 [17]

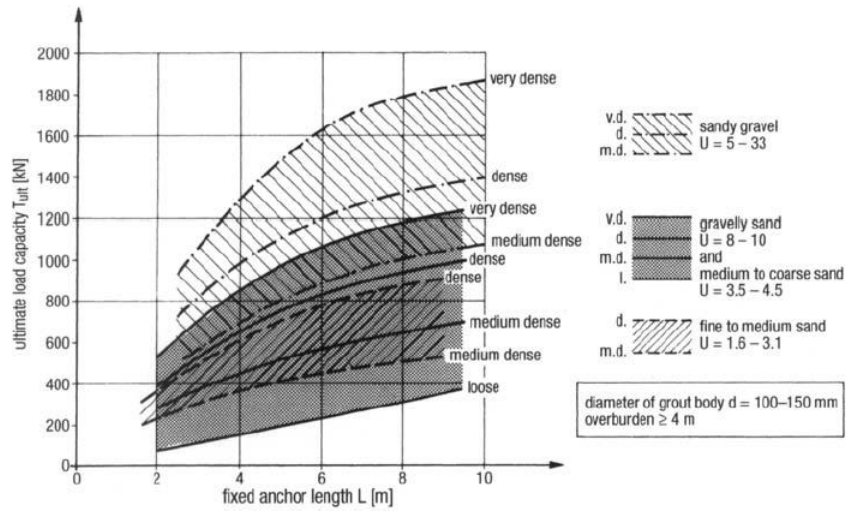


Figure A.3: Ultimate bearing capacity for non-cohesive soils

A.2. Bayesian updating

A.2.1 Algorithms

Metropolis-Hastings algorithm [18]

1. Generate candidate sample v from $\phi_n(\cdot)$
 - (a) Generate pre-candidate state ξ from the pdf $q(\cdot|u_0)$
 - (b) Accept or reject ξ

$$v = \begin{cases} \xi, & \text{with probability } \tilde{a}(u_0, \xi) \\ u_0, & \text{with probability } 1 - \tilde{a}(u_0, \xi) \end{cases} \quad (\text{A.1})$$

$$\tilde{a}(u_0, \xi) = \min\left(1, \frac{\phi_n(\xi)q(u_0|\xi)}{\phi_n(u_0)q(\xi|u_0)}\right)$$

2. Accept or reject v

$$u_1 = \begin{cases} v, & v \in F_j \\ u_0, & v \notin F_j \end{cases} \quad (\text{A.2})$$

Metropolis-Hastings Algorithm with conditional sampling and adaptive scaling [18]

1. Choose starting values of the standard deviation
 - (a) Set $\sigma_{0i} = 1, i = 1, \dots, n$
 - (b) Compute samples mean and standard deviation according to 3.44
2. Get N_a samples from the previous subset as seeds
3. Start iteration process with $iter = 1, \dots, N_s/N_a$

-
- (a) Calculation of correlation parameter ρ_i according to 3.45
 - (b) Generate samples for specific Markov chain, in accordance to the conditional sampling procedure
 - (c) Calculation of the average acceptance rate \hat{a} according to 3.45
 - (d) Calculation of a new scaling parameter λ_{iter} for the next iteration

B. Appendix - Practical Elaboration

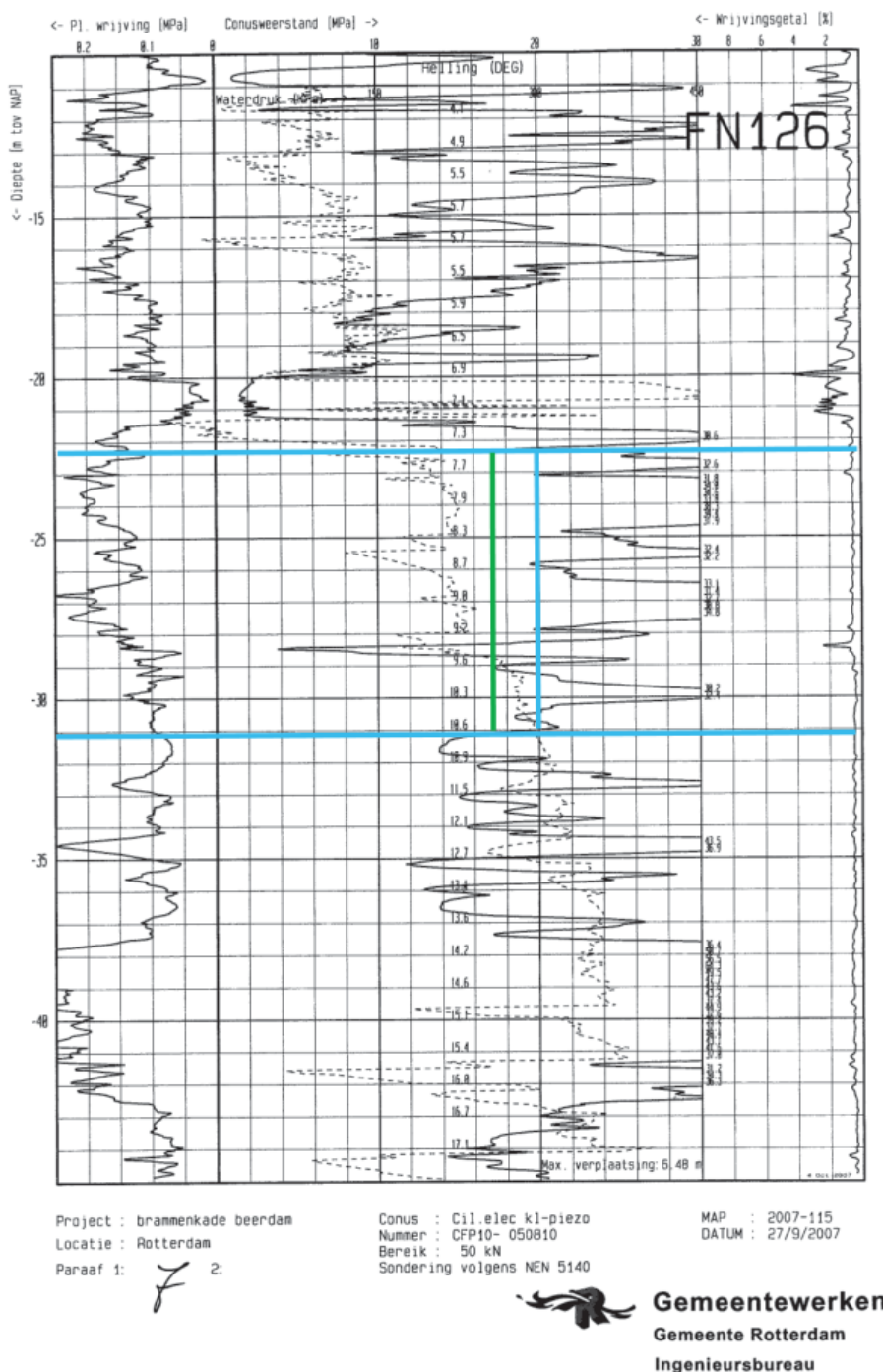


Figure B.1: CPT data corresponding to the site, [22]

C. Appendix - Anchor Modelling

C.1. HHTT Test Data:

C.2. HHTT Structural Parameters:

| | |
|------------------------------|------------|
| H_L [m] | 13.0 |
| b [m] | 1.34 |
| E_{Wall} [kPa] | 21 000 000 |
| I_{Wall} [m ⁴] | 0.0006362 |
| ϕ [°] | 35.0 |

Table C.3: Wall Parameters, Investigation tests

| | | |
|-----------------|------------|----------------------|
| L [m] | 46.60 | total length |
| a [m] | 12.40 | grout body length |
| H [m] | 34.20 | free length |
| D [m] | 0.335 | diameter grout body |
| P_0 [kN] | 5100 | max. anchor load |
| D_o [m] | 0.1397 | outer diameter rod |
| W_L [m] | 0.04 | wall thickness rod |
| E_{rod} [kPa] | 21 000 000 | Youngs modulus steel |

Table C.4: Anchor Parameters, Investigation tests

| | | | |
|------------------------------|------------|------------|------------|
| H_L [m] | 13.0 | 13.0 | 13.0 |
| b [m] | 1.34 | 1.47 | 1.47 |
| E_{Wall} [kPa] | 21 000 000 | 21 000 000 | 21 000 000 |
| I_{Wall} [m ⁴] | 0.0006362 | 0.0006362 | 0.0006362 |
| ϕ [°] | 35.0 | 35.0 | 35.0 |

Table C.5: Wall Parameters, Suitability tests

| | | | | |
|-----------------|------------|------------|------------|-----------------------|
| L [m] | 50.7 | 42.5 | 44.0 | total length |
| a [m] | 15.5 | 7.5 | 10.75 | grout body length |
| H [m] | 35.2 | 35.0 | 33.25 | free length |
| D [m] | 0.325 | 0.325 | 0.325 | diameter grout body |
| P_0 [kN] | 3507 | 1465 | 2653 | max. anchor load |
| D_o [m] | 0.1397 | 0.085 | 0.103 | outer diameter rod |
| W_L [m] | 0.04 | 0.038 | 0.043 | wall thickness rod |
| E_{rod} [kPa] | 21 000 000 | 21 000 000 | 21 000 000 | Young's modulus steel |

Table C.6: Anchor Parameters, Suitability tests

| | time step 1 | total time 1 | Force 1 | u1 | time step 2 | total time 2 | Force 2 | u2 |
|------------|-------------|--------------|---------|-------|-------------|--------------|---------|-------|
| 0,40 Ptest | 1 | 7 | 2054 | 17,21 | 1 | 7 | 2054 | 16,7 |
| | 2 | 8 | 2054 | 17,22 | 2 | 8 | 2054 | 16,98 |
| | 3 | 9 | 2054 | 17,39 | 3 | 9 | 2054 | 17,25 |
| | 4 | 10 | 2054 | 17,38 | 4 | 10 | 2054 | 17,25 |
| | 5 | 11 | 2054 | 17,54 | 5 | 11 | 2054 | 17,22 |
| | 7 | 13 | 2054 | 17,54 | 7 | 13 | 2054 | 17,22 |
| | 10 | 16 | 2054 | 17,52 | 10 | 16 | 2054 | 17,29 |
| | 15 | 21 | 2054 | 17,49 | 15 | 21 | 2054 | 17,38 |
| 0,55 Ptest | 1 | 30 | 2825 | 26,43 | 1 | 30 | 2825 | 27,1 |
| | 2 | 31 | 2825 | 26,42 | 2 | 31 | 2825 | 27,18 |
| | 3 | 32 | 2825 | 26,4 | 3 | 32 | 2825 | 27,18 |
| | 4 | 33 | 2825 | 26,56 | 4 | 33 | 2825 | 27,27 |
| | 5 | 34 | 2825 | 26,56 | 5 | 34 | 2825 | 27,27 |
| | 7 | 36 | 2825 | 26,54 | 7 | 36 | 2825 | 27,37 |
| | 10 | 39 | 2825 | 26,7 | 10 | 39 | 2825 | 27,37 |
| | 15 | 44 | 2825 | 26,7 | 15 | 44 | 2825 | 27,42 |
| 0,70 Ptest | 1 | 53 | 3595 | 36,82 | 1 | 53 | 3595 | 37,38 |
| | 2 | 54 | 3595 | 36,75 | 2 | 54 | 3595 | 37,52 |
| | 3 | 55 | 3595 | 36,98 | 3 | 55 | 3595 | 37,52 |
| | 4 | 56 | 3595 | 36,95 | 4 | 56 | 3595 | 37,77 |
| | 5 | 57 | 3595 | 36,91 | 5 | 57 | 3595 | 37,78 |
| | 7 | 59 | 3595 | 37,09 | 7 | 59 | 3595 | 37,93 |
| | 10 | 62 | 3595 | 37,22 | 10 | 62 | 3595 | 37,95 |
| | 15 | 67 | 3595 | 37,18 | 15 | 67 | 3595 | 38,02 |
| | 20 | 72 | 3595 | 37,39 | 20 | 72 | 3595 | 38,04 |
| | 25 | 77 | 3595 | 37,45 | 25 | 77 | 3595 | 38,1 |
| 30 | 82 | 3595 | 37,52 | 30 | 82 | 3595 | 38,24 | |
| 0,80 Ptest | 1 | 91 | 4109 | 45,6 | 1 | 91 | 4109 | 46,26 |
| | 2 | 92 | 4109 | 45,52 | 2 | 92 | 4109 | 46,26 |
| | 3 | 93 | 4109 | 45,83 | 3 | 93 | 4109 | 46,52 |
| | 4 | 94 | 4109 | 45,77 | 4 | 94 | 4109 | 46,52 |
| | 5 | 95 | 4109 | 45,98 | 5 | 95 | 4109 | 46,71 |
| | 7 | 97 | 4109 | 45,95 | 7 | 97 | 4109 | 46,71 |
| | 10 | 100 | 4109 | 46,1 | 10 | 100 | 4109 | 47,08 |
| | 15 | 105 | 4109 | 46,19 | 15 | 105 | 4109 | 47,05 |
| | 20 | 110 | 4109 | 46,28 | 20 | 110 | 4109 | 47,17 |
| | 25 | 115 | 4109 | 46,42 | 25 | 115 | 4109 | 47,29 |
| | 30 | 120 | 4109 | 46,57 | 30 | 120 | 4109 | 47,3 |
| | 0,90 Ptest | 1 | 129 | 4622 | 56,86 | 1 | 129 | 4622 |
| 2 | | 130 | 4622 | 56,83 | 2 | 130 | 4622 | 57,7 |
| 3 | | 131 | 4622 | 57,28 | 3 | 131 | 4622 | 57,7 |
| 4 | | 132 | 4622 | 57,26 | 4 | 132 | 4622 | 57,7 |
| 5 | | 133 | 4622 | 57,23 | 5 | 133 | 4622 | 57,7 |
| 7 | | 135 | 4622 | 57,49 | 7 | 135 | 4622 | 57,99 |
| 10 | | 138 | 4622 | 57,67 | 10 | 138 | 4622 | 57,99 |
| 15 | | 143 | 4622 | 57,95 | 15 | 143 | 4622 | 58,25 |
| 20 | | 148 | 4622 | 57,91 | 20 | 148 | 4622 | 58,25 |
| 25 | | 153 | 4622 | 58,07 | 25 | 153 | 4622 | 58,21 |
| 30 | | 158 | 4622 | 58,24 | 30 | 158 | 4622 | 58,2 |
| 1,00 Ptest | | 1 | 167 | 5100 | 71,03 | 1 | 167 | 5100 |
| | 2 | 168 | 5100 | 71,03 | 2 | 168 | 5100 | 60,00 |
| | 3 | 169 | 5100 | 71,55 | 3 | 169 | 5100 | 60,96 |
| | 4 | 171 | 5100 | 71,55 | 5 | 171 | 5100 | 60,96 |
| | 5 | 172 | 5100 | 72,05 | 4 | 172 | 5100 | 61,01 |
| | 7 | 173 | 5100 | 72,04 | 7 | 173 | 5100 | 61,49 |
| | 10 | 176 | 5100 | 72,17 | 10 | 176 | 5100 | 61,49 |
| | 15 | 181 | 5100 | 72,45 | 15 | 181 | 5100 | 61,85 |
| | 20 | 186 | 5100 | 72,57 | 20 | 186 | 5100 | 61,84 |
| | 25 | 191 | 5100 | 72,79 | 25 | 191 | 5100 | 62,33 |
| | 30 | 196 | 5100 | 73,07 | 30 | 196 | 5100 | 62,24 |
| | 35 | 201 | 5100 | 73,3 | 35 | 201 | 5100 | 62,45 |
| | 40 | 206 | 5100 | 73,3 | 40 | 206 | 5100 | 62,42 |
| | 45 | 211 | 5100 | 73,4 | 45 | 211 | 5100 | 62,6 |
| | 50 | 216 | 5100 | 73,65 | 50 | 216 | 5100 | 62,58 |
| | 55 | 221 | 5100 | 73,67 | 55 | 221 | 5100 | 62,76 |
| 60 | 226 | 5100 | 73,68 | 60 | 226 | 5100 | 62,76 | |

Table C.1: Investigation test data

| Time [min] | A1 [mm] | A2 [mm] | A3 [mm] | A4 [mm] | A5 [mm] | A6 [mm] | A7 [mm] | A8 [mm] | A9 [mm] |
|------------|---------|---------|---------|---------|---------|---------|---------|---------|---------|
| P 40 % | | | | | | | | | |
| 0 | 14,63 | 15,6 | 16,87 | 12,08 | 18,05 | 19,79 | 18,9 | 16,5 | 14,89 |
| 1 | 14,72 | 15,73 | 17,32 | 12,3 | 18,08 | 19,85 | 18,94 | 16,55 | 15,03 |
| 2 | 14,76 | 15,74 | 17,5 | 12,32 | 18,14 | 19,9 | 18,96 | 16,55 | 15,11 |
| 3 | 14,82 | 15,74 | 17,68 | 12,32 | 18,19 | 19,93 | 18,98 | 16,56 | 15,15 |
| 3 | 14,82 | 15,74 | 17,7 | 12,32 | 18,21 | 19,93 | 18,98 | 16,56 | 15,15 |
| 5 | 14,82 | 15,74 | 17,83 | 12,32 | 18,21 | 19,93 | 19,06 | 16,56 | 15,16 |
| 7 | 14,83 | 15,74 | 17,87 | 12,33 | 18,21 | 19,93 | 19,2 | 16,56 | 15,16 |
| 10 | 14,83 | 15,74 | 17,93 | 12,33 | 18,21 | 19,96 | 19,27 | 16,56 | 15,16 |
| 15 | 14,83 | 15,74 | 17,99 | 12,34 | 18,22 | 19,98 | 19,41 | 16,56 | 15,16 |
| P 55 % | | | | | | | | | |
| 0 | 22,17 | 26,05 | 28,85 | 19,14 | 28,32 | 31,92 | 33,8 | 28,55 | 27,04 |
| 1 | 22,5 | 26,32 | 29,55 | 19,24 | 28,38 | 32,07 | 33,98 | 28,58 | 27,1 |
| 2 | 22,51 | 26,33 | 29,75 | 19,27 | 28,4 | 32,12 | 34,04 | 28,6 | 27,15 |
| 3 | 22,58 | 26,33 | 29,81 | 19,29 | 28,42 | 32,15 | 34,06 | 28,63 | 27,15 |
| 3 | 22,6 | 26,33 | 29,9 | 19,31 | 28,42 | 32,16 | 34,06 | 28,63 | 27,15 |
| 5 | 22,68 | 26,33 | 29,96 | 19,33 | 28,42 | 32,2 | 34,09 | 28,67 | 27,16 |
| 7 | 22,74 | 26,35 | 30,15 | 19,35 | 28,4 | 32,25 | 34,12 | 28,7 | 27,22 |
| 10 | 22,76 | 26,35 | 30,42 | 19,39 | 28,4 | 32,29 | 34,17 | 28,75 | 27,25 |
| 15 | 22,8 | 26,35 | 30,43 | 19,4 | 28,4 | 32,29 | 34,32 | 28,81 | 27,29 |
| P 70 % | | | | | | | | | |
| 0 | 31,75 | 34,44 | 42,56 | 26,7 | 40,31 | 44,99 | 48,56 | 41,91 | 38,04 |
| 1 | 31,85 | 34,89 | 44,18 | 26,87 | 40,33 | 45,15 | 48,71 | 42,02 | 38,35 |
| 2 | 31,93 | 34,92 | 44,5 | 26,9 | 40,33 | 45,26 | 48,74 | 42,07 | 38,38 |
| 3 | 31,96 | 34,94 | 44,63 | 26,93 | 40,34 | 45,28 | 48,76 | 42,12 | 38,4 |
| 3 | 31,96 | 34,94 | 44,78 | 26,94 | 40,34 | 45,31 | 48,76 | 42,15 | 38,43 |
| 5 | 31,96 | 34,97 | 45,02 | 26,96 | 40,34 | 45,33 | 48,78 | 42,18 | 38,43 |
| 7 | 31,97 | 34,97 | 45,32 | 26,98 | 40,35 | 45,36 | 48,83 | 42,2 | 38,44 |
| 10 | 32,01 | 34,99 | 45,58 | 27,01 | 40,34 | 45,42 | 48,95 | 42,24 | 38,46 |
| 15 | 32,06 | 34,99 | 45,7 | 27,1 | 40,36 | 45,42 | 49,11 | 42,29 | 38,46 |
| 20 | 32,1 | 34,99 | 45,72 | 27,12 | 40,38 | 45,46 | 49,24 | 42,3 | 38,46 |
| 30 | 32,1 | 35,01 | 45,79 | 27,19 | 40,41 | 45,43 | 49,34 | 42,41 | 38,49 |
| P 85 % | | | | | | | | | |
| 0 | 41,79 | 46,82 | 61,61 | 34,29 | 55,02 | 60,34 | 65,21 | 57,2 | 51,76 |
| 1 | 42,18 | 46,85 | 62,56 | 35,16 | 55,13 | 60,58 | 65,79 | 57,71 | 51,89 |
| 2 | 42,32 | 46,85 | 62,87 | 35,21 | 55,25 | 60,7 | 65,92 | 57,8 | 51,93 |
| 3 | 42,33 | 46,9 | 63,05 | 35,24 | 55,25 | 60,76 | 66 | 57,91 | 51,96 |
| 3 | 42,42 | 46,94 | 63,09 | 35,27 | 55,24 | 60,8 | 66,04 | 57,96 | 51,98 |
| 5 | 42,53 | 46,96 | 63,11 | 35,3 | 55,26 | 60,84 | 66,07 | 57,98 | 51,99 |
| 7 | 42,53 | 46,99 | 63,33 | 35,33 | 55,27 | 60,96 | 66,15 | 58,04 | 51,99 |
| 10 | 42,54 | 46,99 | 63,51 | 35,4 | 55,27 | 61,07 | 66,21 | 58,15 | 51,99 |
| 15 | 42,55 | 47,08 | 63,7 | 35,41 | 55,27 | 61,2 | 66,25 | 58,2 | 51,99 |
| 20 | 42,57 | 47,12 | 63,8 | 35,46 | 55,29 | 61,38 | 66,32 | 58,21 | 51,99 |
| 30 | 42,57 | 47,14 | 63,92 | 35,5 | 55,33 | 61,47 | 66,4 | 58,37 | 52,01 |
| P 100 % | | | | | | | | | |
| 0 | 55,69 | 55,59 | 78,82 | 46,74 | 75,22 | 80,06 | 87 | 75,32 | 68,02 |
| 1 | 55,73 | 55,86 | 79,28 | 46,95 | 75,36 | 80,24 | 87,15 | 76,46 | 68,71 |
| 2 | 55,78 | 55,92 | 79,43 | 47,03 | 75,56 | 80,31 | 87,19 | 76,51 | 68,85 |
| 3 | 55,85 | 55,94 | 79,63 | 47,07 | 75,61 | 80,44 | 87,23 | 76,57 | 68,97 |
| 3 | 55,89 | 55,94 | 79,77 | 47,08 | 75,63 | 80,55 | 87,26 | 76,6 | 69,15 |
| 5 | 55,93 | 55,98 | 79,92 | 47,11 | 75,63 | 80,69 | 87,28 | 76,65 | 69,25 |
| 7 | 55,99 | 55,99 | 80,02 | 47,16 | 75,67 | 80,81 | 87,33 | 76,65 | 69,46 |
| 10 | 56,04 | 55,99 | 80,21 | 47,23 | 75,72 | 80,94 | 87,38 | 76,67 | 69,7 |
| 15 | 56,21 | 56,04 | 80,54 | 47,28 | 75,79 | 81,08 | 87,44 | 76,77 | 69,89 |
| 20 | 56,29 | 56,05 | 80,69 | 47,33 | 75,85 | 81,19 | 87,52 | 76,89 | 70,08 |
| 30 | 56,37 | 56,05 | 80,88 | 47,53 | 75,91 | 81,23 | 87,65 | 77,02 | 70,23 |
| 45 | 56,41 | 56,1 | 81 | 47,55 | 75,96 | 81,32 | 87,78 | 77,09 | 70,32 |
| 60 | 56,45 | 56,1 | 81,07 | 47,68 | 76 | 81,36 | 87,78 | 77,12 | 70,38 |

Table C.2: Suitability test data

C.3. Results Investigation tests, Set 1 - tabular:

| | An. 1 40 % | An. 1 55 % | An. 1 70 % | An. 1 80 % | An. 1 90 % | An. 1 100 % |
|--------------------|------------|------------|------------|------------|------------|-------------|
| ν [-] | 0,35 | 0,35 | 0,35 | 0,35 | 0,35 | 0,35 |
| G [kPa] | 9,25E+04 | 1,37E+05 | 1,68E+05 | 1,61E+05 | 1,34E+05 | 1,02E+05 |
| K [kPa] | 2,80E+05 | 4,11E+05 | 5,08E+05 | 4,87E+05 | 4,04E+05 | 3,09E+05 |
| μ_M [kPa·s] | 9,00E+11 | 3,57E+11 | 5,51E+09 | 4,68E+09 | 5,63E+09 | 4,80E+09 |
| μ_{KV} [kPa·s] | 6,86E+07 | 9,83E+08 | 4,45E+08 | 2,41E+07 | 4,38E+08 | 1,59E+08 |
| G_M [kPa] | 1,01E+05 | 1,39E+05 | 1,75E+05 | 2,33E+05 | 1,38E+05 | 1,08E+05 |
| G_{KV} [kPa] | 8,02E+05 | 2,83E+06 | 3,23E+06 | 5,00E+05 | 2,02E+06 | 1,07E+06 |

Table C.7: Soil parameters from Investigation Test calibration, Set 1

| | An. 2 40 % | An. 2 55 % | An. 2 70 % | An. 2 80 % | An. 2 90 % | An. 2 100 % |
|--------------------|------------|------------|------------|------------|------------|-------------|
| ν [-] | 0,35 | 0,35 | 0,35 | 0,35 | 0,35 | 0,35 |
| G [kPa] | 7,26E+04 | 9,74E+04 | 1,22E+05 | 1,22E+05 | 1,13E+05 | 1,44E+05 |
| K [kPa] | 2,19E+05 | 2,93E+05 | 3,67E+05 | 3,66E+05 | 3,41E+05 | 4,32E+05 |
| μ_M [kPa·s] | 5,72E+09 | 6,83E+11 | 9,21E+09 | 9,84E+09 | 7,80E+09 | 6,44E+09 |
| μ_{KV} [kPa·s] | 1,00E+07 | 9,75E+08 | 2,91E+08 | 4,76E+08 | 1,47E+08 | 1,25E+08 |
| G_M [kPa] | 9,83E+04 | 9,79E+04 | 1,25E+05 | 1,25E+05 | 1,13E+05 | 1,58E+05 |
| G_{KV} [kPa] | 2,44E+05 | 3,28E+06 | 1,94E+06 | 1,81E+06 | 1,86E+06 | 8,06E+05 |

Table C.8: Soil parameters from Investigation Test calibration, Set 1

C.4. Results Investigation tests

C.4.1 Set 1

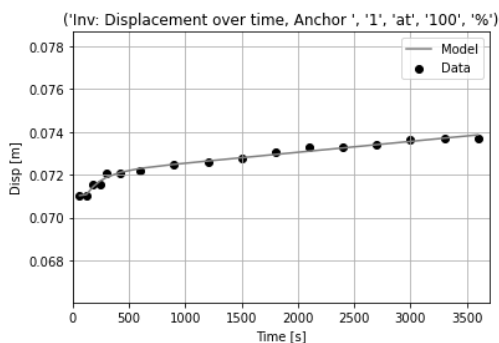


Figure C.1: Inv. test, Anchor 1 at 100 %

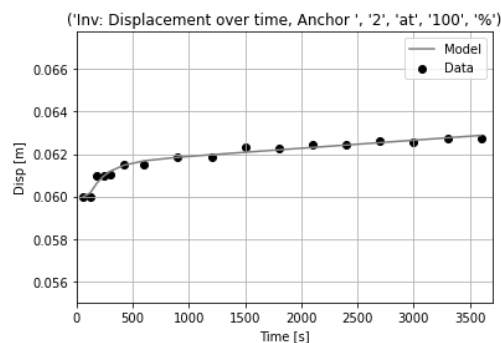


Figure C.2: Inv. test, Anchor 2 at 100 %

C.4.2 Set 3

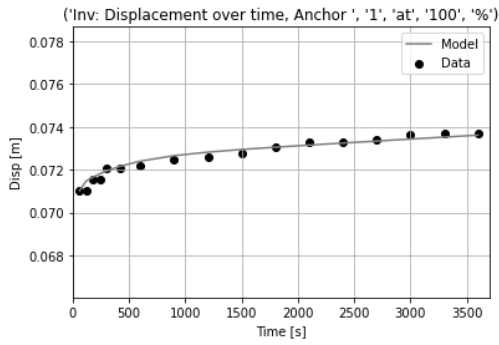


Figure C.3: Inv. test, Anchor 1 at 100 %

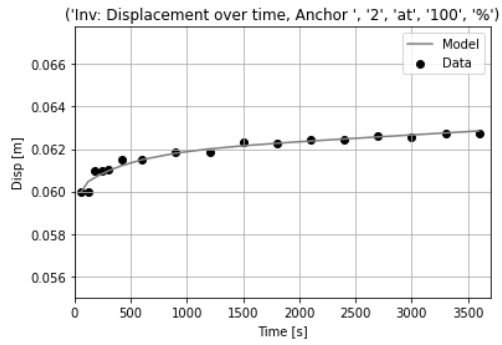


Figure C.4: Inv. test, Anchor 2 at 100 %

C.5. Results Suitability tests

C.5.1 Set 1

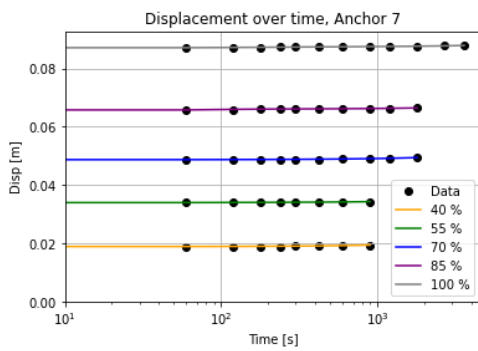


Figure C.5: Suit. test calibration, Anchor 7

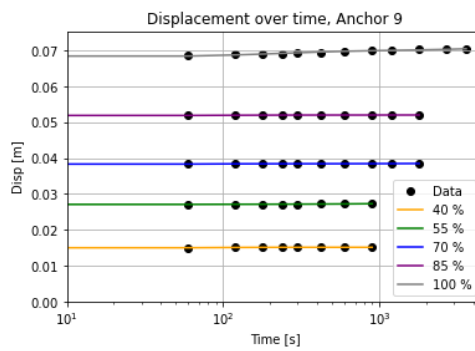


Figure C.6: Suit. test calibration, Anchor 9

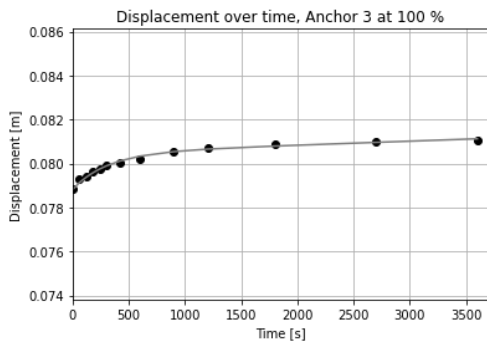


Figure C.7: Suit. test Anchor 3 at 100 %

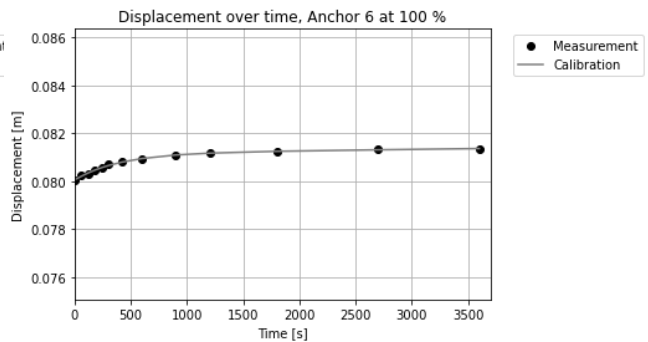


Figure C.8: Suit. test Anchor 6 at 100 %

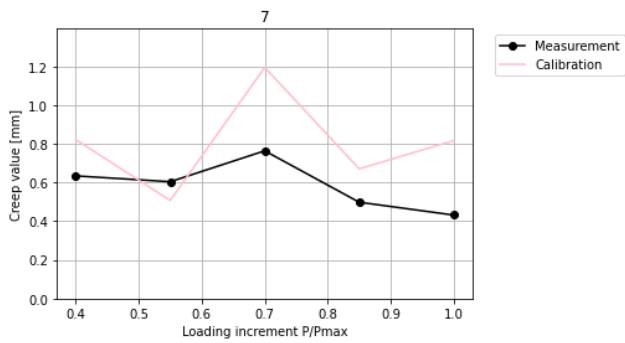


Figure C.9: Suit. test creep, Anchor 7

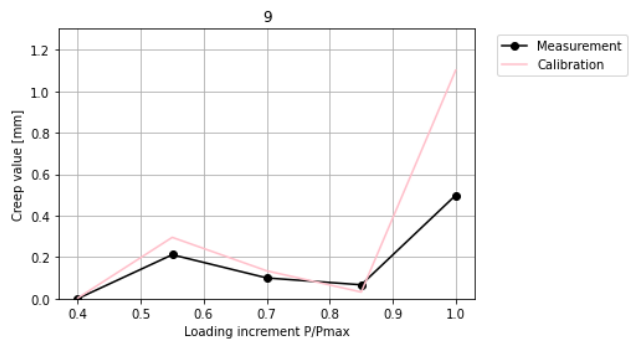


Figure C.10: Suit. test creep, Anchor 9

C.5.2 Set 2

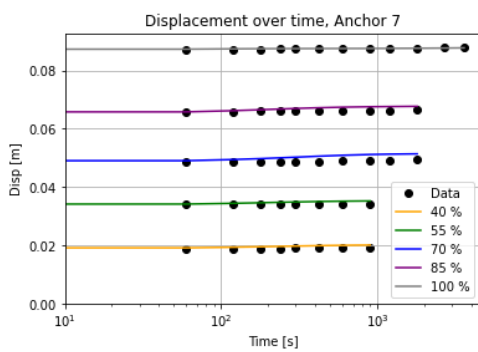


Figure C.11: Suit. test calibration, Anchor 7

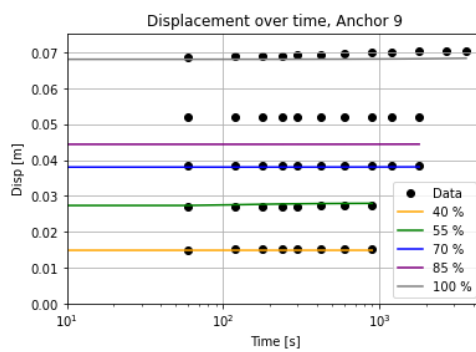


Figure C.12: Suit. test calibration, Anchor 9

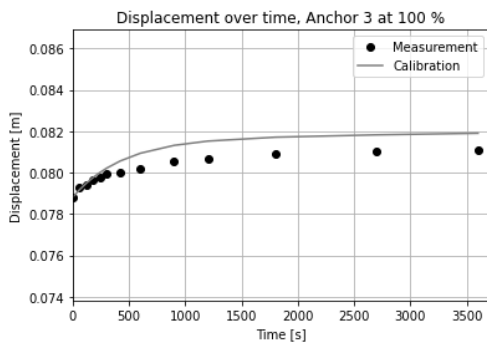


Figure C.13: Suit. test Anchor 3 at 100 %

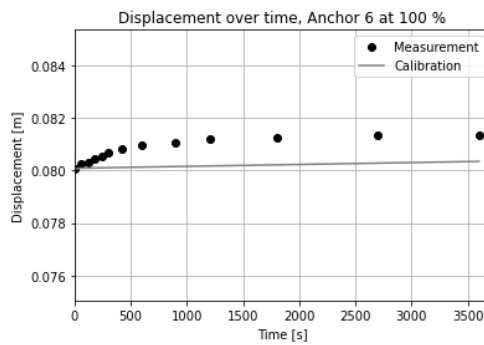


Figure C.14: Suit. test Anchor 6 at 100 %

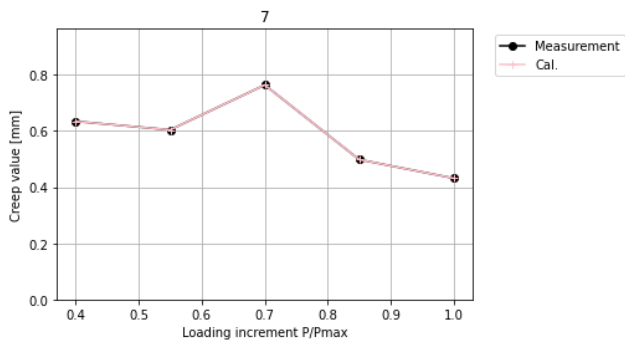


Figure C.15: Suit. test creep, Anchor 7

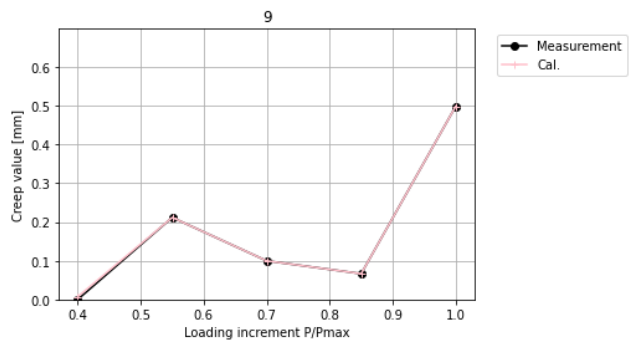


Figure C.16: Suit. test creep, Anchor 9

C.5.3 Set 3

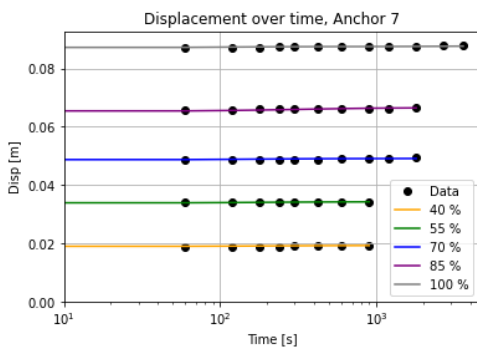


Figure C.17: Suit. test calibration, Anchor 7

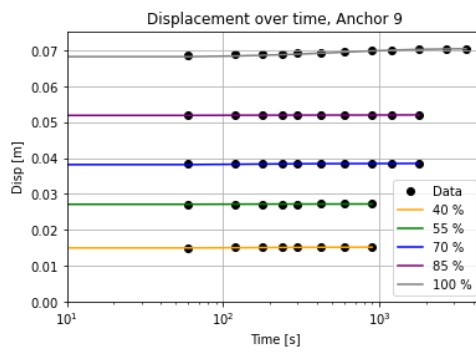


Figure C.18: Suit. test calibration, Anchor 9

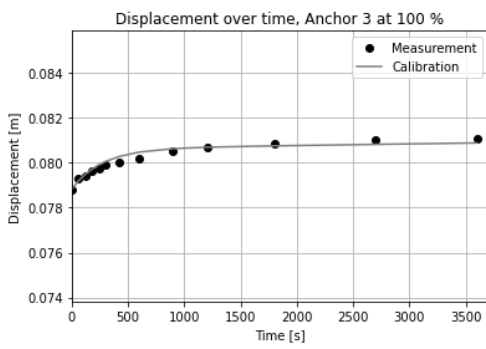


Figure C.19: Suit. test Anchor 3 at 100 %

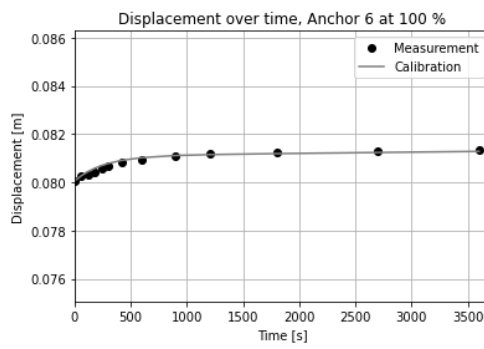


Figure C.20: Suit. test Anchor 6 at 100 %

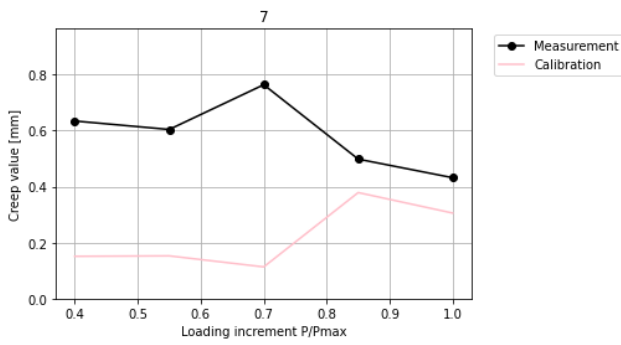


Figure C.21: Suit. test creep, Anchor 7

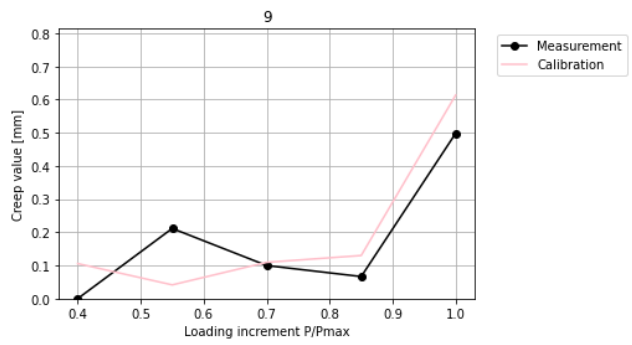


Figure C.22: Suit. test creep, Anchor 9

D. Appendix - Bayesian Updating

D.1. Investigation Tests

D.1.1 Set 1 - Results second anchor

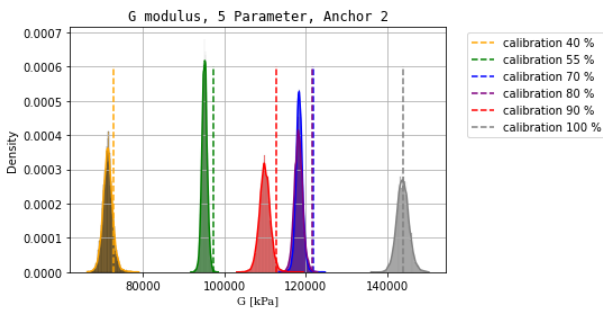


Figure D.1

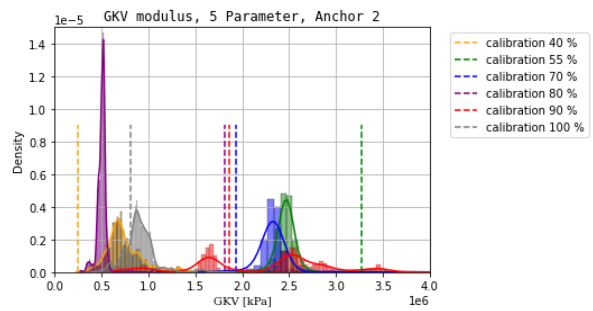


Figure D.2

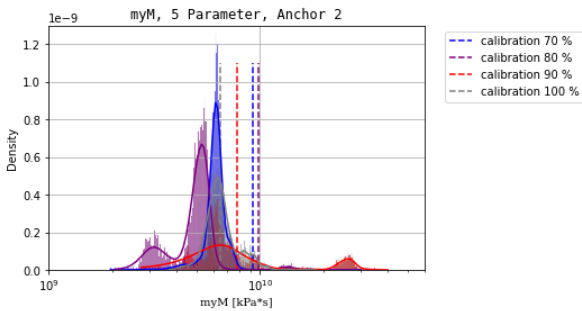


Figure D.3

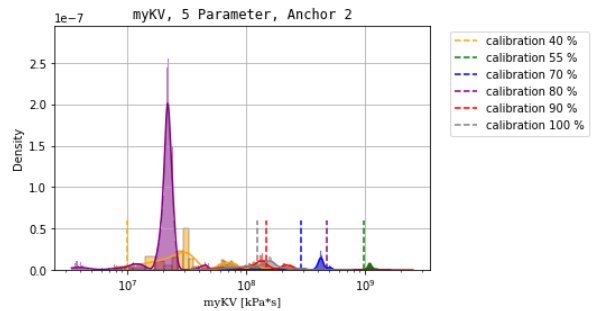


Figure D.4

D.1.2 Set 3 - Results second anchor

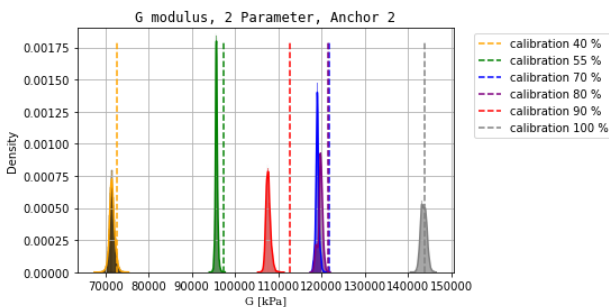


Figure D.5

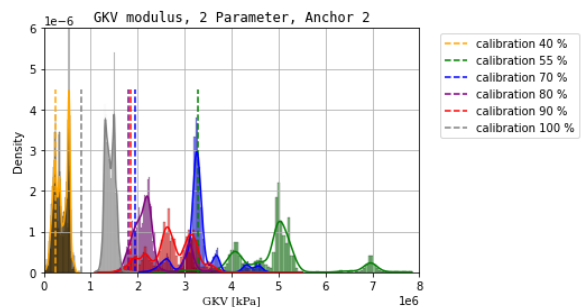


Figure D.6

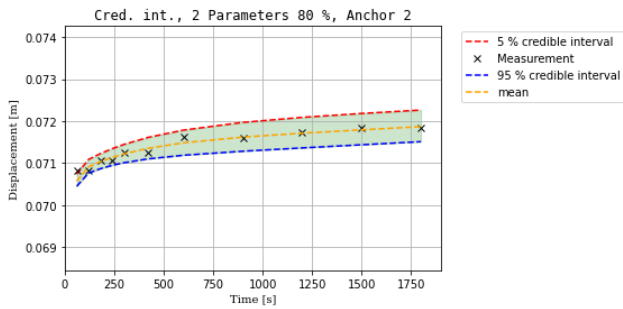


Figure D.7

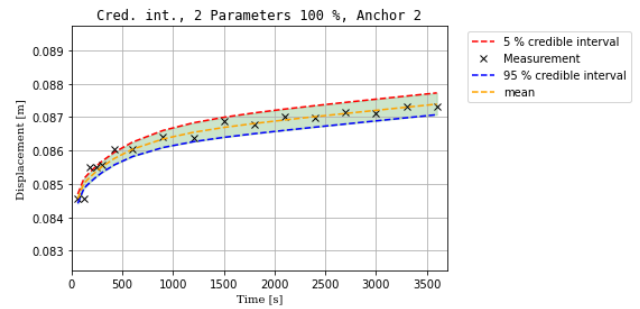


Figure D.8

D.1.3 Set 4 - Results second anchor

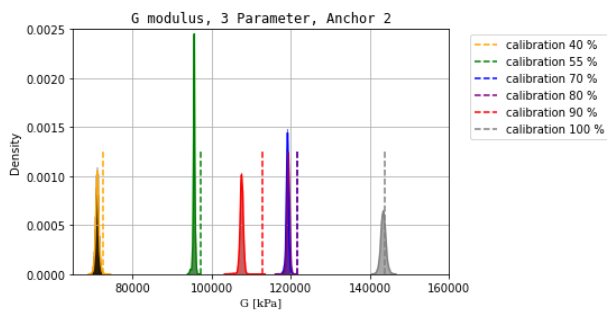


Figure D.9: Posterior distributions, Shear modulus

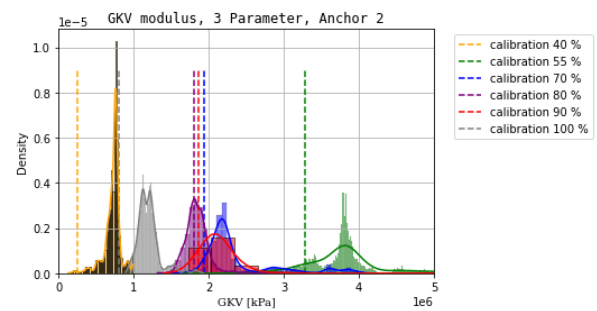


Figure D.10: Posterior distributions, Kelvin-Voigt shear modulus

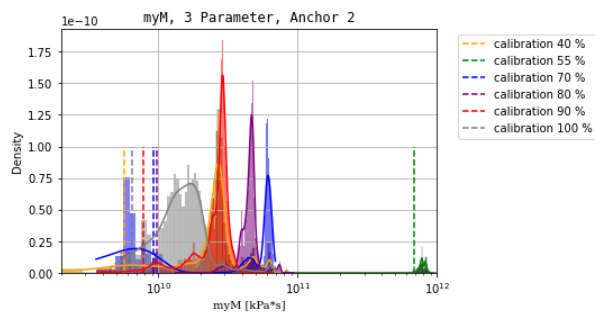


Figure D.11: Posterior distributions, Maxwell viscosity

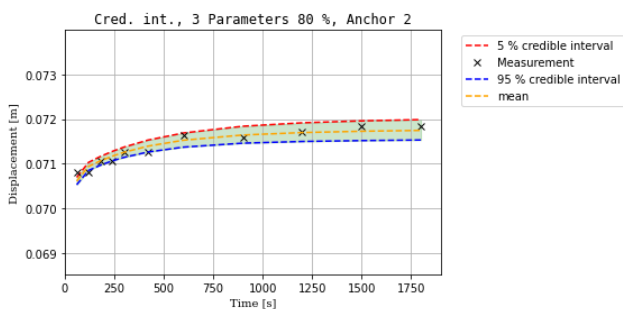


Figure D.12: Credible intervals, 80 % loading

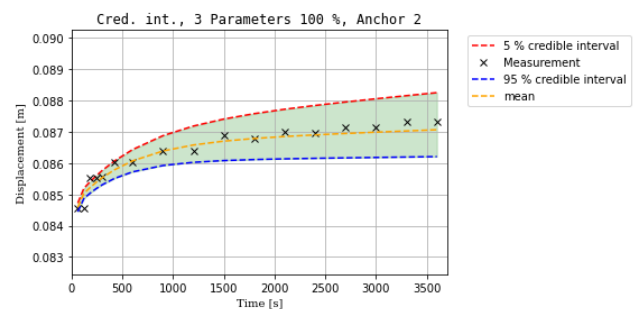


Figure D.13: Credible intervals, 100 % loading

D.1.4 Comparison with truncated normal priors

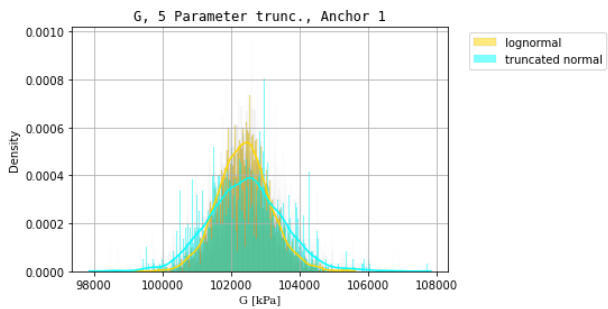


Figure D.14

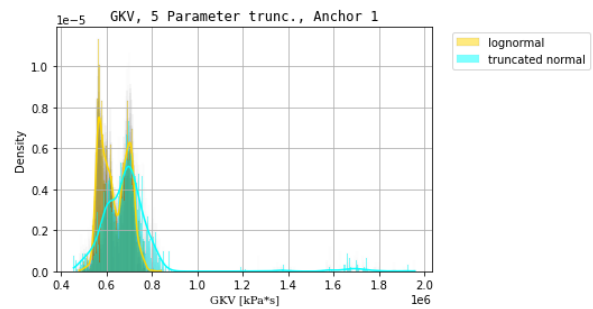


Figure D.15

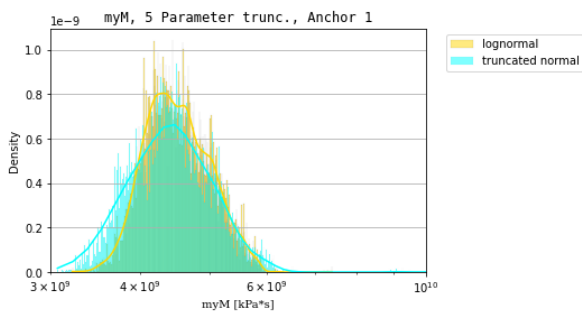


Figure D.16

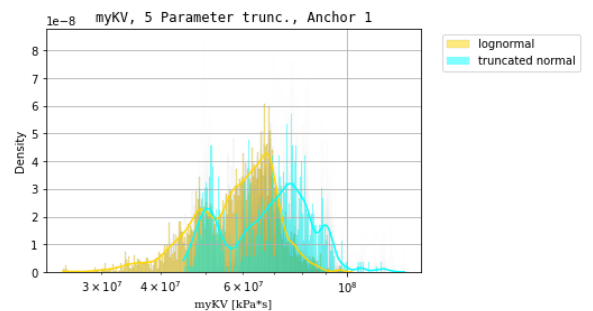


Figure D.17

D.2. Suitability Tests

D.2.1 Reliability investigation

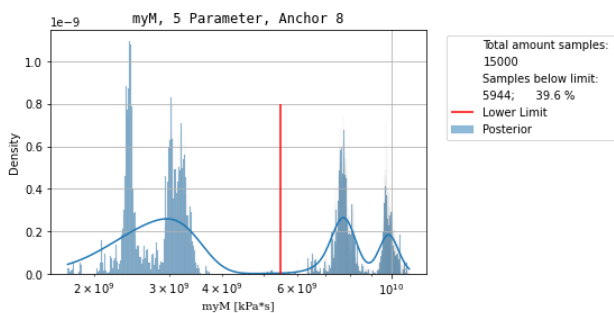


Figure D.18

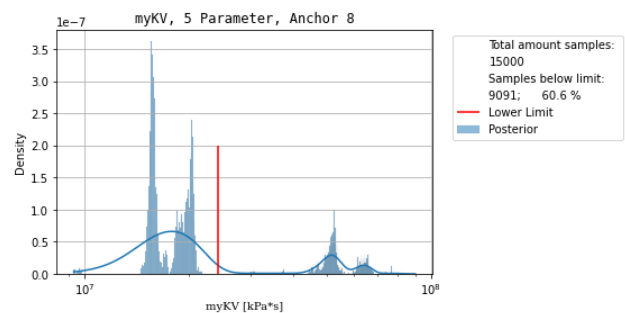


Figure D.19

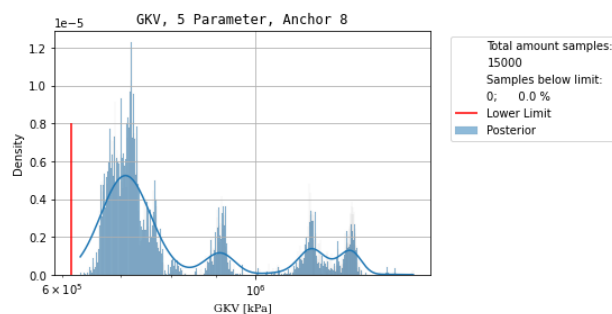


Figure D.20

E. Appendix - Codes

All the code that has been developed within this research, cannot be shown here, therefore the most useful equations to solve for are presented.

E.1. Analytical model

E.1.1 General Displacements

This equation is the overall outline of displacement calculations. This equation is solved for in the calibration, limit parameters or Bayesian updating and can be adjusted depending on which parameter shall be solved for.

```
def TDelta (self):
    t = self.mPar.t
    ny = self.SPar.ny
    b = self.mPar.b
    PO = self.AnPar.PO
    H = self.mPar.H
    a = self.mPar.a
    z = self.mPar.z
    re = self.mPar.re
    ri = self.mPar.ri
    D = self.mPar.D
    kL = self.AnPar.kL
    HL = self.mPar.HL
    EIstr = self.mPar.EIstr
    phi = np.radians(self.mPar.ph)

    G = self.SPar.G
    K = self.SPar.K
    GM = self.SPar.GM
    myM = self.SPar.myM
    myKV = self.SPar.myKV
    GKV = self.SPar.GKV

    #####
    # Wall stiffness
    Ka = (1 - np.sin(phi))/(1+ np.sin(phi))
    Kp = (1+ np.sin(phi))/(1- np.sin(phi))
    ta = HL / (np.sqrt(Kp/Ka) -1)
    LT = HL + ta
    kstr = 3 * EIstr/ (LT**3)

    # Stiffness kpc
    kpcinv = (1-ny)/( 4*b * (1+ny) *G)
    kpc = 1/kpcinv

    # Stiffness kpt
    za1 = H
    za2 = H+a
    intphi31 = ( (za2*np.sqrt(b**2+za2**2))/2 + (b**2 * np.log(za2 +
```

```

np.sqrt(b**2 + za2**2))/2 - (za2**2)/2 ) -
((za1*np.sqrt(b**2+za1**2))/2 + (b**2 * np.log(za1 + np.sqrt(b**2 +
za1**2)))/2 - (za1**2)/2 )

intphi32 = ( (b**2 * np.log(za2+np.sqrt(b**2+za2**2)))/2 - (za2 *
np.sqrt(b**2 +za2**2))/2 + (za2**2)/2 ) - ( (b**2 *
np.log(za1+np.sqrt(b**2+za1**2)))/2 - (za1 * np.sqrt(b**2 +za1**2))/2 + (za1**2)/2 )

kptinv = 1/(np.pi * a * b**2 *G) * ((1- ny) * intphi31 + 0.5 * intphi32)
kpt = 1/kptinv

# Stiffness kA
z1 = z-H
NM = 2*H*z *(z+H)**2
NK = (3-4*ny)*(z+H)**2 - 2*H*z
NB = 3-4*ny
NC = 5 - 12*ny +8*ny**2
NR1e = np.sqrt((z-H)**2 + re**2)
NR2e = np.sqrt((z+H)**2 + re**2)
NR1i = np.sqrt((z-H)**2 + ri**2)
NR2i = np.sqrt((z+H)**2 + ri**2)
NIre = NB*NR1e - (z1**2)/NR1e + NC *NR2e - NK/NR2e - NM/(NR2e**3)
NIri = NB*NR1i - (z1**2)/NR1i + NC *NR2i - NK/NR2i - NM/(NR2i**3)
NDifI = NIre-NIri
NIntDifI = trapz(NDifI, z)

invkA = 1/(2*np.pi*D**2*G*(1-ny)) * NIntDifI
kA = 1/invkA

# Initial displacement
d0 = (1/kL + 1/kpc -1/kpt + 1/kA) * P0

#####
# Time dependent displacements

TG = 1 /(1/GM + t/myM + (1-np.exp(-t*GKV/myKV))/GKV)
Tny1 = []
for i in range(len(TG)):
    Tnyx = (3*K - 2*TG[i])/(2*(3*K+TG[i]))
    if Tnyx < 0:
        Tny1.append(0.)
    else:
        Tny1.append(Tnyx)
Tny = np.array(Tny1)

TkL = np.ones(np.shape(t)) * kL

# Stiffness kpc
Tkpcinv = (1-Tny)/( 4*b * (1+Tny) *TG)
Tkpc = 1/Tkpcinv

# Stiffness kpt
Tkptinv = 1/(np.pi * a * b**2 *TG) * ((1- Tny) * intphi31 + 0.5 * intphi32)
Tkpt = 1/Tkptinv

# Stiffness kA
z1 = np.zeros(np.shape(z))
R1e = np.zeros(np.shape(z))
R2e = np.zeros(np.shape(z))

```

```

R1i = np.zeros(np.shape(z))
R2i = np.zeros(np.shape(z))
M = np.zeros(np.shape(z))
K = np.zeros((len(z), len(t)))
B = np.zeros(np.shape(t))
C = np.zeros(np.shape(t))
Ire = np.zeros((len(z), len(t)))
Iri = np.zeros((len(z), len(t)))

for i in range(len(t)):
    for k in range(len(z)):
        z1[k] = z[k] - H
        R1e[k] = np.sqrt((z[k]-H)**2 + re**2)
        R2e[k] = np.sqrt((z[k]+H)**2 + re**2)
        M[k] = 2*H*z[k] *(z[k]+H)**2
        K[k,i] = (3-4*Tny[i])*(z[k]+H)**2 - 2*H*z[k]
        B[i] = 3-4*Tny[i]
        C[i] = 5 - 12*Tny[i] +8*Tny[i]**2
        Ire[k,i] = B[i]*R1e[k] - (z1[k]**2)/R1e[k] + C[i] *R2e[k]
        - K[k,i]/R2e[k] - M[k]/(R2e[k]**3)

        R1i[k] = np.sqrt((z[k]-H)**2 + ri**2)
        R2i[k] = np.sqrt((z[k]+H)**2 + ri**2)
        Iri[k,i] = B[i]*R1i[k] - (z1[k]**2)/R1i[k] + C[i] *R2i[k]
        - K[k,i]/R2i[k] - M[k]/(R2i[k]**3)
DifI = Ire-Iri
IntI = []
for i in range(len(t)):
    DifIx = DifI[:,i]
    IntDifIx = trapz(DifIx, z)
    IntI.append(IntDifIx)

TinvkA = 1/(2*np.pi*D**2*TG*(1-Tny)) * IntI
TkA = 1/TinvkA

# Total stiffness
Tks = 1/( 1/TkL + 1/Tkpc - 1/Tkpt + 1/TkA)

Tdelta = P0/Tks
delta0 = d0

# Time dependent displacement loop
dDelta = np.zeros(len(t))
dP = np.zeros(len(t))
du =np.zeros(len(t))
ddP = np.zeros(np.shape(t))

for i in range(1, len(t)):
    dDelta[0] = 0
    dDelta[1] = Tdelta[1]-delta0
    dP[1] = dDelta[1]/((1/kstr) + (1/TkL)[0])
    du[1] = dDelta[1] - (dP[1]/TkL[0])

    dDelta[i] = Tdelta[i] - Tdelta[i-1]
    dP[i] = dDelta[i]/((1/kstr) + (1/TkL)[0])

    ddP[0] = dP[0]
    ddP[i] = ddP[i-1] + dP[i]
    if ddP[i] >= P0:

```

```

        ddP[i] = P0
        dP[i] = 0

    du[i] = dDelta[i] - (dP[i]/TkL[0])

P = np.ones(len(t)) * P0
dPc = np.zeros(len(t))
for i in range(len(t)):
    dPc[0] = dP[0]
    dPc[i] = dPc[i-1] + dP[i]
    P[i] = P[i] - dPc[i]
    if P[i] < 0:
        P[i] = 0

CdDelt = np.cumsum(dDelta)
TDelt = CdDelt+d0
return TDelt

```

E.1.2 Calibration - Least squares

This equation solves for the calibrated Burger Parameter, or time dependent soil parameter values. In the script, the elastic, non-time dependent parameters are solved for in different steps in the same fashion.

```

def parafitLSU (tframe, Delta, M, A, S):
    def f (tframe, myMO, myKVO, GMO, GKVO):
        MyModelx = Afun.AnalyticalModel(M, A, S)
        Tss = MyModelx.AllbP(tframe, myMO, myKVO, GMO, GKVO)
        return Tss

    y = Delta
    def residual(p, tframe, y):
        return y - f(tframe, *p)

    # p0 = [myM, myKV, GM, GKV],
    # setting G as lower bounds for the stiffness parameters
    p0 = [1e10, 5e8, S[1], 1e6]
    bounds = ([1e8, 9e11], [1e7, 9e10], [S[1], 400000], [S[1], 5e8])
    boT = np.transpose(bounds)
    popt = opt.least_squares(residual, p0, max_nfev=1000, bounds = boT,
        ftol = 1e-10, xtol= 1e-10, gtol = 1e-15, args=(tframe, y))
    print(popt)

    SPar2 = {'ny': S[0],
            'G': S[1],
            'K': S[2],
            'myM': popt.x[0],
            'myKV': popt.x[1],
            'GM': popt.x[2],
            'GKV': popt.x[3],
            }

    SPar2 = pd.Series(SPar2)

    OptModel1 = Afun.AnalyticalModel(M, A, SPar2)
    TDelta = OptModel1.Tdelta()
    return TDelta, SPar2

```

E.1.3 Limit Parameters

```

def parafitICF (tframe, Delta0, M, An, S, LimGKV):

```

```

def f (tframe, FmyM, FmyKV, FGKV):
    MyModelx = Afun.AnalyticalModel(M, An, S)
    Tss = MyModelx.AllCreepI(tframe100, FmyM, FmyKV, S[1], FGKV)
    return Tss

y = Delta0
def residual(p, tframe, y):
    return y - f(tframe, *p)

# p0 = [myM, myKV, GM, GKV]
p0 = [1e8, 1e8, S[1]]
bounds = ([1e6,S[3]],[5e7, 1e11], [S[1], LimGKV])
boT = np.transpose(bounds)
popt = opt.least_squares(residual, p0, max_nfev=1000, bounds = boT,
ftol = 1e-16, xtol= 1e-15, gtol = 1e-15, args=(tframe, y))
print(popt)

return popt.x[0], popt.x[1], popt.x[2]

```

```

def AllCreepI (self, t, myM, myKV, GM, GKV):

    G = self.SPar.G
    ny = self.SPar.ny
    K = self.SPar.K
    b = self.mPar.b
    PP = self.AnPar.PO
    H = self.mPar.H
    a = self.mPar.a
    z = self.mPar.z
    re = self.mPar.re
    ri = self.mPar.ri
    D = self.mPar.D
    kL = self.AnPar.kL
    HL = self.mPar.HL
    EIstr = self.mPar.EIstr
    phi = np.radians(self.mPar.ph)

    def creepGen100 (Y):
        ds = (Y[-1]-Y[-7]) * 1000
        ks = ds/(np.log10(tframe100[-1]/tframe100[-7]))
        return ks

    def creepGen85 (Y):
        ds = (Y[-1]-Y[-3]) * 1000
        ks = ds/(np.log10(tframe70[-1]/tframe70[-3]))
        return ks

    def creepGen55 (Y):
        ds = (Y[-1]-Y[-3]) * 1000
        ks = ds/(np.log10(tframe40[-1]/tframe40[-3]))
        return ks

    if len(t) == len(tframe40):
        creep = creepGen55(TDelta(t, G, ny, K, myM, myKV, GM, GKV))
    if len(t) == len(tframe70):
        creep = creepGen85(TDelta(t, G, ny, K, myM, myKV, GM, GKV))
    if len(t) == len(tframe100):
        creep = creepGen100(TDelta(t, G, ny, K, myM, myKV, GM, GKV))
    return creep

```

E.2. Bayesian Updating

E.2.1 aBUS-SuS Call, general

This formulation is the same ones as used of the authors of the algorithm in their example scripts.

```
def Up_3_Par_queue (prior_pdf, tframe, Yi, percent, queue, indicator):
    f_d = lambda x: Afun.AnalyticalModel(mParFun(tframe), AnParFun1(percent),
    SParMy).Up_3_Par(x[0], x[1], x[2])
    likelihood = lambda theta: mvn.pdf(f_d(theta), Yi,
    np.diag((theta[3]**2 * np.ones(len(Yi))))))
    realmin = np.finfo(np.double).tiny # to prevent log(0)
    log_likelihood = lambda theta: np.log(likelihood(theta) + realmin)

    N = int(20000) # number of samples per level
    p0 = 0.1 # probability of each subset

    print('\naBUS with SUBSET SIMULATION: \n')
    h, samplesU, samplesX, logcE, c, sigma = aBUS_SuS(N, p0, log_likelihood, prior_pdf)

    nsub = len(h.flatten()) # number of levels + final posterior
    u1p, u0p = list(), list()
    x1p, x2p, x3p, x4p, pp = list(), list(), list(), list(), list()

    for i in range(0, nsub):
        # samples in standard
        u1p.append(samplesU['total'][i][:,0])
        u0p.append(samplesU['total'][i][:,1])
        # samples in physical
        x1p.append(samplesX[i][:,0])
        x2p.append(samplesX[i][:,1])
        x3p.append(samplesX[i][:,2])
        x4p.append(samplesX[i][:,3])
        pp.append(samplesX[i][:,4])

    res = np.array([x1p, x2p, x3p, x4p, pp])
    print(res)
    queue.put([res, indicator])
    return res, indicator
```

E.2.2 Multiprocessing function call

This formulation was used to calculate several load steps at the same time. This might be not the best way of implementation, but it worked for this purpose. Since the results leave the function unsorted, a indicator is used to make sure that the load steps can be identified afterwards.

```
print('Start: ', time_print())
if __name__=="__main__":

    queue = multiprocessing.Queue()
    prc1 = multiprocessing.Process(target=(Up_3_Par_queue), args=(prior40,
    tframe40, xDel140, 0.4, queue, 0))
    prc2 = multiprocessing.Process(target=(Up_3_Par_queue), args=(prior55,
    tframe55, xDel155, 0.55, queue, 1))
    prc3 = multiprocessing.Process(target=(Up_3_Par_queue), args=(prior70,
    tframe70, xDel170, 0.70, queue, 2))
    prc4 = multiprocessing.Process(target=(Up_3_Par_queue), args=(prior80,
    tframe80, xDel180, 0.80, queue, 3))
    prc5 = multiprocessing.Process(target=(Up_3_Par_queue), args=(prior90,
```

```
tframe90, xDel190, 0.90, queue, 4))
prc6 = multiprocessing.Process(target=(Up_3_Par_queue), args=(prior100,
tframe100, xDel1100, 1.0, queue, 5))

prc1.start()
prc2.start()
prc3.start()
prc4.start()
prc5.start()
prc6.start()

res_i = queue.get()
print('1.1 Process done!')
res_j = queue.get()
print('2.1 Processes done!')
res_k = queue.get()
print('3.1 Processes done!')
res_l = queue.get()
print('4.1 Processes done!')
res_m = queue.get()
print('5.1 Processes done!')
res_n = queue.get()
print('All Processes done!', time_print())

prc1.join()
prc1.close()
prc2.join()
prc2.close()
prc3.join()
prc3.close()
prc4.join()
prc4.close()
prc5.join()
prc5.close()
prc6.join()
prc6.close()
```